Connectivity and Mobility in Wireless Networks

Peter Pratt

A dissertation submitted to the University of Bristol in accordance with the requirements for award of the degree of Doctor of Philosophy in the Faculty of Mathematics
June 23, 2019

Word Count: 56785

To my Wife and Son

Abstract

With the ever continuing increase in the number of devices connecting to one another, forming the Internet of Things (IoT), understanding how the performance of these networks connect is of paramount importance. Modelling the location of devices/base stations by random sets, tools from stochastic geometry can be leveraged creating a framework which is far more tractable than previous lattice models. As such there has been significant progress into the fundamental capabilities of wireless networks, including connectivity and scalability. To date, the majority of literature has presumed a uniform Poisson Point Process in $\mathbb{R}^2$ to model the distribution of points which represent base stations or smart devices. Although very tractable, the model loses some important features that heavily influence real world networks. For example, within this model there is a notion of a "typical user", which is that the network performance (such as the probability you can send a signal) is independent of location. Naturally, this contradicts what we as consumers experience in reality, since connectivity varies due to base stations being far away, or buildings/hills etc causing signal degradation.

Furthermore, as the IoT continues to grow, the network becomes increasingly dynamic due to portable smart devices requiring connectivity. Motivated by this, we study the impact boundaries (examples are geographical features like the body of water surrounding New York city) and human mobility have on the connectivity properties of wireless networks, both over single and multiple time slots. To achieve this, we use a Poisson Point Process with non-uniform measure in some finite domain and model the links between points as probabilistic connection function. Through this general model, referred to as a Soft Random Geometric Graph, we are able to study a range of different networks even within the wireless communication literature. These include the classical device to base station architecture, to device-to-device networks where information is relayed in a multihop fashion, to ultra dense 5G networks where the base stations may themselves be mobile, for instance

as drones. We later extend our work to spatio-temporal networks where we analyse how these graphs evolve over multiple time slots. Our results therefore have a variety of applications ranging from the routing information and scalability of mobile ad hoc networks to how 5G networks should be deployed in urban environments to maximise user experience.

Acknowledgements

I would firstly like to thank Carl Dettmann, Orestis Georgiou and Woon Hau Chin for their invaluable expertise, guidance and support that has made the last four years so enjoyable. I would also like to extend that thank you to everyone from the Spatially Embedded Networks group based in both Bristol and Oxford; I know the continued dialogue between both groups has greatly helped my research. I would also like to acknowledge the financial support of the EPSRC and Toshiba who have helped to fund me during my studies.

My final thank you goes to my wife for helping to make the last four years so enjoyable, and without whom this thesis would have been completed six months earlier.

Author's Declaration

I declare that the work in this dissertation was carried out in accordance with the requirements of the University's Regulations and Code of Practice for Research Degree Programmes and that it has not been submitted for any other academic award. Except where indicated by specific reference in the text, the work is the candidate's own work. Work done in collaboration with, or with the assistance of, others, is indicated as such. Any views expressed in the dissertation are those of the author.

Signed: Peter W Pratt

Date: February 2019

Contents

List of Tables

List of Figures

Chapter 1

Introduction

As our dependency on technology continues to increase, so does our need to be connected. We have all experienced the frustrations of not being able to send that all important text message when we needed to most. These random failures that occur locally can be very annoying from a personal perspective, but can also have detrimental effects to the whole network when information is instead relayed from device-to-device, leaving everyone unhappy. Categorising why our smart devices suddenly fail to connect to the network is a problem this work aims to address, and it turns out it is probably not because your phone hates you[1]. So whether it be for business purposes or simply because you need to share that joke you thought over that last cup of coffee, this work aims to provide insight into why our smart devices fail and hopefully influence future network deployment to maximise user experience.

1.1 So what is a Wireless Network?

Lets first take a step back and consider the different types of networks we are interested in. The traditional (Macro Cell) architecture of wireless networks consists of base stations (BSs) and end users. Typically when one end-user

[1] although I cannot guarantee this

tries to send a packet to another (reasonably far away), it first sends the packet to its nearest BS, it then gets routed through the backhaul network to a different BS which then transmits it to the intended target. A conventional model is to do a Voronoi tessellation of the network, where every user in a cell is served by the same BS, meaning a single BS serves many users [Kou16a]. This type of network is unlikely to scale well with the number of users. That is, as the number of devices in the network increases, so does the strain on the network architecture, after all a BS can serve only so many users at any one time, all the rest will impact negatively on the performance through interference. One solution is to introduce more sophisticated network protocols, where instead of everyone transmitting at once, only a subset can access the channel at any one time, or alternatively you could include more antennas and/or channels in which devices can communicate. However, these mechanisms are unlikely to cope with the exponential growth in devices, and simply adding more BS is not a viable solution mainly due to financial and geographical restrictions.

The antithesis of the archetypal network consisting of BSs and users, are wireless mesh networks. A wireless mesh network has no centralised system, but instead information is transferred through the network in a multihop fashion. One example of a mesh network is a mobile ad hoc network (MANET) where mobile smart devices continually make and break links as they move around. MANETs have various advantages over a fixed network architecture with the main advantage being they can easily resolve problems of isolated nodes due to their self-configuring nature. Other advantages of MANETs include: they are easily deployable since they require no fixed infrastructure; easily scalable since devices can easily be added to the network and random node failures are less likely to cause cascading network failures as data can take multiple paths [Hel14]. However, MANETs are not without their flaws, for example they are susceptible to: variations in network performance (no fixed connections); interference depends on location and can lead to isolated users or a waste of resources (data has to be repeatedly resent

due to links failing), and the allocation of resources as devices have to relay information [Hel14].

Another solution to meet the increasing demand of cellular traffic are heterogeneous networks (HetNets) [Boc14b, DR13]. HetNets are formed by adding smaller versions of BSs, namely pico and femto cells, more generally called Access Points (APs). There is a general consensus that network densification, both spatially and over the frequency domain, can help cope with the expected 1000-fold increase in traffic demand over the coming decade whilst remaining cost effective [Bhu14, DR13]. By deploying smaller pico and femto cells can help to improve network throughput, bring about higher data rates along with improving mobile user coverage [Bhu14]. Moreover, HetNets have the added appeal of being far more scalable, as smaller APs are cheaper and easier to deploy, with fewer initial costs compared with their macro cell counterparts. Furthermore, smaller APs provide greater network flexibility, for example drones have been proposed to offset spikes in traffic demand during sporting events or music festivals [Ors17].

1.2 Network Models

Traditional models for wireless networks assumed a hexagonal lattice structure for cells in which a BS is located at the centre [Rin47]. Naturally, this is a very idealised model since it simply would not be possible to build such a network in reality both financially and due to geographically restrictions. It turns out that the locations of BS appear far more random [Li15], probably because few foresaw such rapid growth in technology and didn't plan accordingly; people are generally opposed to having a BS in their front room to ensure a nice regular structure.

As a result it has become common practice to model the location of BSs via a point process embedded in $\mathbb{R}^2$. The usual model utilises a uniform Poisson Point Process (PPP) for mathematical tractability, but the point set can be modelled by a wide range of different point patterns found in

Stochastic Geometry [Bac09, Hae12, Det18b] and they need not be uniform. However, other point processes have been used to model different network features with varying degrees of success. For example, the Gibbs process is an extremally powerful point process as it allows the user to interpolate between networks with attraction and repulsion via a density function that is defined by the pairwise interaction of points, but rarely results in a tractable solution [Guo13, Det18b]. On the other hand the determinantal point process, first used to model the distribution of fermions in thermal equilibrium [Kul12], has been used to model the intrinsic repulsion between BSs with far more success, see [Miy14] for example. Regardless of the point process chosen, the question of whether any network analysis can be done often boils down to whether the spatial average can be computed; one of the reasons the PPP is so popular is due to its complete spatial randomness yielding a nice form for the probability generating functional (PGFL). As a consequence we now have a mathematical framework for calculating network metrics such as the coverage probability which was not previously possible. However, creating these networks with a fixed architecture is both costly and time consuming, and as early as the 1960's it was proposed that mesh networks, which have little start up cost and time, could be used for wireless communications [Gil61]. It is these mesh networks, with mobility, that we are particularly interested in and are discussed in more detail below.

In 1961, Gilbert introduced the Random Plane network [Gil61], more commonly referred to now as the Random Geomtric Graph (RGG), where points are randomly dropped in some space and and pairs of nodes are linked if they are mutually close [Wal11, Bar11, Det18b]. The location of points in a RGG are modelled by a spatial point pattern, with the original model being a uniform PPP where N points are uniformly distributed in the domain and N is a Poisson random variable (rv). RGGs have been applied to the study of wireless sensor networks where the power of devices is relatively low [Kar08]. The scope of RGGs are certainly not limited to communication networks, for example they have also been to used model the spread of diseases [Bal08],

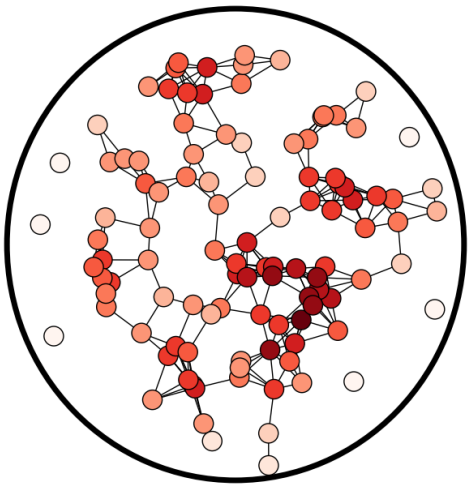

Figure 1.1: A RGG in a circular region with radius $R = 5$, and a non-uniform PPP with density $\lambda_0 = 1.5$ and a connection range of $r_0 = 1$. The darker colours represent a higher degree.

and are studied in combinatorics as unit disk graphs [Cla90]. It should be noted that most rigorous statements are for infinite RGGs, for example on $\mathbb{R}^2$, or on a sequence of RGGs in finite domains for which $\bar{N} \to \infty$, with further discussion on how the system scales left to [Coo15, Det18b].

More recently, the RGG has been generalised to the *Soft Random Geometric Graph* (SRGG) which includes an additional source of randomness in terms of link probabilities. Similar to the RGG, the points are modelled by a point process, but instead of a deterministic connection model, the probability two nodes connect depends on some link function $\mathcal{H} : r \to [0, 1]$, where r is the separation between the two nodes. In most cases $\mathcal{H}(r)$ decays as a function of distance, but this is not always true as we will discuss in the following chapter. As a result, SRGGs are able to model a wider variety of networks including neural [Shi92, Rou04], social [Cho11, Won06] and more diverse communication networks [Det18b], simply by choosing a suitable $\mathcal{H}$. As is sometimes the case in mathematics, different communitiies refer to it with different names which include the Waxman graph (named after its

creator) [Wax88], the random connection model [Pen16, Kri16, Mül15] and spatially embedded random networks [Bra14, Iye18, Mao17] which once again is indicative of its wide array of applications. One particular connection function of interest is the interference-limited connection function. In this case, the connection probability not only depends on the distance between the receiver and transmitter, but the locations of all other transmitting devices in the network (which are acting as interferers). Interestingly, for this model it is possible to obtain closed form expressions for network metrics using stochastic geometry which was not previously possible from a purely information theoretic standpoint [Bac97]. In the following chapters we will see why this is such a powerful model in understanding wireless networks.

1.3 Results for the Random Geometric Graph and its generalisations

The main question addressed in [Gil61] was one of network criticality. Namely, what are the conditions needed for a RGG to transition from being comprised of connected components of finite size almost surely, to one where there is almost surely an infinite (giant) component [Det18b]: a phenomenon known as percolation [Gri99]. In fact, the original paper on RGGs [Gil61] provides an upper bound by tiling the plane and drawing from results on bond percolation and a lower bound using a branching process [Wal11]. Improvements on these bounds have since been given, largely by refining the original techniques used in Gilbert's paper [Hal85].

However, perhaps a more pertinent question is *when does a finite RGG become fully connected?* A graph is said to be fully connected when there exists a multihop path between any two nodes in the network. One of the most celebrated results was by Penrose [Pen97] who showed that for points uniformly distributed on the unit cube, the RGG becomes fully connected when there are no more isolated nodes with high probability, as the number

of nodes goes to infinity. This phenomenom also appears in classical random graphs [Bal08] and SRGGs [Mao13,Mao17,Pen16], albeit only for a particular class of connection functions. This result not only identifies the bottleneck to full connectivity, but also a simple approximation which has been used extensively in the study of wireless networks. Interestingly in 1D this result does not hold as the network is more likely to split into two disconnected clusters, and remains an open problem.

1.4 Finite Mobile networks

The scaling adopted in the above results means the impact of boundaries are hidden. It turns out that in more realistic networks where the number of nodes is large but finite, boundaries play an important role when studying network connectivity. Moreover, these results assume that points are uniformly distributed within a domain, but this is unlikely to be the case in reality. As networks become increasingly mobile, the distribution of devices becomes less uniform: mobility induces inhomogeneity. As people with smart devices move around in their every day lives, a higher proportion of network traffic will occur in popular places such as shopping centres and sporting events.

In fact, it is the impact user mobility has on network performance that is of particular interest to us in this thesis. Human mobility itself is a very rich area of research with a wide range of models claiming to capture the key behaviours that categorise human mobility [Bet02, Ben07, Lee12]. The importance of mobility on network performance is illustrated by the results in [Gup00] and [Gro01]. When the network is *not* mobile, the performance in terms of its ability to transmit data (network capacity) decreases as the number of nodes increases, due to the increased competition for resources [Gup00]. On the other hand, Grossglauser and Tse [Gro01] showed that the converse is true if the nodes are mobile, even for an interference-limited environment; albeit at the cost of increased delay. Essentially, a

mobile network can handle more data but it is transferred at a slower rate. In this work we largely focus on the Random Waypoint (RWP) model to represent human mobility, as it is both intuitive and tractable. The RWP model converges to a stationary distribution which can be computed exactly (see Chapter 3) where the distribution of users is highest in the middle of the domain and decreases towards the boundaries, making for a very intuitive model for cities. The stationary distribution of the RWP model, coupled with tools from stochastic geometry, allows for a more mathematical analysis when compared with other models. However, we do not limit ourselves to analysing the RWP, but study more general non-uniform distribution of users, allowing us to capture a wider range of human mobility behaviour. This has the further benefit of enabling us to more precisely isolate whether it is boundaries, inhomogeneity or both that determine network connectivity.

1.5 About this thesis

In this thesis our primary aim is to address the following question: *how does mobility impact the performance of Soft Random Geometric Graphs?*

To tackle this question we first begin by trying to understand how we can model mobility in wireless networks. We particularly focus on the popular Random Waypoint Mobility model that has been widely studied as it converges to a stationary distribution. In chapter 3 we calculate, for the first time, the exact spatial distribution for the rectangle and triangle cases, and compare them with existing approximations within the literature. Although the approximations differ quantitatively to the exact calculations, they still capture the same qualitative nature; the density goes to zero at the boundary and is highest in the bulk. Motivated by this we study a more general distribution of points which allows us to interpolate between the RWP model, the widely studied uniform model and one where the density of points is highest near the boundary (referred to as convex). By using a PPP with non-uniform measure and a general connection function it allows us to capture the diverse

array of impacts of inhomogeneity, a result of mobility, on a wide range of networks, which we can compare with existing results in the literature.

Indeed, within this general framework we first highlight the impact inhomogeneity and boundaries have on the average number of connections a device can have in MANET in chapter 4. Of particular interest is the interference model where the probability a link is formed also depends on the locations of other nodes. In this case the mean degree is not only highly location dependent, but also very sensitive to the choice of path loss function; for a non-singular path loss function the mean degree has a distinct density which maximises the mean degree, beyond which it decays to zero.

Our second main contribution comes in chapter 5 which regards ultra-dense networks and looks at how HetNets can bring about the improved performance promised by 5G networks. Here we use a nearest neighbour communication model to represent how devices and APs communicate, and provide insight into the optimal deployment of APs for a range of different network scenarios.

Our final main contribution in chapter 7 is to use the insight from the previous chapters and apply it to mobile networks over multiple time slots. In this case we provide two methods to approximate the probability a node is isolated near a corner in a range of different networks, and discuss how these boundary nodes influence the overall connectivity. The insight obtained is then applied to how routing in wireless mesh networks could be optimised.

A publication list is provided in Appendix A, along with a break down of my contributions for each paper.

The thesis is divided into the following chapters.

Chapter 2: A discussion of the mathematical preliminaries used throughout the thesis.

Chapter 3: The Random Waypoint Model is formally defined, and exact expressions for the spatial distribution are computed for the triangle and rectangle.

Chapter 4: The average degree is computed for a range of SRGGs in a rectangle with different non-uniform densities, including the stationary distribution of the RWP. The result is then related to percolation in SRGGs with interference.

Chapter 5: We analyse the coverage probability in ultra-dense heterogeneous networks with non-uniform measures. We then use these results to analyse how to deploy access points in order to optimise user experience.

Chapter 6: We build upon the work of Chapter 5, and apply it to Low Power Wide Area networks, which have a modified connection model yielding some interesting results.

Chapter 7: A range of different SRGGs are analysed over multiple time slots, analysing how boundaries and non-uniform distribution of points affect network connectivity.

Chapter 8 We extend our analysis beyond a single node to how long clusters of size two or more are isolated for.

Chapter 9: We draw together our results and highlight some interesting open problems.

1.5.1 List of Notation

Notation	Description
Φ	Point Process
$\Lambda(\cdot)$	Intensity measure of the point process
$\lambda(\boldsymbol{x}), \rho(\boldsymbol{x})$	Intensity of points in the point process
λ_0, ρ_0	Density of the point process
λ_c	Critical density for which a graph percolates
$\bar{N}$	Mean number of points in the point process
R	Radius of a circular domain
$\mathcal{B}_{\boldsymbol{x}}(r)$	The ball centred at the point $\boldsymbol{x}$ with radius r.
$\mathcal{A}_{\boldsymbol{x}}(r_1, r_2)$	The annulus centred at the point $\boldsymbol{x}$ with inner radius r_1 and outer radius r_2.
$V_{\mathcal{B}}(\boldsymbol{x}, r)$	The void probability at the point $\boldsymbol{x}$ with radius r.
$\mathcal{H}(r)$	The connection probability that two points separated by a distance r connect.
r_0	Typical connection range, used to scale the connection function
r_c	Critical connection range for the network to percolate
$g(\cdot)$	Path loss function
η	Path loss exponent
σ^2	The amount of noise in the channel
γ	A parameter that thins the number of points in the process, often used to reduce the number of interferes.
$\wp$	Probability a node is transmitting.
$\lvert h\rvert^2$	Channel gain, assumed to be exponential random variable with mean one

Notation	Description
q	Threshold required for a successful transmission to take place
$\mathcal{L}_{\mathcal{I}}(s)$	Laplace transform of the interfering signals in the point process evaluated at s
q_{sf}	Threshold required for a successful transmission to take place, where SF refers to the spreading factor
ψ	The carrier wavelength
$\bar{l}$	The mean length between consecutive waypoints in the random waypoint model.
$\mu(\boldsymbol{x})$	The mean degree of a point at $\boldsymbol{x}$
$F_{\boldsymbol{x}}(r)$	The Cumulative density function of the nearest neighbour distribution
$f_{NND}(\boldsymbol{x})$	The probability density function of the nearest neighbour distribution
$C(\boldsymbol{x})$	The location dependent coverage probability.
$C_K(\boldsymbol{x})$	The coverage probability in a network where K nodes cooperate.
$\bar{C}(\cdot)$	The average coverage probability.
$P_{iso}(\boldsymbol{x})$	The probability a node at $\boldsymbol{x}$ is isolated from the rest of the nodes in the network.
P_{fc}	Probability of full connectivity
$\mathcal{G}_K$	A connected subgraph of size K nodes.
$\mathcal{C}^T_{\mathcal{G}_K}$	The expected number of clusters of size K that are connected within themselves, but are disconnected from the rest of the network.

Table 1.1: A Table of all the notation used in this Thesis.

1.5.2 Table of Abbreviations

Abbreviation/ Initialism	**Full name/ Description**
AP	Access Point
BPP	Binomial Point Process
BS	Base station
CoMP	Cooperative Multipoint transmission scheme
CSMA/CA	Carrier-Sense Multiple Access with Collision Avoidance (channel access scheme)
HetNet	Heterogeneous Network
IoT	Internet of Things
LoRa	Long Range (Type of Low Power Wide Area Network)
LPWAN	Low Power Wide Area Network
LTE	Long term evolution standard for the fourth generation (4G) of networks
MANET	Mobile Ad hoc network
MIMO	Multiple input Multiple output model
PGFL	Probability Generating Functional
PPP	Poisson Point Process
QD	Quasi Disk (connection model)
RGG	Random Geometric Graph
RW	Random Walk (mobility model)
RWP	Random Waypoint (mobility model)
SA	Soft Annulus (connection model)
SD	Soft Disk (connection model)
SF	Spreading Factor
SINR	Signal-to-Interference-plus-Noise-Ratio
SIR	Signal-to-Interference-Ratio

Abbreviation/ Initialism	**Full name/ Description**
SLAW	Self-similar Least Action Walk (mobility model)
SNR	Signal-to-Noise-Ratio
SRGG	Soft Random Geometric Graph
MU	Mobile User

Table 1.2: A Table of all the abbreviations and initialisms used in this thesis.

Chapter 2

Mathematical Preliminaries

The purpose of this chapter is to introduce the key concepts that are continually used throughout. Many of the results stated can also be found in the review I did jointly with Carl Dettmann and Orestis Georgiou Ref [Det18b]. My main contributions in the review were the chapters on point processes (Sec 2 of Ref [Det18b]); percolation (Sec4.2 of Ref [Det18b]); temporal networks (Sec 7 of Ref [Det18b] and mobility (Sec 8 of Ref [Det18b]), much of which is discussed below. This chapter will also contain some overlap with the introductions in Ref [Pra16, Pra17, Pra18] of which I was a co-author where my contributions to each are outlined in the publication list in Appendix A. Finally, I also edited the following Wikipedia pages: Edgar Gilbert, Mobile ad hoc network and Random Geometric Graph [Wik18a, Wik18b, Wik18c] as part of the spatially embedded networks project between Oxford and Bristol, as such there may also be some overlap in some of the discussions.

The spread of diseases, fires and information through real world networks depends greatly on the underlying spatial structure [Det18b]. The first spatial model was the RGG [Gil61], originally called a Random Plane network but has since been generalised to SRGGs to model a wider variety of networks. In this work we focus on the applications of SRGGs to wireless communication networks where the nodes represent either a smart device (which is possibly mobile), a base station (BS) in the classical architecture,

or an AP in HetNets with the links representing channel conditions.

Before we discuss some results on RGGs we first need to introduce stochastic geometry and the definition of a Poisson Point Processes (PPP), along with some key results including Campbell's theorem for sums and the Probability generating functional for the PPP. These results and definitions are fundamental to the study of wireless networks and can be found in the following books and/or reviews [Hae12, Bac09, Bac10b, Las17, Det18b, Bła18]. Throughout this chapter we will aim to motivate each definition by an associated application that we use in the subsequent chapters, with that in mind we will largely focus on the space $\mathbb{R}^2$ for brevity, although it is easily generalisable to higher dimensions. Other PPs, such as the determinantal PP, can be used to model different situations in wireless networks but are not discussed here; the reader is referred to the following references for a general discussion on point processes [Dal07, Der17], and Ref [Hae12, Bła18, Det18b] which focus on their application to wireless networks.

2.1 Stochastic Geometry

Stochastic geometry is the study of random sets in space, most notably point processes, that is, random sets of individual points. Initially, stochastic geometry was first used to further understanding in fields such as material science, astronomy and biology [Sos00, Tor08, Bac10b]. Generally speaking, in stochastic geometry, point processes need not model just collections of points in some space, they can be used for more general sets such as balls, lines, planes and fibres which are then mapped back into point processes using a suitable representation [Ken10, Sch14]. Examples of other applications include: material science to model fibres and the hard core particle structure of concrete [Bal06]; astronomy of which Olbers' paradox is a nice example; biology and ecology to model forestry distributions, the statistics of legionnaires outbreaks [MB06] and wrinkles [Bat12]; vehicular networks [Che18b] and more recently in machine learning [Kul12]. Our interest lies in the ap-

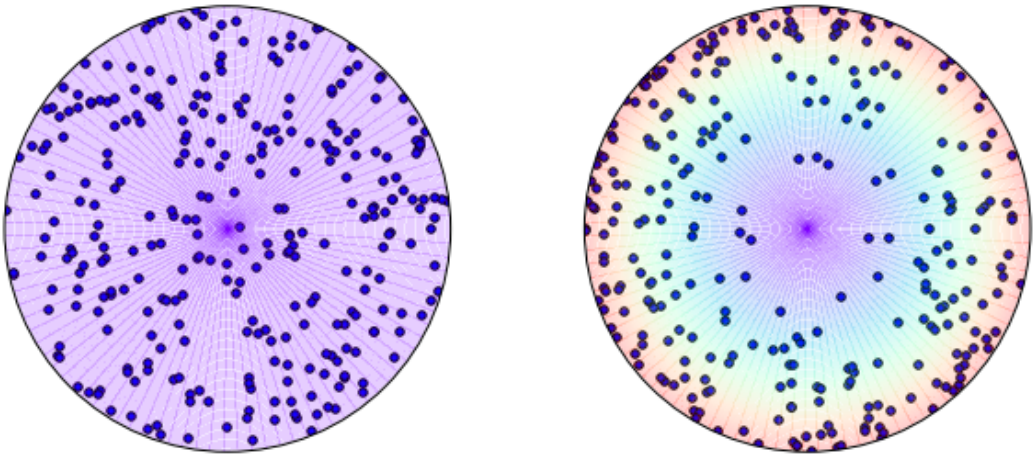

Figure 2.1: A realisation of two PPP with different density functions $\lambda(r)$ in a disk with radius R. The blue dots represent point in Φ and the background shading representing the density function $\lambda(r)$. Left: A single realisation of a PPP with uniform intensity measure. Right: A realisation of a PPP with density $\lambda(r) = \frac{2}{\pi R^4} r^2$.

plication of Stochastic Geometry to modelling wireless networks.

Prior to using random point models, traditional practice was to assume a hexagonal lattice to model each cell with a corresponding BS located at the centre that serves all the associated users within it [Rin47]. Already a highly idealised approach, obtaining closed form expressions within this lattice model for network performance metrics using a standard information theoretic approach was not possible; the restriction largely being the spatial average could not be computed. However, Ref [Bac97] showed that by allowing the locations of BSs to be modelled by a random point pattern, and leveraging standard techniques from stochastic geometry often resulted in closed form expressions for metrics such as coverage and average rate. The original model proposed in Ref [Bac97] used a uniform PPP in $\mathbb{R}^2$ to model the locations of macro base stations (cell towers) which has been shown to be consistent in terms of the spatial statistics of BSs in cities [Lu15]. Intu-

itively, this random model has the benefit of being able to incorporate the irregularity in the distribution of base stations due to several factors, including the availability of space and costs of building large cell towers in certain locations. The Poisson model for BSs is highly generalisable to other cities as the analysis is not based on a fixed data set but rather a *typical* urban environment, allowing for key network features such as scalability to be studied more easily. Furthermore, the Point Process Φ can be more general in order to capture different features of a network, including non-uniformity, clustering or the repulsion of points.

In this thesis we will use a non-uniform Poisson point process, but other point processes have been proposed to model different network scenarios such as the Neyman-Scott process which can model user clustering [Zho13].

2.1.1 Poisson Point Process

We now formally define the PPP and discuss some of its useful properties. Let Φ be a general Point Process (PP) on $\mathbb{R}^d$ with smooth density $\lambda(\boldsymbol{x})$ where the mean number of points in a compact set $A \subset \mathbb{R}^d$ is defined as

$$\Lambda(A) = \int_A \lambda(\boldsymbol{x}) \mathrm{d}x. \tag{2.1}$$

Definition 2.1 (Poisson Point Process (PPP), Ref [Hae12] Definition 2.10)**.** The PPP on $\mathbb{R}^d$ with intensity measure Λ is defined by the following two properties,

1. For every compact set $A \subset \mathbb{R}^d$, the number of points in A (denoted $\Phi(A)$), is a Poisson random variable with mean $\Lambda(A)$.

2. The number of points in mutually disjoint compact subsets $A_1, A_2, ..., A_n$ are independent Poisson random variables.

The first point indicates that the probability that the number of points

in a set $A \subset \mathbb{R}^d$ is k is given as,

$$\mathbb{P}[\Phi(A) = k] = \frac{1}{k!} e^{-\int_A \lambda(\boldsymbol{x}) \mathrm{d}\boldsymbol{x}} \left(\int_A \lambda(\boldsymbol{x}) \mathrm{d}\boldsymbol{x} \right)^k. \tag{2.2}$$

Note that the number of points in the process Φ may still be finite even if the density function has global support (over $\mathbb{R}^d$), for example if the PPP has Gaussian intensity [Hae12, Det18a]. The second property ensures complete spatial randomness of the PPP, which has led to it often being the preferred model due to its tractability [Bac09].

We adopt the random set formalism to describe the point process which ensures that all Point Processes are simple. That is the point process $\Phi = \{x_1, x_2, x_3, ...\} \subset \mathbb{R}^d$ is a collection of points $x_i \in \mathbb{R}^d$ and there is at most one point at any given location [Hae12].

The following two definition of stationary and isotropic point processes are fundamental to understanding why the PPP in $\mathbb{R}^d$ is so tractable.

Definition 2.2 (Stationarity, (Ref [Hae12] Definition 2.27))**.** A point process is *stationary* on $\mathbb{R}^d$ if its distribution is translation invariant.

Definition 2.3 (Isotropic, (Ref [Hae12] Definition 2.28))**.** A PP in $\mathbb{R}^d$ is *isotropic* if its distribution is rotationally invariant about the origin.

Combining the above two definitions gives the definition of *motion-invariance* (Ref [Hae12] Definition 2.29) which gives rise to the concept of a "typical user". That is to say, the performance of a node is the same irrespective of its location. Arguably it is the special case of a uniform PPP in $\mathbb{R}^d$ which yields such elegant closed form expressions which ultimately lead to the surge in interest in using stochastic geometry as a model for wireless networks. The majority of this work will be focused on PPPs that are not motion-invariant (although we do make use of some isotropic PPPs in Chapters 5 and 6) and all notion of a typical user is lost as network performance becomes location dependent.

An extremely useful property of a PPP is that a new (sparser) PPP is easily obtained from another PPP via a random thinning and they need not have the same distribution.

Theorem 1 (Thinning, Ref [Hae12], Theorem 2.36)**.** *Let* $\wp : \mathbb{R}^d \to [0,1]$ *be a thinning function and apply it to a PPP* Φ *by deleting each point* $\boldsymbol{x}$ *with probability* $1 - \wp(\boldsymbol{x})$*, independently of all other points. This thinning procedure generates a new PPP with intensity function* $\wp(\boldsymbol{x})\lambda(\boldsymbol{x})$*.*

The proof follows by computing the conditional distribution of the thinned process. Importantly, this theorem provides an easy way to numerically generate a non-uniform PPPs in more interesting domains. For example, one can obtain a non-uniform PPP Φ_B with distribution $\lambda_B(\boldsymbol{x})$, $\Lambda(B) > 0$, in $B \subset A$ from a uniform PPP Φ_A in A with distribution $\lambda_A(\boldsymbol{x}) = \lambda_A$ and $\Lambda(A) > 0$, provided $\lambda_B(x) \leq \lambda_A(x)$ almost everywhere.

1. Generate the uniform PPP Φ_A such that $\Lambda(A) \gg \Lambda(B)$. For simplicity let A be the rectangle $A = \{(x,y)|0 \leq x \leq L_x, 0 \leq y \leq L_y\}$. This is obtained by generating M uniform random variables for each dimension (in this case two for the rectangle), where M is a Poisson random variable with mean $\Lambda(A)$.

2. Retain only those points where $\frac{\lambda_{\mathcal{B}}(\boldsymbol{x})}{\lambda_{\mathcal{A}}} \geq U(0,1)$ and $\boldsymbol{x} \in \mathcal{B}$

Some example code written in Python is given in Appendix B.

This random thinning can be used to model a random transmission scheme. The simplest example of a random access channel scheme is the ALOHA model [Abr70], where $\wp$ represents the probability that a device is on (off) or, when devices have a single antenna, transmitting (receiving). For example, in a city centre there may be more competition for resources so more devices will need to be turned off so $\wp(\boldsymbol{x})$ will be lower, conversely nearer the suburbs $\wp(\boldsymbol{x})$ may be high due to a lack of competition.

Now we have a way to model the locations of points in the network, we need to understand how links between nodes are formed. Generally speaking

a network has a transmission scheme which controls how devices connect, and these can differ greatly depending on the network. Examples of different transmission schemes include: a bipolar network where there is an assigned receiver transmitter pair, short range communication for low power devices or a cooperative network where nodes receive information concurrently from its K nearest neighbours. As such the nearest neighbour distribution is often required in the analysis which itself requires the definition of the void probability.

Definition 2.4 (Void Probability)**.** The void probability is defined as the probability that there are no nodes from Φ in the ball $B_{\boldsymbol{x}}(r)$ centred at $\boldsymbol{x}$ with radius r and can be written as

$$\mathbb{P}[|\Phi(B_{\boldsymbol{x}}(r))| = 0] = e^{-\int_{B_{\boldsymbol{x}}(r)\cap A} \lambda(\boldsymbol{y}) \mathrm{d}\boldsymbol{y}}. \tag{2.3}$$

Here $B_{\boldsymbol{x}}(r) \cap A$ is the region of the ball centred at $\boldsymbol{x}$ with radius r that intersects the domain A where the PPP is defined. The relatively nice expression for the void probability means that the nearest neighbour distribution is often easily computed [Sri10], as discussed below and in Sec 5.

For the nearest neighbour communication model, one which is often employed in wireless mesh networks, the distribution is straightforward to calculate from the void probability.

Definition 2.5 (Nearest Neighbour Distribution)**.** For a PPP Φ in A the cumulative density function (CDF) of the nearest neighbour distances for a particular node located at $\boldsymbol{x}$ is given by the complement of the probability that there is no node in $B_{\boldsymbol{x}}(r)$,

$$F_{\boldsymbol{x}}(r) = 1 - \mathbb{P}[|\Phi(B_{\boldsymbol{x}}(r))| = 0] = 1 - e^{-\int_{B_{\boldsymbol{x}}(r)} \lambda(\boldsymbol{y}) \mathrm{d}\boldsymbol{y}}. \tag{2.4}$$

Therefore the pdf of the Nearest neighbour distribution (NND) is just the derivative of eq.(2.4), or minus the derivative of the void probability. The

K^{th} nearest neighbour distribution for a Binomial Point process (BPP) and PPP has also been analysed [Sri10] and is formulated in the same manner. First consider the probability there are $K-1$ points in $B_{\boldsymbol{x}}(r_K)$,

$$\mathbb{P}[|\Phi(B_{\boldsymbol{x}}(d_K))| = K-1] = \sum_{i=0}^{K-1} \frac{(\Lambda(B_{\boldsymbol{x}}(d_K) \cap A))^i}{i!} \exp\Big(-\Lambda(B_{\boldsymbol{x}}(d_K) \cap A)\Big), \tag{2.5}$$

then the probability density function of the K^{th} nearest neighbour is minus the derivative of eq.(2.5), which as usual simplifies for the uniform case with no boundaries. In Chapter 5 we will use the K^{th} NND to analyse cooperative transmission schemes such as the Coordinated Multipoint (CoMP) scheme for LTE [Nig14], where multiple nodes transmit to a single device, maybe by exploiting a large antenna array on the receiver.

2.1.2 Binomial Point Process

In the later chapters we also need the Binomial Point Process (BPP), which is equivalent to a PPP conditioned on there being N points. This conditioning on the number of points in the PPP means that there is no longer complete spatial independence. For example let there be N points in a BPP defined in $A = A_1 \cup A_2$, where A_1, A_2 are disjoint sets. If there are m points in A_1 then there *must* be $N-m$ points in A_2. The close relationship between the BPP and PPP is well known and often a BPP is approximated by a PPP for simplicity in the regime when the number of points is large; the validity of this assumption is discussed more rigorously in [Pen16].

2.1.3 Results from Stochastic Geometry

The complete spatial randomness of the PPP means that it is possible to analyse a particular point in the network through Palm theory [Hae09, Bac10a, And11]. A Palm process is the result of conditioning on there being a point $\boldsymbol{x}$

in Φ, provided $\boldsymbol{x}$ is in the support of $\lambda(x)$, and is the probability of an event happening given $\boldsymbol{x} \in \Phi$ [Hae12]. Notice that the probability of there being a point at $\boldsymbol{x}$ in the PPP is a null event, since the PP is diffuse, but Palm theory can still make sense of this. With the point $\boldsymbol{x}$ added to Φ, it is often desirable to compute a metric for $\boldsymbol{x}$ based on the remaining set of points (i.e. excluding the point $\boldsymbol{x}$), such as its connection probability; this is called the reduced palm measure. For a PPP, Slivnyak's theorem [Ken10] tells us that the reduced palm measure has the same distribution as the original PPP. Simply put, conditioning on $\boldsymbol{x} \in \Phi$ for a PPP is the same as adding a point at $\boldsymbol{x}$ to Φ. Certainly in most of the literature Slivnyak's theorem has been used extensively, and formalises the idea of a *typical user*.

One of the primary tools needed to analyse wireless networks is to compute the spatial average, this is achieved through the probability generating functional (PGFL).

Theorem 2 (Probability Generating Functional (PGFL) for a PPP (Ref [Hae12] Theorem 4.9))**.** *Let $\mathcal{V}$ be the family of all measurable functions $v : \mathbb{R}^d \to [0, 1]$ such that $1 - v$ has bounded support and Φ be a Poisson process with intensity measure Λ. Then*

$$\mathbb{E}\left[\prod_{\boldsymbol{x}\in\Phi} v(\boldsymbol{x})\right] = \exp\left(-\int_{\mathbb{R}^d} (1 - v(\boldsymbol{x}))\Lambda(d\boldsymbol{x})\right). \tag{2.6}$$

As we alluded to earlier, the ability to compute the spatial average of the network has led to closed form expressions not previously possible. Another important result is Campbell's theorem that shows that the sum of measurable functions of the point process is a random variable [Chi13]. More formally,

Theorem 3 (Campbell's Theorem (Ref [Chi13] Theorem 4.1))**.** *The sum of a measurable function $f : \mathbb{R}^d \to \mathbb{R}$ over the point process Φ is a random*

variable with mean,

$$\mathbb{E}\left[\sum_{x\in\Phi} f(x)\right] = \int_{\mathbb{R}^d} f(x)\lambda(x)\,dx, \tag{2.7}$$

Later on in this thesis we will apply Campbell's theorem to study the differences in how signals are typically modelled, see section 2.2.2.

The final theorem we discuss is the Campbell-Mecke theorem which is a combination of the two previous statements, and is needed to analyse approximate the connectivity in cooperative networks in chapter 5.

Theorem 4 (Campbell-Mecke for PPP, Theorem 8.9 [Hae12])**.** *Let* Φ *be a PPP with mean* Λ *and measurable* $f : \mathbb{R}^d \to \mathbb{R}$ *and* $v : \mathbb{R}^d \to [0, 1]$*,*

$$\mathbb{E}\left[\sum_{x\in\Phi} f(x)\prod_{y\in\Phi} v(y)\right] = \exp\left(-\int_{\mathbb{R}^d}(1-v(\boldsymbol{x}))\Lambda(d\boldsymbol{x})\right)\int_{\mathbb{R}^d} f(\boldsymbol{x})v(\boldsymbol{x})\Lambda(d\boldsymbol{x}). \tag{2.8}$$

This theorem has since been further generalised in Ref [Sch12] allowing the computation of the expected values of sum-products of functions over a PPP. In general, the above expressions can be given in closed form for a PPP with uniform intensity measure in $\mathbb{R}^d$, but this is not often the case in finite networks [Geo15].

We conclude this section by remarking that the uniform assumptions in $\mathbb{R}^2$ provide insight into network performance but do not account for spatial inhomogeneities or boundaries and in particular mobility, which is a particular focus of this thesis.

2.2 Random Geometric Graphs and their generalisations

2.2.1 RGGs

In 1961 Gilbert introduced one of the first spatial models to study how information flows through a network. In the original RGG the location of points were modelled by a uniform PPP in $\mathbb{R}^2$ with constant density λ_0, and points were connected if their Euclidean separation was less than some critical value r_0.

RGGs have since been generalised to SRGGs by allowing for an extra source of randomness in terms of the link probabilities, this allows for a wider array of applications including: neural [Shi92, Rou04], social [Cho11, Won06] and a longer range communication model. In addition SRGGs has also been extended to non-Euclidean spaces. As an example, SRGGs in hyperbolic space have also been studied which share the same characteristic features as real world networks such as high clustering and heavy tailed degree distributions whilst still being receptive to a more mathematical analysis [Kri10, Kle07, Gug12]. A network is said to have a high clustering if a node's immediate neighbours are themselves neighbours (lots of local triangles in the graph, an individual's friends are also likely to be friends) whilst the heavy tailed degree distributions are a result of there existing a fraction of the nodes that have a very high degree, for example influencers or celebrities on social networks) [Wat98, Boc14a].

More formally, a SRGG is a random collection of points embedded in some space X where points are joined by a probabilistic connection function $\mathcal{H} : \mathbb{R} \to [0, 1]$ based on a notion of distance, with the usual case being longer links are increasingly less likely. Interestingly, in wireless communication networks each of the metric space axioms are violated [Det18b]. Consider the distance function $\mathcal{D} : X \times X \to \mathbb{R}$, then:

1. The distance $\mathcal{D}(x, y)$ between two points x and y, with $x \neq y$ can

be zero when two smart devices are located at the same point but with different antenna orientations, assuming a non-simple PP has been used.

2. The triangle inequality is violated if signals are not allowed to propagate through obstacles and instead are reflected around them.

3. $\mathcal{D}(x, y) \neq \mathcal{D}(y, x)$ due to differing transmission powers of devices at x, y respectively. This is apparent in interference-limited networks, where the graph can become highly directional.

Due to the many variations of wireless networks there is no universal model that accurately describes the network, rather there are a range of connection functions that are used in different network scenarios. For example, when nearby nodes transmit on the same channel they generate interference which may result in outage; to mitigate this the network can employ different protocols to ensure both a fairer distribution of resources and connectivity. We now introduce two different classes of connection functions that model a diverse range of network scenarios: those with compact support and those with infinite or global support. The choice of connection function is naturally dependent on what is being modelled. For example, RGGs are more likely to model smart devices that are battery powered since they typically have smaller transmission ranges, whilst "softer" connection functions are better suited to capture the longer range transmission power of BSs. We will often include a parameter r_0 (or some variant thereof) as the "typical connection range" which acts to scale the connection function.

2.2.2 Connection Functions

In this work we focus on the following connection functions found in the wireless literature and begin with discussing the soft disk model.

The classical RGG discussed previously is sometimes referred to as the (hard) disk model, or unit disk model if $r_0 = 1$. By construction this is

a deterministic connection model, but can be generalised to one which is probabilistic by including the parameter $\wp \in (0, 1]$, that is $\mathcal{H}(r) = \wp \mathbb{1}_{r \leq r_0}$, where $\wp = 1$ is the usual RGG and $\wp = 0$ is normally excluded else the edge set is empty. This generalisation allows the modelling of random link failures in the network or a simple ALOHA transmission protocol as described earlier. The soft disk (SD) model is an interpolation between the classical hard disk model and the Erdos-Renyi graph with fixed probability $\wp$ [Det16, Pen16], where the latter is independent of the spatial configuration of points. We include the probability $\wp$ for all the connection functions with compact support, largely due to our interest in spatio-temporal networks which are discussed in Chapter 7.

The soft annulus model (SA) is defined as $\mathcal{H}(r) = \wp \mathbb{1}_{r_- \leq r \leq r_+}$, where $\wp$ is as above. Intuitively, the SA model can be thought of as employing an interference management scheme where it introduces a "guard zone" where pairs of node closer than r_- do not connect. Similar to the SD model the parameter $\wp$ acts to model temporal variations in the channel.

The Quasi Disk (QD) model has connection function

$$\mathcal{H}(r) = \begin{cases} \wp & r \leq r_-, \\ \wp \left(\frac{r_+ - r}{r_+ - r_-} \right) & r_- < r \leq r_+, \\ 0 & \text{otherwise.} \end{cases}$$

Initially the QD model behaves like the soft disk model and then the probability decays linearly to zero on the interval $(r_-, r_+]$. Intuitively, this can be thought of as the medium being clutter/obstacle/interference free on the interval $[0, r_-]$ and then transitioning into an environment which has increasingly more clutter/obstacles/interference which degrade the channel. There are further examples of connection functions with compact support that are used in the literature but these capture the main characteristics of short range networks.

Next we discuss those connection functions with infinite support and start

with the most interesting case which models interference for neighbouring nodes.

The interference connection function has two particular cases, the *uplink* and *downlink* cases. The *downlink* (respectively *uplink*) case refers to when a device tries to receive (send) a message from (to) a particular transmitter (receiver). For the large part we will mainly focus on the *downlink* case except in chapter 6 where we discuss a modified connection model for Low Power Wide Area (LoRa) networks. As such, we will proceed by discussing the connection probability in the *downlink* case and only discuss the uplink case when needed.

Let Φ denote a PPP with density $\lambda(\boldsymbol{x})$ in $A \subset \mathbb{R}^d$. Let $\boldsymbol{X}_{\mathcal{R}}$ be the receiver[1] trying to decode a message from the intended transmitter $\boldsymbol{X}_{\mathcal{T}} \in \Phi$. The probability a link is formed between transmitter and receiver pair $\boldsymbol{X}_{\mathcal{R}}, \boldsymbol{X}_{\mathcal{T}}$ is equal to the probability that the *signal to interference plus noise ratio* (SINR) measured at the receiver is greater than some threshold value q, where q is a parameter of the device. If q is low then the device has little sensitivity and can connect more frequently under more interference, whilst the converse is true for larger q. To understand the SINR we first need to be able to model the transmission of signals.

The quality of signal that is measured at the receiver is determined by various different factors, which are usually decomposed into two categories: *small scale effects* (of the order of a wavelength) and *large scale fading* (of the order of many wavelengths). *Large scale* effects are those that capture the average signal strength over a distance r due to scattering, reflections, refractions, absorption, path loss etc and small scale effects are those that account for the fluctuations around this average, for example due to multi-path interference where waves arrive at the same point via multiple paths causing both constructive and destructive interference [Tse05].

Statistical channel models are adopted to allow for a tractable analysis of network performance, with the simplest case being the *Rayleigh fading*

[1] not necessarily a point in Φ

model. The Rayleigh fading model assumes there is no dominant path between receiver and transmitter and instead the number of possible reflected and scattered paths is large, and statistically independent [Tse05]. The received signal h can be decomposed into an in-phase and quadrature component, which are assumed to be independent Gaussian random variables and therefore can be written as, [KG16, Tse05]

$$h = \varrho + i\varphi \tag{2.9}$$

The pdf of h is the joint pdf of the real and imaginary parts, and since they are independent normals the joint pdf (and CDF) is the product of two normally distributed random variables with zero mean and ζ variance. The pdf of the absolute value of h can be found by first calculating the CDF in polar coordinates,

$$\begin{aligned} \mathbb{P}[-x \leq h \leq x] = 2\mathbb{P}[h \leq x] - 1 &= \frac{2\pi}{2\pi\zeta} \int_0^x e^{-\frac{r^2}{2\zeta}} r \mathrm{d}r - 1 \\ &= 2(1 - e^{-\frac{x^2}{2\zeta}}) - 1 = 1 - 2e^{-\frac{x^2}{2\zeta}}. \end{aligned} \tag{2.10}$$

Thus, differentiating the CDF to obtain the pdf of $|h|$ gives,

$$f_X(x) = \frac{x}{\zeta} \exp\left(-\frac{x^2}{2\zeta}\right), \tag{2.11}$$

which is Rayleigh distribution, hence the name *Rayleigh fading*. We are interested in the distribution of the amplitude of the received signal, $|h|^2$, so we make the transformation $X = \Psi(Y) = Y^2$ and use the following formulae

$$f_Y(y) = f_X(\Psi^{-1}(y)) \frac{\mathrm{d}}{\mathrm{d}y} \Psi^{-1}(y). \tag{2.12}$$

Direct application of eq.(2.12) gives

$$f_Y(y) = f_X(\sqrt{x}) \cdot \frac{1}{2\sqrt{x}} = \frac{\sqrt{x}}{2\sqrt{x}\zeta} \exp\left(-\frac{x}{2\zeta}\right) = \frac{1}{2\zeta} \exp\left(-\frac{x}{2\zeta}\right). \quad (2.13)$$

The channel gain is therefore an exponential random variable, where the parameter $\frac{1}{2\zeta}$ is set to one for simplicity (the parameter is effectively absorbed in the subsequent calculations for connectivity in threshold parameter q).

The Rayleigh model assumes that there is no line of sight between the receiver and transmitter, with there being no constant component of the signal, however in models where a LoS connection is guaranteed then the fading is more often modelled by a Rician distribution [Hae12, Tse05]. All of the subsequent work that is done in this thesis can be generalised to the Rician models, but we much prefer the Rayleigh model due to its tractability.

Next we need to understand how the signal behaves over larger distances, and this is captured through the path loss function $g(.)$. The most common path loss function used to model how the signal decays with distance is,

$$g(r) = r^{-\eta}, \quad (2.14)$$

where r is the separation between a transmitter and receiver pair, and η is the path loss exponent. Typically $\eta \in [2, 6]$, where $\eta = 2$ models free space, the usual inverse square law found in physics, and larger η represents a more cluttered environment. Empirical values show for a typical urban environment $\eta = 4$ and $\eta = 6$ models cities that are very *cluttered* such as New York city [Mac13]. Intuitively, a larger η corresponds to a decreasing likelihood of making long range connections. This singular model provides a more tractable analysis but can lead to some interesting behaviour due to it not being well defined when r goes to zero. For example, if a signal is modelled as the product of the channel gain (assumed to be exponential with mean one) and a path-loss function with power law decay, the mean interference in the network is infinite for any η [Geo15, Hae12]. For a set Φ

of interferers modelled by a uniform PPP in $\mathbb{R}^2$,

$$\mathbb{E}[\sum_{\boldsymbol{x}\in\Phi}|h|^2|\boldsymbol{x}|^{-\eta}] = 2\pi\lambda_0\int_0^\infty r^{1-\eta}\mathrm{d}r = \begin{cases}\frac{2\pi\lambda_0}{2-\eta}r^{2-\eta}\big|_0^\infty \\ 2\pi\lambda_0\log r\big|_0^\infty\end{cases} = \infty. \tag{2.15}$$

In fact the mean interference diverging can be shown to be true in any dimension [Hae12]. The important behaviour here is not that the mean of the interference diverges, but that the sum of the interfering signals is absolutely convergent a.s only if $\eta >$ dimension [Hae12]. We will see in subsequent chapters that when $\eta =$ dimension the impact of interference goes from being a local one ($\eta >$ dimension) to a global one ($\eta \leq$ dimension) ultimately leading to outage [Geo15]. In the literature this phenomenon is often likened to Olbers paradox, where the sky should be uniformly bright if the stars constitute a uniform PPP in $\mathbb{R}^3$, yet we still see a dark night sky [Bad07, Geo15]

To overcome this behaviour, often a small parameter ϵ is included into the path loss function to overcome this

$$g(r) = \frac{1}{\epsilon + r^\eta} \tag{2.16}$$

In a rather unimaginative fashion we refer to these two models as the singular and non-singular path loss models. Variants of the latter path loss model are included in [Hae12].

Now we have all the ingredients for calculating the connection probability with interference. To achieve this, first lets define the connection function as the probability that the SINR is greater than the threshold parameter q. Then condition on the set of interferers, and then compute the spatial average using the PGFL. We outline the derivation below.

Let $d_{\mathcal{R}}$ be the distance between the receiver $\boldsymbol{X}_{\mathcal{R}}$ and the intended transmitter $\boldsymbol{X}_\tau$, and $d_{\mathcal{I}}$ be the distance between receiver and all other interfering

signals located at $\boldsymbol{X}_{\mathcal{I}} \in \Phi \backslash \boldsymbol{X}_{\tau}$.

$$
\begin{aligned}
\mathcal{H}(r) &= \mathbb{P}\left[SINR \geq q\right] = \mathbb{P}\left[\frac{|h_{\tau}|^2 g(d_{\mathcal{R}})}{\sigma^2 + \gamma \sum_{\boldsymbol{X}_{\mathcal{I}} \in \Phi \backslash \boldsymbol{X}_{\mathcal{T}}} |h_I|^2 g(d_{\mathcal{I}})} \geq q\right] \\
&=^{(0)} \mathbb{E}_{|h_{\mathcal{I}}|^2, d_I}\left[\mathbb{P}\left[\frac{|h_{\tau}|^2 g(d_{\mathcal{R}})}{\sigma^2 + \gamma \sum_{\boldsymbol{X}_{\mathcal{I}} \in \Phi \backslash \boldsymbol{X}_{\mathcal{T}}} |h_I|^2 g(d_{\mathcal{I}})} \geq q \middle| |h_{\mathcal{I}}|^2, d_{\mathcal{I}}\right]\right] \\
&=^{(1)} \mathbb{E}_{|h_{\mathcal{I}}|^2, d_I}\left[\exp\left(-\frac{q\sigma^2 + q\gamma \sum_{\boldsymbol{X}_I \in \Phi \backslash \boldsymbol{X}_{\mathcal{T}}} |h_{\mathcal{I}}|^2 g(d_{\mathcal{I}})}{g(d_{\mathcal{R}})}\right) \middle| |h_{\mathcal{I}}|^2, d_{\mathcal{I}}\right] \\
&=^{(2)} \exp\left(-\frac{q\sigma^2}{g(d_{\mathcal{R}})}\right) \mathbb{E}_{|h_{\mathcal{I}}|^2, d_I}\left[\prod_{\boldsymbol{X}_I \in \Phi \backslash \boldsymbol{X}_{\mathcal{T}}} \exp\left(-\frac{q\gamma |h_I|^2 g(d_{\mathcal{I}})}{g(d_{\mathcal{R}})}\right) \middle| |h_{\mathcal{I}}|^2, d_{\mathcal{I}}\right] \\
&= \exp\left(-\frac{q\sigma^2}{g(d_{\mathcal{R}})}\right) \mathbb{E}_{d_{\mathcal{I}}}\left[\prod_{\boldsymbol{X}_{\mathcal{I}} \in \Phi \backslash \boldsymbol{X}_{\mathcal{T}}} \frac{1}{1 + \frac{q\gamma g(d_{\mathcal{I}})}{g(d_{\mathcal{R}})}} \middle| d_{\mathcal{I}}\right]
\end{aligned}
$$

$$
\begin{aligned}
\mathcal{H}(r) &=^{(3)} \exp\left(-\frac{q\sigma^2}{g(d_{\mathcal{R}})}\right) \exp\left(-\int_A \left(1 - \frac{1}{1 + \frac{q\gamma g(d_{\mathcal{I}})}{g(d_{\mathcal{R}})}}\right) \lambda(\boldsymbol{X}_{\mathcal{I}}) \mathrm{d}\boldsymbol{X}_{\mathcal{I}}\right) \\
&= \exp\left(-\frac{q\sigma^2}{g(d_{\mathcal{R}})}\right) \exp\left(-\int_A \frac{1}{1 + \frac{g(d_{\mathcal{R}})}{q\gamma g(d_{\mathcal{I}})}} \lambda(\boldsymbol{X}_{\mathcal{I}}) \mathrm{d}\boldsymbol{X}_{\mathcal{I}}\right) \qquad (2.17)
\end{aligned}
$$

In (1) and (2) we have used that $|h|^2$ is an exponential r.v with mean one, and that the channel gains are i.i.d, (3) uses the PGFL for Poisson Point Processes given in eq.(2.6), and the last term in the final line is the Laplace transform of the random variable $\sum_{\boldsymbol{X}_{\mathcal{I}} \in \Phi \backslash \boldsymbol{X}_{\mathcal{T}}} |h_I|^2 g(d_{\mathcal{I}})$ evaluated at $\frac{q\gamma}{g(d_{\mathcal{R}})}$ $\left(\mathcal{L}_{\mathcal{I}}\left(\frac{q\gamma}{g(d_{\mathcal{R}})}\right)\right)$. The parameter $\gamma \in [0, 1]$ acts as a random independent thinning of the interfering signals (see Sec.1 on ALOHA) with the extremal cases being $\gamma = 1$ where all nodes share the same channel and are transmitting, and $\gamma = 0$ corresponds to no interference.

The Laplace transform cannot be given in closed form for an arbitrary density $\lambda(\boldsymbol{x})$ in a domain A, but special cases can be given including for a uniform density in the plane [Bac97], centre of a circular disk, see Sec 4

(including an illustrative example in Fig 4.3) and Sec 5 for further details. We do however remark that whilst a closed form expression can be obtained for a uniform PPP in $\mathbb{R}^d$, it is independent of location and transmission power making it rather unrealistic. In this scenario the connection probability depends only on the point to point distance between two devices, but it should also depend on the underlying distribution of all other devices. For example, if the distribution of devices is non-uniform then the interference field varies as a function of position, thus so should the outage probability.

The interference model is the only connection model we consider that depends on the underlying point process. The other connection models can be thought of as having networking protocols which mitigate the impact of interference, hence the restriction that $r_0 \ll L$ due to a finite amount of network resources.

The Signal-to-Noise-Ratio (SNR) model is obtained from the SINR model by setting $\gamma = 0$ ensuring there is no interfering signal, i.e.

$$\mathcal{H}(r) = \exp\left(-\frac{q\sigma^2}{g(d_R)}\right), \tag{2.18}$$

We will use the terms SNR and Rayleigh model interchangeably, with the latter being a reference to the assumed channel conditions. For simplicity we will often write $q\sigma^2 = \frac{1}{r_0}$ making clear that r_0 acts to scale the connection function. Prior to this now more standard model, Waxman [Wax88] introduced the connection function $\mathcal{H}(r) = \beta e^{-\frac{r}{r_0}}$, which can be obtained from the Rayleigh case by introducing a constant before the exponential and allowing $\eta = 1$. In addition when $\eta \to \infty$ we retrieve the disk model used in RGGs, therefore we can see that for higher η longer links become increasingly unlikely.

Finally, the last connection function we study is the Multiple Input and Multiple Output (MIMO) connection function. In this network scenario nodes have multiple antennas such that they can conceivably transmit and receive a signal to/from neighbouring nodes simultaneously provided the cross

channel interference is not too great. In fact, the increased diversity at the node (increased number of antennas) has been shown to improve network capacity [Kan03a]. The connection probability in MIMO systems is simply the CDF of the output SNR which was initially given in closed form (in the form of a determinant) by Ref [Dig03] through calculation of the largest eigenvalue in the case of i.i.d Rayleigh channels. This has since been extended to independent channels with non-identical Rician channels [Kan03b, Kan02], and then again to incorporate cross channel interference [Kan03a].

Later on in Chapter 7 we apply the MIMO model with Rayleigh channels to a mesh network where the nodes represent mobile devices, thus due to power/size/financial constraints it is unlikely devices will have more than two antennas. This allows us to write $\mathcal{H}$ in a much simpler expression to that given in [Dig03],

$$\mathcal{H}(r) = e^{-\left(\frac{r}{r_0}\right)^{\eta}} \left(2 + \left(\frac{r}{r_0}\right)^{2\eta} - e^{-\left(\frac{r}{r_0}\right)^{\eta}}\right). \tag{2.19}$$

Naturally there are many other connection functions used in the literature [Det16], including MISO (multiple input and single output), SIMO (single input multiple output), with a comprehensive tableau found in Ref [Det16]. Now we can discuss some of the main results found in the literature on RGGs and SRGGs.

2.3 Percolation

From their introduction one of the main questions regarding RGGs was one of network criticality [Gil61]. Namely, what are the conditions needed for the network to transition from being comprised of connected components of finite size almost surely, to one where there is almost surely an infinite (giant) component [Det18b]: a phenomenon known as percolation [Gri99]. At the time the question of percolation was based on the lattice

Model	Connection Function, $\mathcal{H}(r)$
SD	$\wp \mathbb{1}_{r \leq r_0}$
SA	$\wp \mathbb{1}_{r_- \leq r \leq r_+}$
QD	$\begin{cases} \wp & 0 \leq r \leq r_- \\ \wp \left(\frac{r_+ - r}{r_+ - r_-} \right)^{\mu} & r_- \leq r \leq r_+ \\ 0 & \text{otherwise} \end{cases}$
Rayleigh	$e^{-\frac{1}{r_0^{\eta} g(r)}}$
Waxman	$\beta e^{-\frac{r}{r_0}}$
Interference	$e^{-\frac{1}{r_0^{\eta} g(r)}} \exp\left(- \int_A \frac{1}{1 + \frac{g(r)}{q \gamma g(\lvert \boldsymbol{x} - \boldsymbol{y} \rvert)}} \lambda(\boldsymbol{x}) \mathrm{d}\boldsymbol{x} \right)$
MIMO	$e^{-\left(\frac{r}{r_0}\right)^{\eta}} \left(2 + \left(\frac{r}{r_0} \right)^{2\eta} - e^{-\left(\frac{r}{r_0}\right)^{\eta}} \right)$

Table 2.1: Table of connection functions for a PPP defined in A which are discussed in section 2.2. The location of the receiver is at $\boldsymbol{y}$, with the distance between the receiver and transmitter pair being r. Parameters: r_0 is the typical connection range, $\wp \in (0, 1]$ is the probability a node is active; $\eta \in [2, 6]$ is the path loss exponent; $\mu > 0$ defines how fast the function decays with distance; q is the threshold signal quality and σ^2 is the channel noise.

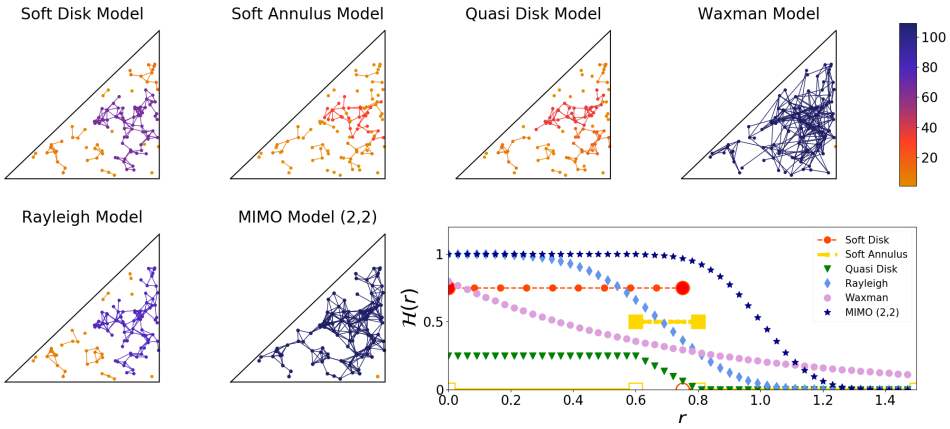

Figure 2.2: A realisation of Φ in a triangular region for the different connection functions in Table 2.1, and a representation of how the link probability behaves as a function of distance. The colours represent the size of the connected components of the corresponding graphs. Parameters are $L = 10; r_0 = 0.5; \eta = 4; \beta = 1; \wp = 0.5; \mu = 1; r_- = 0.5; r_+ = 0.8$.

model [Bro57], and Gilbert extended the question of percolation to this random point model which led to the field of "continuum percolation". Since then percolation has been used to explain the composite material phenomena such as electrical conductivity, magnetism and the localisation of electrons [Bor88, OG06, Kiw01]. In fact, a nice example of percolation is given in Ref [Gri99]. Initially a glass of Pernod is transparent, and adding a single drop of water does nothing to change this. Even when additional drops of water are added the Pernod still retains its transparency, until at some point a drop is added then the Pernod suddenly becomes opaque. This is exactly the percolation point/transition where the global behaviour of the system changes; the straw that broke the camel's back if you will.

Returning to Gilbert's question of percolation on the RGG, he aimed to find the critical value where the network has a positive probability of percolating through increasing the mean degree of the network ($\lambda_0 \pi r_0^2$). Recent convention is to express network criticality in terms of either the density (denoted λ_0) or transmission range (denoted r_0), rather than both, where we

adopt the former by fixing r_0.

To obtain an upper bound on the critical density, which we denote as λ_c, Gilbert drew from established results from bond percolation. By tiling the plane with squares of size $\frac{r_0}{\sqrt{8}}$ so any points in adjacent squares are connected, then the corresponding edge can be labelled as open if the square contains at least one point. By construction this means the probability an edge is open is independent due to the spatial independence of the PPP. All that remains is to use the results from bond percolation on the square lattice to provide an upper bound for continuum percolation, albeit a rather loose one. A suggested improvement for this bound was provided in the same paper[2] by tiling the plane using hexagonal tiles and using results from site percolation on the triangular lattice (or face percolation on the hexagonal lattice) [Wal11].

A lower bound was also obtained by relating the problem to a branching process. Starting with an arbitrary point in the process (this exploits the stationarity property of the PPP in $\mathbb{R}^d$) explore its nearest neighbours, i.e. find all nodes within distance r_0, and call these the daughters of the starting node. After which, find all subsequent "grand-daughters" (or daughters of the daughters) of the starting node, and repeat this approach until it dies out. By introducing a growth model where each node has a Poisson number of offspring with mean $\lambda_0 \pi r_0^2$, we have an associated branching process which can now be solved [Hae12]. The double counting of points results in a lower bound for λ_c. For example, the connection disks in the RGG overlap meaning a sixth generation node may have two fifth generation nodes as its neighbours and "recount them", thus the total number of points in the n^{th} generation of the branching process stochastically dominate that of the disk graph.

Percolation on SRGGs has largely been unexplored. Initial investigations have drawn inspiration from continuum percolation with interference to derive for example the network capacity [Fra07]. One interesting result is for

[2]originally Gilbert assumed that the critical probability for percolation was 1/2 which was later proved to be correct [Kes82]

a SRGG in $\mathbb{R}^2$ generated by a uniform PPP and links are made according to the SIR link function. This model has the additional complexity of the link probabilities between any two points also depending on the underlying spatial distribution of the PPP. These models are constructed such that they are not directional by constructing links if and only if the SIR condition can be met at both end points. First note that we should expect percolation in the RGG with soft connectivity (as for the case with hard connectivity) to be monotonic in λ_0, such that the probability of percolation is zero when $\lambda_0 < \lambda_c$, and the $\lambda_0 > \lambda_c$ the graph percolates almost surely. An SIR graph can be shown to percolate for a small enough $\gamma > 0$ (recall that γ is the random thinning of interferers) provided $\lambda_0 \geq \lambda_c$ and the path loss function is integrable on $\mathbb{R}^2 \backslash B_0(\epsilon)$ [Dou06]. Namely, by randomly thinning the number of nodes transmitting concurrently on the same channel the graph can percolate, provided the density is larger than the critical density needed for percolation when there is no interference. In a similar vein, [Vaz12] showed that for small enough q (recall q is the minimum threshold value for the signal measured at the receiver in order for there to be a successful link, assuming a non-singular path loss with no thinning), percolation only occurs for a certain interval of densities; when the number of nodes in the network is small percolation is obstructed due to large gaps, whilst when the density is too large interference effects begin to dominate. So once again, it is possible for the network to transition from sub-critical to super-critical back to sub-critical again as the node density increases for a fixed set of network parameters.

2.4 Full connectivity

Percolation in networks describes the transition from one where the network is disconnected a.s, to one where only a fractional set of nodes are isolated. Often in a wireless network having *any* nodes that are disconnected is usually not good enough. A better, and more desirable question is, *what is the*

probability there is a multihop path between every node in the network?

One of the most celebrated results for RGGs was by Penrose [Pen97] who showed that for a RGG with uniform measure on the unit cube, the network becomes fully connected with high probability when the last isolated node forms a link[3]. The result is based on showing that the longest edge in the minimum spanning tree and the longest edge in the nearest neighbour graph (the minimum r_0 needed to connect the network) converge in probability as $\bar{N} \to \infty$, which is done through application of the Chen Stein method [Pen03, Mao13, Hsi05]. The proof uses the fact that edges of a node only depend on its neighbourhood, as very long edges are extremely rare, then using the Chen stein method to show the asymptotic distribution of the longest edge of the MST. A more detailed proof can be found in Ref [Wal11]. It turns out that the isolated nodes in this case are located far from the boundaries due to the adopted scaling of $r_0 \to 0$ as $\bar{N} \to \infty$ such that P_{fc} remains fixed [Pen03][4].

Similar work has been done on the RGG with a large class of densities in 2 dimensions by Hsing and Rootzen [Hsi05], in higher dimensions when nodes are normally distributed [Pen98] and when the connection range is location dependent [Iye12]. So far all the above work assumes that the transmissions range is identical throughout the network but perhaps a more accurate model is one where r_0 is location dependent, devices in sensor networks may have different transmit powers if they are in a highly populated region to those in regions where the network is sparse. This problem was addressed in Ref [Iye12] who provided a location dependent critical r_0 for densities with polynomial rates of decay. For a more comprehensive review of the many results on RGGs the reader is referred to Ref [Wal11].

This work has since been generalised to SRGGs where isolated nodes are also the last to connect. Mao and Anderson [Mao13, Mao17] looked at

[3]This phenomenon also appears in classical random graphs [Bal08]

[4]For networks in $\mathbb{R}^d$ where the location dependent connectivity mass is finite, the probability a node at $\boldsymbol{x}$ is isolated is non-zero resulting in the network being disconnected. As a result, much of the analysis is done on networks in a finite domain.

a uniform PPP on the unit cube with a connection function $\mathcal{H}(r/r_0)$ that satisfies the more restrictive condition of $\mathcal{H}(x) = o(1/(x^2 \log^2 x))$ as opposed to the usual $\mathcal{H}(x) = o(1/x^2)$ [Mao12],and once again make use the Chen Stein method to show the number of isolated nodes converges to a Poisson distribution. Moreover, they show that the network is a.a.s fully connected if and only if there is no isolated nodes in the network [Mao13, Mao17].

These results are of great importance in the wireless literature community as they provide not only insight into the bottleneck of P_{fc} but also a simple approximation, $P_{fc} \approx \mathbb{P}$[No Isolated Nodes]. It is straight forward to use the PGFL (eq.(2.6)) to explicitly write the probability a node at $\boldsymbol{x}$ is isolated from every other node in the network.

$$\begin{aligned} P_{iso}(\boldsymbol{x}|\Phi) &= \prod_{\boldsymbol{y}\in\Phi\setminus\{\boldsymbol{x}\}} 1 - \mathcal{H}(|\boldsymbol{x}-\boldsymbol{y}|) \\ P_{iso}(\boldsymbol{x}) &= \exp\Big(-\int_A \mathcal{H}(|\boldsymbol{x}-\boldsymbol{y}|)\Lambda(\mathrm{d}\boldsymbol{y})\Big). \end{aligned} \tag{2.20}$$

The integral is the mean degree of the node at $\boldsymbol{x}$, and for the uniform case the isolation probability is sometimes written as $P_{iso}(\boldsymbol{x}) = e^{-\lambda M(\boldsymbol{x})}$ where $M(\boldsymbol{x})$ is the location dependent connectivity mass [Coo12a]. Realising that isolated nodes are the bottleneck to full connectivity we have,

$$\begin{aligned} P_{fc} &\approx \mathbb{P}[\text{No Isolated Nodes}] \approx \exp\Big(-\int_A \exp^{-\int_A \mathcal{H}(|\boldsymbol{x}-\boldsymbol{y}|)\Lambda(\mathrm{d}\boldsymbol{y})}\,\Lambda(\mathrm{d}\boldsymbol{x})\Big) \\ &= e^{-e^{-\lambda M(x)}}. \end{aligned} \tag{2.21}$$

The simple approximation of P_{fc} is used widely throughout the literature provided the connection function is not too "long range". In uniform RGGs isolated nodes can be modelled by a limiting Poisson Point Process. An important difference between RGGs and SRGGs is that isolated nodes are unable to be close to each other else they would connect, but this is not the case for SRGGs.

So far the results we have discussed have either no boundaries or negate their impact via the adopted scaling. It is reasonable to think that as boundaries restrict the number of close neighbours, boundary nodes are likely to be more isolated and thus dominate connectivity. However, since there are fewer nodes near the boundary, the isolated nodes in the bulk dominate. This is not the case in dense but finite networks. For a SRGG with an exponential connection function, a cluster expansion approach was utilised by Coon, Georgiou and Dettmann to show that P_{fc} can be decomposed into contributions from the bulk and the different types of boundary, where the latter tend to dominate [Coo12a]. This result was later extended to a more general class of connection functions showing that boundaries can obstruct P_{fc} in dense networks [Det16]. Conversely, in interference-limited networks, boundary nodes can be more connected due to a reduction in the interference field [Geo15, Coo12b]. Importantly all these results assume a uniform PPP, and neglect any variations in the node density due to mobility, which we will discuss in the following two subsections.

2.5 Spatio-temporal Networks

Having focused so far on the single snapshot connectivity behaviour of SRGGs under various limits, we now turn our attention to spatio-temporal networks. There are many different examples of a spatio-temporal networks, with varying degrees of complexity. In general, a spatio-temporal network is one which changes with time due to fluctuations in channel conditions, mobility and nodes disconnecting and reconnecting to the network. Of particular interest are the impacts of spatial structure and boundaries on network properties such as the expected delay (the time it takes for a node to make a link), or the minimum time for paths to form. Even when ignoring any underlying spatial geometry of the network it is often difficult to provide closed form expressions for things such as path formation. Recently, [Taj17] provided upper and lower bounds for the probability of accessibility (probability there

is a path between i and j at time T) of a network for the general case when links between nodes are random, and possibly time dependent, and is only tractable when the link probabilities are identical across the network. Interestingly, their predictions for the accessibility probability perform well when compared with the inter-contact time of taxis in Rome, where taxis are said to be connected if they are within some critical distance [Taj17]. By modelling the probability a link is made in a given time slot by an exponential random variable they are able to capture the characteristics of a spatio-temporal network. For further discussions on space free temporal networks,the reader is referred to [Hol12] for a review while [Boc14a] provides a thorough overview of dynamics on multi-layer networks.

Incorporating the spatial structure of wireless networks naturally increases the complexity of the analysis. One solution is to model the network dynamics by fixing the underlying structure of the point process Φ and only allowing for the set of edges to vary with time. Indeed, by this model [Det17] obtained closed form expressions for the probability the network is fully connected as a function of time by analysing the distribution of isolated nodes for a uniform PPP on the torus (enabling $\bar{N} < \infty$ which negates the impact of boundaries) where the pairwise link probability depends on their Euclidean separation. In these uniform static networks, it is again those nodes that are highly isolated that hinder the flow of information through the network but can be improved if a random re-wiring of the network is done, akin to that in space free random graphs.

An interesting variation of this model is when an ALOHA channel access scheme is employed, in this scenario a node can either transmit or receive (referred to as half-duplex) a message during each time step. This model adds directionality to the network where the possible edge set varies with time. By considering a connection function where two nodes connect if they form a receiver-transmitter pair, a noise condition is met and there is no intermediate node that is transmitting, [Gan09] showed that the time for a path to form between a source and destination scales linearly with their

Euclidean separation. Moreover, [Bac10a] highlighted that for the SIR model there is a phase transition for a critical transmit probability $\wp$ where the mean delay becomes infinite. Even conditioning on there being two points in Φ, the expected shortest delay between the points grows faster than their Euclidean separation [Bac11]. This work was extended to nearest neighbour communication models by [Hae13], where they also provide bounds on the delay of Poisson networks.

Alternatively, it is often convenient to assume an infinite mobility model in the network where there is a new, independent, realisation of Φ at each time slot, i.e. there is no spatial correlation between time slots, and as a consequence the analysis simplifies significantly. By employing this method, coupled with the static case, one can obtain upper and lower bounds for the performance of these spatial-temporal networks with mobility. For the high mobility case the local delay is always finite for the SIR model [Hae13] due to lack of correlation between time slots, this alludes to how mobile networks have the potential to resolve problems of disconnectivity.

2.6 Mobility

In mobile networks there is no fixed network topology; instead, nodes move around the domain according to a particular set of rules. This resultant mobility causes links to be continually made and broken. Wireless communication networks are a natural application where the nodes could represent hand-held smart devices or vehicles say. Of particular interest are decentralised MANETs since they can help alleviate the strain on the pre-existing network architecture. By relaying packets in a multi-hop fashion, rather than through a centralised router, the network becomes easily scalable without large overheads (no need for costly base stations) [Hel14], and provided the devices are mobile can resolve problems of node isolation due to their self configuring nature. The importance of mobility on network performance was highlighted by both [Gup00] and [Gro01]. For the static case, comprised

of n nodes with fixed transmit power, Ref [Gup00] showed the capacity per node of the network scales like $O\left(\sqrt{\frac{1}{n \log n}}\right)$, suggesting network performance decreases with node density. However, Grossglauser and Tse [Gro01] showed that in an interference-limited environment mobility can in fact improve network capacity, albeit at the cost of increased delay. Furthermore, one can show that mobile networks perform better than their static counterparts by studying the extremal case where nodes have infinite mobility [Hae13];and any realistic mobility model falls somewhere in between these two cases.

As one might expect, network performance remains sensitive to the choice of mobility model used, for instance [Lin04, Sha04, Nee05] showed that the delay-capacity trade-off differs for the random waypoint and Brownian motion models (see below), and thus characterising the level of inhomogeneity is important [Sch17]. For the remainder of this chapter we discuss a number of interesting and practical mobility models.

2.6.1 Random walk

One of the simplest mobility models is the random walk (RW). The RW models the random displacement of small particles such as Pollen, and is often referred to as "Brownian" motion after Robert Brown who studied (amongst other things) the motion of pollen on the surface of water [Mör10, Kla96]. Since then, random walks have been applied to numerous areas of research including: the movement of animals [Hof83]; the modelling of financial markets [Fam95] and even in Psychology to model decision making [Nos97]. In this work, we use a random walk to model the mobility of humans, and their associated smart devices.

In one RW model that has been used to model human mobility nodes move independently from one another, and at each time step T a node has a new velocity chosen uniformly at random. A particular nodes position at

time t is therefore described by the following equation,

$$\boldsymbol{x}(t) = \left(t - T\left\lfloor \frac{t}{T} \right\rfloor\right) \boldsymbol{v}_{\lfloor \frac{t}{T} \rfloor} + \sum_{i=0}^{\lfloor \frac{t}{T} \rfloor - 1} \boldsymbol{v}_i T, \tag{2.22}$$

where $\boldsymbol{v}_i$ is the velocity at time i, and $\lfloor \cdot \rfloor$ is the usual floor function. The sum represents all the random displacements in all the previous time steps, whilst the first term represents the latest displacement.

The RW is diffusive and for dim ≤ 2 it is recurrent, resulting in a uniform spatial node distribution [Ban07], with the usual approach for finite domains being to reflect off the boundary[5]. As a consequence, RW mobility is often analysed in terms of MANETs through a uniform point process [Gon14] (non-uniformity is very short lived and averages out over time) and results are compared with other models that have an asymptotic stationary distribution.

Discrete variations have also been proposed where vertices represent intersections in cities like New York, thus the mobility of a vehicle/pedestrian can be seen as a 2D RW on a lattice. One such example is the correlated RW, which is a generalised version of the standard RW [Ban07]. On the two dimensional lattice a user continues in the same direction with probability $\wp$, opposite direction with probability q and orthogonal direction with probability $2r$, such that $\wp + q + 2r = 1$. A further extension of the RW is the Manhattan model where $q = 0$, i.e you never revisit the last lattice site, and the speed between consecutive time steps and other users on the same street are correlated [Ban07].

2.6.2 Random waypoint model

The next, and arguably most popular mobility model for MANETs, is the Random waypoint (RWP) mobility model. In the RWP node movements are independent from one another and a single node chooses a waypoint uni-

[5]alternatively one could "wrap" the domain round, for example in 1D forming a circle, 2D a Torus

formly at random, travels to it with a constant speed, pauses with a probability $\wp$ then repeats the process. The time a node waits at each waypoint, i.e. its "think time", can be either be constant or vary from waypoint to waypoint depending on the model. In the RWP model, unlike the RW, a node continues on a path often for multiple time slots. Its simple formulation, coupled with the fact it converges to a stationary distribution, makes it a very good starting point for a more mathematical analysis. The continual crossing of paths in the middle of the domain means the probability of finding a node in the bulk is higher compared with the boundaries; intuitively this is what we might expect in cities where the centres are densely populated during working hours or busy shopping periods. The stationary distribution of the RWP has a simple closed form in 1D [Bet03a] and an integral form for any convex polygon which is easily computed numerically [Hyy06], see Sec 3 for further details. Interestingly the spatial distribution of the RWP model is proportional to the betweenness centrality of a uniform RGG in a disk (and other convex domains), in the limit as the number of nodes goes to infinity [Gil]. Betweenness centrality measures the proportion of shortest paths a particular node lies on between any two nodes in the graph and is thus a measure of a node's "importance". Therefore, nodes within the bulk have a higher betweenness as they are more likely to lie on the shortest multi-hop path between any pair of nodes. This is of particular importance in wireless routing where a network could easily become disconnected due to a cascading of node failures originating from a failed single node which had a high betweenness; for example a node could be a bridge between two clusters or a hub in a star graph. The mobility of the RWP leads to the outage probability being both spatially, and temporally, correlated [Kou16b, Gon14] in an interference-limited environment; an effect which increases in a dense network with blockages [Kou17].

The RWP model can be modified to include "hot spots" where the distribution of waypoints is no longer uniform, or else focused along the boundaries [Bet03b]; although interesting extensions they provide little further

insight whilst increasing the complexity of the problem and more general non-uniform measures are usually preferred.

2.6.3 Lévy

A Lévy mobility model is a modified RW where the path lengths are taken from a heavy tailed distribution $f_X(l) \sim l^{-\alpha-1}$, with $0 < \alpha < 2$, which has infinite second moment [Rhe11, Hug95, Che06]. As a consequence, the long "flights" occur with a power law frequency rather than being exponentially rare , as is the case for the RW [Man94]. In contrast to a typical RW, the Lévy mobility model has no characteristic length scale for the flight lengths and is sometimes referred to as a scale free RW [Ben07]. Simply put, Lévy mobility models how a small neighbourhood is explored then a large jump occurs which is subsequently explored, this process repeats until the end of the simulation. It turns out that heavy tailed distributions of path lengths are characteristic of human mobility [Ben07, Bro06, Lee11], which was observed from the traces of bank notes [Bro06]. As such, Levy mobility has been used to model the spread of infectious diseases due to air travel, and the mobility of portable smart devices in wireless networks [Lee11].

There are typically two cases studied: the Lévy flight and Lévy walk, the former has each flight taking a fixed time, and the latter having finite velocity culminating in a strong spatial-temporal correlation [Lee11]. The scale free nature of Lévy mobility models leads to a super-diffusive behaviour [Rhe11].

Analogously to how the normalised sum of i.i.d random variables with zro mean and finite second moment converges to a Gaussian under the CLT, the sum of these i.i.d random variables with infinite second moment tends to a symmetric stable Lévy distribution law with density [Kol68, Che08, Deta]

$$f^{\alpha,c}_{stable}(x) = \frac{1}{2\pi}\int_{-\infty}^{\infty} \exp\left(-itx - |ct|^{\alpha}\right) \mathrm{d}t,$$

where $c > 0$ is a scale factor. For $\alpha = 1$ it reduces to the Cauchy distribution,

whilst the Gaussian distribution is recovered when $\alpha \to 2$. For the Lévy flight model Ref [Lee11] show that the critical delay[6] behaves like $\bar{N}^{\alpha}$, whereas for the Lévy walk the delay is $\bar{N}^{\frac{1}{2}}$ for $\alpha < 1$ and for $\alpha \geq 1$ it behaves like the Lévy flight. This transitional behaviour at $\alpha = 1$ for the Lévy walk is a consequence of the mean flight length being infinite for $\alpha < 1$ [Lee11, Lu14]

The truncated Lévy flight was later introduced to ensure a finite second moment [Shl86]. Each flight has length l chosen from a Lévy stable distribution, and is re-sampled if the length is less than zero or greater than some cut off length $l_{\max}$. Similar to the normal Lévy flight model the direction of travel and speed are chosen uniformly from $U(0, 2\pi)$ and $U(v_{\min}, v_{\max})$ respectively; as such the mobility can be described by a sequence of flights and pauses. At each destination, the pause time is sampled from a different Lévy stable distribution and is re-sampled if it is less than zero or greater the specified maximum time $t_{\max}$ [Detb].

2.6.4 Self-similar Least Action Walk

Arguably, the Self-Similar Least Action Walk (SLAW) model [Lee12] provides a more accurate model for human mobility when simulations are compared to real life traces, but in contrast to other models lacks a rigorous mathematical formulation. (You can download the simulation in a link provided in the paper). It aims to capture the 4 key features of human mobility: flights and pause-times follow a truncated power-law; inter-contact times also follow a similar power-law decay; human mobility exhibits heterogeneous features and waypoints are fractal in nature. Essentially this model captures how humans continuously revisit the same places (work, home, gym etc) in their daily lives, which defines a concept of a local area of mobility, but they occasionally travel long distances (visit family, days out), whilst the places they do visit tend to be popular.

[6]The critical delay is the minimum delay required to achieve greater throughput per node than that of a static network which is of the order of the square root of the number of nodes [Lee11]

More generally, [San05] studied the (critical) transmission range needed for the graph to become fully connected with high probability for a MANET with a hard-disk connection model where nodes move according to a general mobility model $\mathcal{M}$ (including the RWP model). In particular for the RWP they show that the critical transmission range is $O\left(\sqrt{\frac{\log n}{n}}\right)$ for a non-zero pause time. Their analysis holds more generally for any bounded mobility model without blockages.

There is a plethora of other models which claim to capture at least one feature that characterises human mobility; the reader is referred to Ref [Ban07, Cam02, Har09] for relevant surveys. In Ref [Cam02] they discuss some group models where the mobility of an individual node also depends on the behaviour of other nodes in the network. The analysis of MANETs is primarily focused on comparing them to real life traces and simulating network behaviour. Therefore, for the application of wireless networks it largely remains a balancing act between mathematical tractability and model accuracy. One approach is to focus on particular aspects of human mobility such as regions of high/low densities (such as shopping centres, concerts, sport stadiums etc) or the fractal distribution of waypoints [Che18a, Det18a] that capture mobility through the inhomogeneity of the fixed spatial distribution [Gon08, Rhe11]. In addition, one can compare this approach to one where the nodes have infinite mobility, and thus the performance of real life mobile networks is bounded above and below by the two cases.

Chapter 3

Random Waypoint Model

As discussed in Sec 2.6, the Random Waypoint (RWP) model is a popular model for Mobile Ad hoc networks (MANETs). In this chapter we first provide a formal definition of the RWP model and then discuss the one dimensional case for which the stationary distribution is already known. We then compute the exact spatial distribution of the RWP in the rectangle and triangle for the first time. We compare these results with previous approximations in the literature which are used in the subsequent chapters. We published the result for the RWP in the rectangle in Ref [Pra16], whilst the approximation for the RWP near a boundary was used in Ref [Pra18].

Definition 3.1 (Random waypoint, Ref [Bet04])**.** Initially N points are placed inside a convex domain A via a BPP. Label each node in the model from $i = 1, \dots N$, and at time t the location of the i^{th} node is given by $\boldsymbol{r}_i \in A$. Every node moves independently from all other $N-1$ nodes, so it suffices to describe the motion of a single node i (refer to Fig **??**). At the initialisation of the model, the node i has starting waypoint P_1. The node then chooses its next waypoint $P_2 \in A$ uniformly at random, and a velocity v_1 is drawn from a distribution $f_V(v)$ (which is non-zero for $v \in [v_{\min}, v_{\max}]$ where $0 < v_{\min} < v_{\max} < \infty$) independent of the past. The node then travels from P_1 to P_2 in a straight line with constant speed v_1, called a leg and

denoted as $l_1 = \bar{P_1P_2}$. At P_2 the node pauses with probability $\wp$ for a time $\tau_\wp$ taken from the uniform distribution $U(0, \tau_{\max})$. The process then repeats itself. The result is the path of each node is characterised by a sequence of waypoints $\{P_1, P_2, \ldots\}$ and legs $\{L_1, L_2, \ldots\}$.

The above model is slightly modified to some earlier versions to incorporate a distribution of pause times. This can be generalised further to make the pause times be dependent on location [Hyy06], but this does little to affect the overall nature of the model. The parameter $\wp \in [0, 1]$ is the probability that a node is thinking (i.e. is not moving), and is given by [Bet04]

$$\wp = \frac{\mathbb{E}[T_p]}{\mathbb{E}[T_p] + \mathbb{E}[T]}, \tag{3.1}$$

where $\mathbb{E}[T]$ is the mean time for a single leg and $\mathbb{E}[T_p]$ is the expected pause time. Clearly, $\wp = 0$ corresponds to the case when the nodes do not pause once they reach the waypoint, conversely when $\wp = 1$ then the nodes are static for all time, in which case the spatial distribution of nodes in A is uniform by definition. The expected time taken for a leg is [Bet04]

$$\mathbb{E}[T] = \frac{\log[\kappa]\bar{l}}{(\kappa - 1)v_{\min}} \tag{3.2}$$

where κ is the ratio of the maximum and minimum speeds, $v_{\max}/v_{\min} > 1$, and $\bar{l}$ is the mean leg length given later by eq. (3.6). All of the above enables us to express the spatial distribution of nodes under the weighted sum of the static ($f_{\boldsymbol{X},p} = \frac{1}{|A|}$) and moving ($f_{\boldsymbol{X},m}$) probability density functions [Bet03a],

$$f_{\boldsymbol{X}}(\boldsymbol{x}) = \wp f_{\boldsymbol{X},p}(\boldsymbol{x}) + (1 - \wp) f_{\boldsymbol{X},m}(\boldsymbol{x}), \tag{3.3}$$

where $\int_A f_{\boldsymbol{X}}(\boldsymbol{x}) \mathrm{d}\boldsymbol{x} = 1$. Importantly, the mobile part of eq.(3.3) ($f_{\boldsymbol{X},m}(\boldsymbol{x})$) converges to a stationary distribution, making the RWP model a great mathematical object to study. The continual crossing of the domain as a node travels from waypoint to waypoint results in the probability of finding a node

in the bulk being much higher than at the boundaries, which is zero when the think time is zero ($\wp = 0$), as illustrated by the exact and approximate pdf in Fig 3.4. A non-zero $\wp$ acts to shift the density at the boundaries upwards, and as $\wp$ continues to increase towards one the distribution becomes more and more uniform as the time spent at each waypoint is much larger than the time spent travelling between them.

The RWP for the 1D case was first acehieved in Ref [Bet02] whereby they compute the pdf by recording the locations of a node at a particular time instance in a continuous histogram. In the same paper, they provide a simple approximation of the pdf of a rectangle from two, independent, one-dimensional processes [Bet02]. The same authors later gave an alternate method for the 1D case, and an improved approximation for the unit square by looking at the average time spent on a particular leg [Bet03a]. However, Ref [Hyy06] pointed out that the approximations made in [Bet03a] are in fact not needed and an exact expression can be found via an almost identical method, which results in the following equation,

$$f_{\boldsymbol{X},m}(\boldsymbol{r}) = \frac{1}{\bar{l}|A|^2} \int_0^{\pi} a_1 a_2 (a_1 + a_2) \mathrm{d}\phi \tag{3.4}$$

Here $\bar{l}$ denotes the mean leg length which is the average distance a node travels to its next waypoint; $a_1(\boldsymbol{r}), a_2(\boldsymbol{r})$ are the lengths of the line to the right and left of the point $\boldsymbol{r}$ at an angle ϕ to the horizontal, this is better illustrated in Fig 3.2. The derivation of eq.(3.4) is outlined below.

1. Writing the pdf as the expected portion of time spent in an elemental region $\mathrm{d}A$ per unit area noting that the speeds on each leg are fixed.

$$f_{\boldsymbol{X},m}(\boldsymbol{r}) = \frac{\mathbb{E}\left[\frac{l \cap \mathrm{d}A}{V}\right]}{\mathbb{E}\left[\frac{l}{V}\right] \mathrm{d}A} = \frac{\mathbb{E}[l \cap \mathrm{d}A]}{\mathbb{E}[l]\mathrm{d}A} \tag{3.5}$$

2. Condition on the location of r_1

3. Using simple geometrical arguments involving the area of a segment,

this conditional argument can be written as the product of that elemental region, radial distance r and distance from r_1 to the boundary.

4. Integrating over all possible locations of r_1 then gives the result obtained in eq.(3.4)

This method has since been generalised to $n-$dimensional space by the same authors [Hyy05], for example in 3D the area of interest is a cone rather than a segment.

In the same paper as eq.(3.4) polynomial approximations for 2D domains are given [Hyy06], improving on those originally provided in Ref [Bet03a]. However, the increased complexity of the polynomial approximations limits the potential for analytical analysis and as such are often ignored in favour of a more tractable approach which still captures the important qualitative nature of the problem.

The mean leg length can be directly calculated from eq.(3.4) by integrating both sides over the domain A, and rearranging for $\bar{l}$ since $\int_A f_{\boldsymbol{x},m}(\boldsymbol{r})\mathrm{d}\boldsymbol{r} = 1$. An alternative method is also provided in Ref [Hyy06]. Starting with the definition of the mean leg length

$$\begin{aligned} \bar{l} &= \frac{1}{|A|^2}\int_A\int_A |\boldsymbol{r}_2 - \boldsymbol{r}_1|\mathrm{d}\boldsymbol{r}_1\mathrm{d}\boldsymbol{r}_2 \\ &= \frac{1}{|A|^2}\int_{\mathbb{R}^2} \boldsymbol{r}D(\boldsymbol{r})\mathrm{d}\boldsymbol{r} \end{aligned} \tag{3.6}$$

The first equality is the definition of the mean leg length, the second is achieved by using a change of variable $\boldsymbol{r} = \boldsymbol{r}_2 - \boldsymbol{r}_1$ and introducing the parameter $D(\boldsymbol{r}) = \int_A \mathbb{1}_{\boldsymbol{r}_1 \in A\cap(A-\boldsymbol{r})}\mathrm{d}\boldsymbol{r}$. Although, it doesn't appear so, it is usually straight forward to calculate the mean leg length from this equation, and we give examples for the 1D case and the triangular domain later on in this chapter.

3.1 One-dimensional case

Consider the RWP on the line $[-L, L]$. We begin by first calculating the mean leg length $\bar{l}$ from eq.(3.6). In this example, $D(\boldsymbol{r}) = \int_A \mathbb{1}_{\boldsymbol{r}_1 \in |A \cap (A-\boldsymbol{r})|} \mathrm{d}\boldsymbol{r} = \int_{-L}^{L} |x_2 - x_1| \mathrm{d}x_2$, and all is left is to integrate over all possible locations of x_1.

$$\bar{l}_{1d} = \frac{1}{|A|^2} \int_A \int_A |x_2 - x_1| \mathrm{d}x_2 \mathrm{d}x_1 = \frac{2L}{3} \tag{3.7}$$

Of course, for the 1D case we need not use eq.(3.6), but we can see from inspection that the first integral in the above expression is $\bar{l}$.

To compute the pdf we use the method outlined by [Hyy06], and first start by calculating $\frac{\mathbb{E}[l \cap \mathrm{d}A | \boldsymbol{r}_1]}{\mathrm{d}A}$, where $a_1(x) = L - x$ and $a_2(x) = L + x$.

$$\frac{\mathbb{E}[l \cap \mathrm{d}A | \boldsymbol{r}_1]}{\mathrm{d}A} = \frac{\mathbb{E}[l \cap \mathrm{d}x | x_1]}{\mathrm{d}x} = \frac{1}{2L}(L - x)\mathbb{1}_{x_2 > x_1} + \frac{1}{2L}(x + L)\mathbb{1}_{x_2 < x_1} \tag{3.8}$$

Deconditioning on the location of x_1 gives

$$\frac{\mathbb{E}[l \cap \mathrm{d}x]}{\mathrm{d}x} = \frac{1}{2L} \int_{-L}^{x} \frac{1}{2L}(L - x)\mathrm{d}x + \frac{1}{2L} \int_{x}^{L} \frac{1}{2L}(x + L)\mathrm{d}x = \frac{1}{2L^2}(L^2 - x^2) \tag{3.9}$$

Combining these results yields the pdf of the RWP on the interval $[-L, L]$

$$f^{1d}_{\boldsymbol{X},m}(x) = \frac{1}{\bar{l}} \mathbb{E}[l \cap \mathrm{d}x] = \frac{3}{4L^3}(L^2 - x^2) \tag{3.10}$$

In Ref [Bet02] they propose two 1D processes to model the stationary distribution of the RWP in a rectangle with dimensions $[-a, a] \times [-b, b]$.

$$f^{\square,\mathrm{approx}}_{\boldsymbol{X},m}(x, y) = \frac{9}{16a^3b^3}(a^2 - x^2)(b^2 - y^2), \tag{3.11}$$

We now proceed by comparing this approximation with the exact expression obtained through application of eq.(3.4).

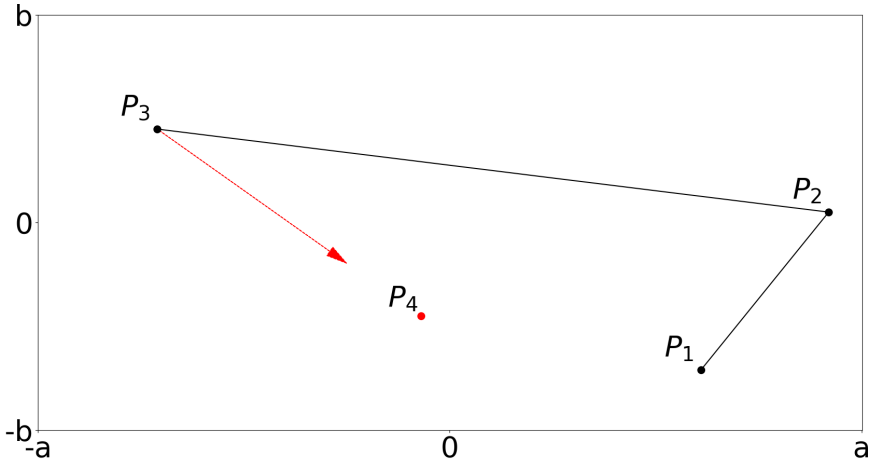

Figure 3.1: A schematic of the RWP in a rectangle, where P_i represents the position of the i^{th} waypoint.

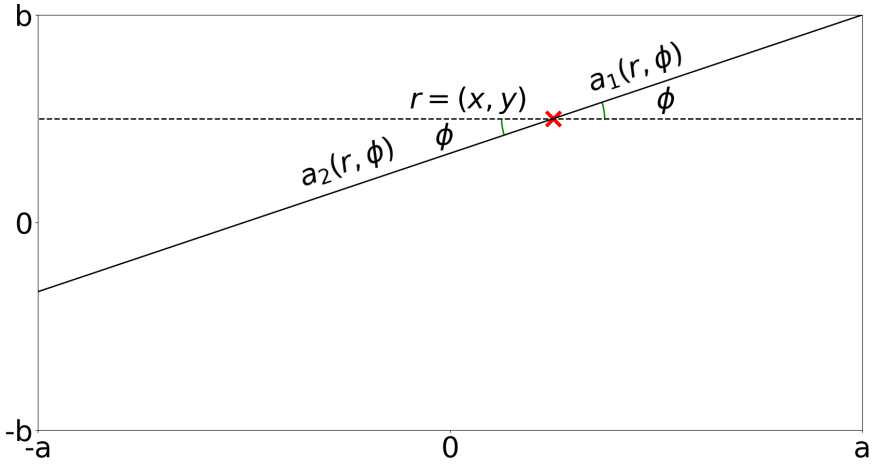

Figure 3.2: A schematic of how $a_1(x, y), a_2(x, y)$ in eq.(3.4) are computed for a specific point $\boldsymbol{r}$.

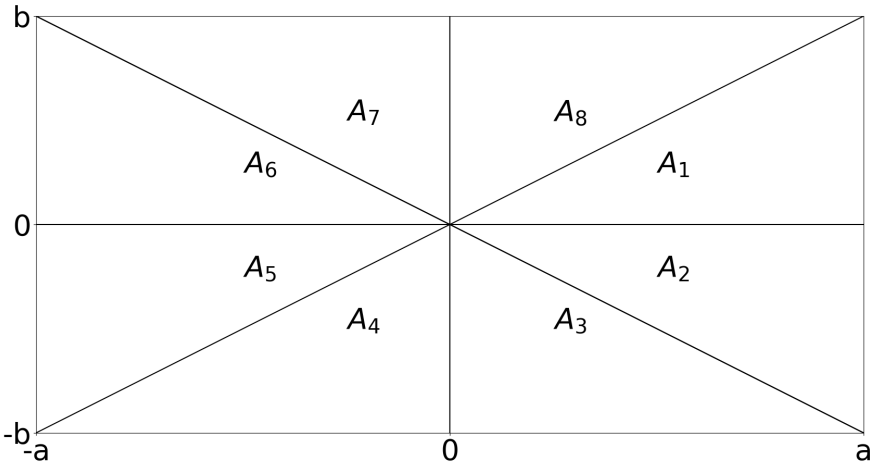

Figure 3.3: A schematic of the symmetry exploited to compute the closed form expression of the RWP in the triangle

3.2 Exact pdf for the RWP in the rectangle

The mean leg length can be computed via eq.(3.6) and was previously given in [Hyy06].

$$\bar{l}_{\square} = \frac{1}{30a^2b^2}\left(2a^5 + 2b^5 + 3a^2b^2c - c(a^4+b^4) + 5a^4b\log\left[\frac{2b+2a+c}{2a+c-2b}\right] - 5ab^4\log\left[\frac{2b}{2a+c}\right]\right) \tag{3.12}$$

where $c = 2\sqrt{a^2+b^2}$.

We now use eq.(3.4) to compute the exact distribution. Due to the symmetry of the problem we need only calculate the pdf for one section (an eighth) of the rectangle, depicted in Fig 3.1. In order to solve eq.(3.4) for the area labelled A_1 we need expressions for $a_1(x,y)$ and $a_2(x,y)$, which are

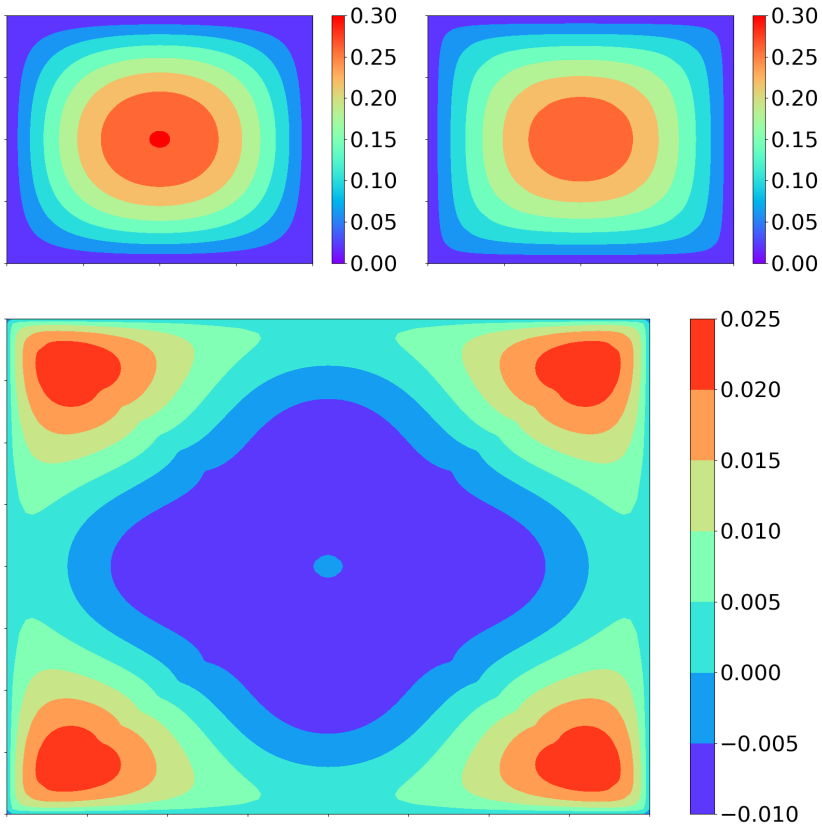

Figure 3.4: *Top Left:* The approximate stationary distribution. *Top right:* The exact stationary distribution in the rectangle. *Bottom:* The difference between the exact and approximate distributions. Parameters: $a = 1, b = 2$.

given below.

$$
\begin{aligned}
a_1(x,y) &= \begin{cases} \frac{a-x}{\cos\theta} & 0 \le \theta < \arctan\left[\frac{b-y}{a-x}\right] \\ \frac{b-y}{\sin(\theta)} & \arctan\left[\frac{b-y}{a-x}\right] \le \theta < \pi - \arctan\left[\frac{b-y}{a+x}\right] \\ -\frac{(a+x)}{\cos(\theta)} & \pi - \arctan\left[\frac{b-y}{a+x}\right] \le \theta < \pi \end{cases} \\
a_2(x,y) &= \begin{cases} \frac{a+x}{\cos\theta} & 0 \le \theta < \arctan\left[\frac{b+y}{a+x}\right] \\ \frac{b+y}{\sin\theta} & \arctan\left[\frac{b+y}{a+x}\right] \le \theta < \pi - \arctan\left[\frac{b+y}{a-x}\right] \\ \frac{x-a}{\cos(\theta)} & \pi - \arctan\left[\frac{b+y}{a-x}\right] \le \theta < \pi \end{cases}
\end{aligned}
\tag{3.13}
$$

For presentation purposes we only state the result here and provide the (some what tedious) calculations in Appendix **??**.

$$
\begin{aligned}
f^{A_1}_{\boldsymbol{X},m}(x,y) = \frac{1}{4\bar{l}_{\square}a^2b^2}\Bigg(& \frac{(2x+a)(b+y)(a-x)}{a+x}c_1 + \frac{(a-x)(b+y)(b-2y)}{b-y}c_2 \\
& \frac{(b-y)(a-x)(b+2y)}{b+y}c_3 + \frac{(a+2x)(b-y)(a-x)}{a+x}c_4 \\
& + (b-y)(a-x)^2\log\left[\frac{(c_3+x-a)(b-y)}{(c_4-a-x)(b+y)}\right] \\
& + (b+y)(a-x)^2\log\left[\frac{(a+x+c_1)(b-y)}{(b+y)(a-x+c_2)}\right] \\
& + (b+y)^2(a-x)\log\left[\frac{(b-y+c_2)(a+x)}{(a-x)(b+y+c_1)}\right] \\
& - a(a+x)(a-x)\log\left[\frac{-b+y+c_4}{c_1-y-b}\right] \\
& + (b-y)^2(a-x)\log\left[\frac{(b+y+c_3)(a+x)}{(a-x)(b-y+c_4)}\right] \\
& + b(b-y)(b+y)\log\left[\frac{(a-x+c_2)\,(b+y)}{(b-y)\,(-a+x+c_3)}\right]\Bigg)
\end{aligned}
\tag{3.14}
$$

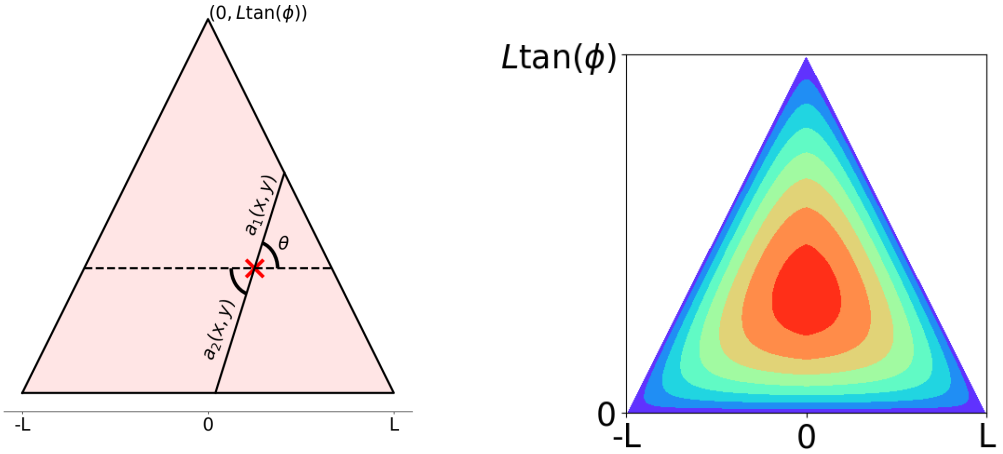

Figure 3.5: Left: Set up of the random waypoint model in an isosceles triangle, where $a_1(x,y), a_2(x,y)$ are drawn on for an arbitrary point (x,y). Right: The exact spatial distribution of the RWP in the triangle, given in Appendix C.2

where $\bar{l}_{\square}$ is the mean leg length calculated earlier and we have defined,

$$\begin{aligned} c_1 &: \sqrt{(a+x)^2+(b+y)^2} \\ c_2 &: \sqrt{(a-x)^2+(b-y)^2} \\ c_3 &: \sqrt{(a-x)^2+(b+y)^2} \\ c_4 &: \sqrt{(a+x)^2+(b-y)^2} \end{aligned} \tag{3.15}$$

We now have all the ingredients for the distribution for the whole rectangle. Using symmetry we can use eq.(3.14) to assemble the pdf for the complete rectangle. The density at any point in the rectangle is given in terms of $f^{A_1}_{\boldsymbol{X},m}(x,y)$.

$$f^{\square}_{\boldsymbol{X},m}(x,y) = \begin{cases} f^{A_1}_{\boldsymbol{X},m}(x,y) & \text{if } 0 \le x \le a, 0 \le y \le \frac{b}{a}x \\ f^{A_1}_{\boldsymbol{X},m}(x,-y) & \text{if } 0 \le x \le a, -\frac{b}{a}x \le y \le 0 \ (A_2) \\ f^{A_1}_{\boldsymbol{X},m}\left(\frac{a}{b}y, -\frac{b}{a}x\right) & \text{if } 0 \le x \le a, -b \le y \le -\frac{b}{a}x \ (A_3) \end{cases} \tag{3.16}$$

$$f^{\square}_{\boldsymbol{X},m}(x,y) = \begin{cases} f^{A_1}_{\boldsymbol{X},m}\left(-\frac{a}{b}y, -\frac{b}{a}x\right) & \text{if } -a \leq x \leq 0, -b \leq y \leq \frac{b}{a}x \ (A_4) \\ f^{A_1}_{\boldsymbol{X},m}(-x,-y) & \text{if } -a \leq x \leq 0, 0 \leq y \leq -\frac{b}{a}x (A_5) \\ f^{A_1}_{\boldsymbol{X},m}\left(-x,y\right) & \text{if } -a \leq x \leq 0, \frac{b}{a}x \leq y \leq 0 \ (A_6) \\ f^{A_1}_{\boldsymbol{X},m}\left(-\frac{a}{b}y, \frac{b}{a}x\right) & \text{if } -a \leq x \leq 0, -\frac{b}{a}x \leq y \leq b \ (A_7) \\ f^{A_1}_{\boldsymbol{X},m}\left(\frac{a}{b}y, \frac{b}{a}x\right) & \text{if } 0 \leq x \leq a, \frac{b}{a}x \leq y \leq b \ (A_8) \end{cases} \tag{3.17}$$

We now proceed by discussing some particular cases, and make comparisons with the approximation in eq.(3.11).

Particular cases

Centre

$$\begin{aligned} f^{\square}_{\boldsymbol{X},m}(0,0) = \frac{1}{8\bar{l}(4ab)^2}\Bigg(&4ab\sqrt{a^2+b^2} + 2b^3 \log\left[\frac{a+\sqrt{a^2+b^2}}{b}\right] \\ &+ 2a^3 \log\left[\frac{b+\sqrt{a^2+b^2}}{a}\right]\Bigg) \end{aligned} \tag{3.18}$$

At the centre of the rectangle the exact distribution still has a logarithm term, meaning that analysis further down the line is likely to rely on numerical calculations. As such we want to now see if the approximation given in eq.(3.11) is suitable.

Square

Letting $a = b = 1$ the density at the centre of the square for each case is given by,

$$\begin{aligned} f^{\square}_{\boldsymbol{X},m}(0,0) &= .695 \\ f^{\square,\text{approx}}_{\boldsymbol{X},m}(0,0) &= .563 \\ f^{\text{uniform}} &= 0.25 \end{aligned} \tag{3.19}$$

Clearly, the density of users in the middle of the domain for the RWP is at least twice that of the uniform model, with the exact and approximate models also deviating.

Approximation near the boundary

Without loss of generality we assume that $b >> a$, and approximate near the boundary with $x \approx a$.

$$f^{\square}_{\boldsymbol{X},m}(x \approx a, 0) = c(x-a) - c^* \log[x-a](x-a) + O((x-a)^2), \quad c, c^* \in \mathbb{R}$$
$$f^{\square,\text{approx}}_{\boldsymbol{X},m}(x \approx a, 0) = -\frac{9}{8a^2 b}(x-a) + O((x-a)^2) \tag{3.20}$$

Qualitatively we can see that the profiles of the exact, approximate and simulated (mobile) distributions are the same, see Fig 3.4. That is to say, the density of nodes is higher in the bulk of the domain, and goes to zero at the boundaries. However, the behaviour of the approximate and exact expressions differ near the boundaries. For the approximate solution of the RWP it grows linearly away from the boundary, whilst the density actually grows like $\log[x-a](x-a)$ away from a vertical boundary. Furthermore, it can be shown near the corner the RWP grows linearly, whilst the approximation actually grows as a quadratic.

To facilitate a more tractable approach we will invariably use the approximate form of the RWP in our analysis. To qualify this, we first point out that we are not analysing the performance of a network with RWP mobility, but instead we are analysing the impact more general mobility models and boundaries have on the performance of MANETs. As a result, we are often not concerned with the exact distribution of the RWP but are interested in its qualitative features, such as having a higher density of nodes in the bulk compared with near the boundary.

3.3 Triangle

We now move onto the RWP in a triangular region defined as $\mathcal{T} = \big\{(x,y)| -a \leq x \leq a, 0 \leq y \leq \min\left[\frac{b}{a}(x+a), -\frac{b}{a}(x-a)\right]\big\}$, illustrated in Fig 3.2. The purpose to analyse the RWP in $\mathcal{T}$ is to see the impact corners have, in particular we look at the role boundaries have on spatio-temporal networks in Sec 7. Most of the working is given in AppendixC.2, since the calculations are similar to those discussed in the rectangle, and we merely state the results.

Mean leg length

$$\bar{l}_{\triangle} = \frac{4}{30(a^2+b^2)^{3/2}}\left(4a^2b^2\log\left[\frac{a}{a+\sqrt{a^2+b^2}}\right] + b^4 - a^4 + 4a^3\sqrt{a^2+b^2}\right) + \frac{a\sqrt{a^2+b^2} + b^2\log\left[\frac{a+\sqrt{a^2+b^2}}{b}\right]}{15a} \tag{3.21}$$

As a sanity check, let $a = \sqrt{3}, b = a\sqrt{3}$ such that we have an equilateral triangle with height 3, then $\bar{l}_{\triangle}$ reduces to the following,

$$\bar{l}_{\triangle} = \frac{a(4+\log[27])}{10} = 1.263 \tag{3.22}$$

which is consistent with that given in Ref [Hyy06].

Triangle pdf

Through symmetry we only need to calculate the pdf for the case when $x \geq 0$, which we denote as $f^{+,\triangle}_{\boldsymbol{X},m}(x,y,a,b)$ to generate the full pdf for the triangle $f^{\triangle}_{\boldsymbol{X},m}(x,y,a,b)$ (for $x<0$ it is equivalent to $f^{\triangle}_{\boldsymbol{X},m}(-x,y,a,b)$) [1]. Even for $f^{\triangle,+}_{\boldsymbol{X},m}(x,y,1,1)$ the expression is very lengthy, and are unable to do any meaningful analysis with it. As such, we will need to use an approximation. The exact expression for $f^{\triangle,+}_{\boldsymbol{X},m}(x,y,a,b)$ is included in Appendix C.2 for completeness.

[1] We could work out the exact distribution for the RWP in any triangular region using the exact same method, but in this case we may not be able to rely on symmetry which doubles the workload.

Triangle Approximation

Lets now consider a translated version of the isosceles triangle $\mathcal{T} = \{(x,y)|0 \leq x \leq L, 0 \leq y \leq \min(x\tan\phi, -(x-L)\tan\phi)\}$. The motivation for this is that in the exact solution making it symmetrical about the origin enabled a simpler final result, whilst here we will ultimately want to approximate it near a corner; doing it at the origin is simpler. Naturally, if we want to switch between the two, a straight forward transformation of coordinates is needed. Our approach is to use three 1D processes (see eq.(3.10)) to model the RWP in a triangle, like that done in for the rectangle with two 1D processes. The justification for this is to try to achieve a more tractable form of the spatial distribution, albeit with the knowledge that it will only capture the qualitative behaviour of the RWP. Furthermore, the simple form of the 1D processes means any numerical computations are far quicker than compared with using the exact form, including the closed form expression we given in Appendix C.2. By translating each 1D process appropriately we obtain the following approximation.

$$\begin{aligned} f^{\triangle}_{\text{approx}}(x,y) &= c_{\triangle} f_{1d}(y) f_{1d}\left(x\cos\left(\frac{\pi}{2}-\phi\right) - y\sin\left(\frac{\pi}{2}-\phi\right)\right) \\ &\quad \times f_{1d}\left((x-L)\cos\left(\frac{\pi}{2}+\phi\right) - y\sin\left(\frac{\pi}{2}+\phi\right)\right) \\ &= c_{\triangle} y(L-2y\cot(\phi))(x-y\cot(\phi))(L+y\cot(\phi)-x) \\ &\quad \times (L-\csc(\phi)(y\cot(\phi)+x))(\csc(\phi)(L+y\cot(\phi)+x)-L) \end{aligned} \tag{3.23}$$

The first term is the density of a one dimensional process in the y-direction (base of the triangle) with length $\frac{L}{2}\tan\phi$, the second and third terms are processes from the corresponding left and right boundary lines respectively with the 1D process with length $L\sin\phi$, $c_{\triangle}$ is an additional normalisation constant such that $\int_T f^{\triangle}_{\text{approx}}(\boldsymbol{x})\mathrm{d}\boldsymbol{x} = 1$, where $c_{\triangle}$ in the second equality has absorbed some extra constants. Since we will largely concern ourselves with what happens near the corner for a large domain, we first transform the

above into polar coordinates and then take the leading order expansion for small $r = \sqrt{x^2 + y^2}$.

$$\begin{aligned} f^{\triangle}_{\text{approx}}(r,\theta) &= -c_{\triangle} L^4 (\csc(\phi) - 1)\sin(\theta)(\cot(\phi)\sin(\theta) - \cos(\theta))r^2 + O(r^3) \\ &\sim \sin(\theta)\sin(\phi - \theta)r^2 + O(r^3), \end{aligned} \tag{3.24}$$

The appeal of this approximation is that the density near the corner is far more tractable. However, we should note that from eq.(3.4) it can be shown that the exact solution grows linearly away from the corner, not quadratically. In this case, we tried the simplest approximation possible to try to achieve a tractable form but, as might be expected, it once again fails to accurately describe the boundary behaviour. However, as a result of us not having a good approximation for the RWP in the triangle, it led us to study a more general non-uniform density near a corner in Chapter 7. In that chapter we use the density $\lambda(r,\theta) = \bar{c} r^{\alpha} g_{\phi}(\theta)$ to model the distribution of points near a corner. Within this model we have the added flexibility of comparing different "levels" of inhomogeneity since we can easily interpolate between different network scenarios by tuning the parameter α and varying $g_{\phi}(\theta)$ leading to a more robust analysis.

3.4 Circular Domain

Unlike in the previous cases the integral in eq.(3.4) cannot be solved explicitly for the circle [Hyy05], instead it is an elliptic integral of the second kind. Interestingly, the same integral form represents the betweenness centrality in dense uniform SRGGs [Gil16].

$$f^{\circ}_{\boldsymbol{X},m}(r) = \frac{2(R^2 - r^2)}{\bar{l}\pi^2 R^4} \int_0^{\pi} \sqrt{R^2 - r^2\cos^2\theta}\,\mathrm{d}\theta \tag{3.25}$$

However, a simple approximation was provided in Ref [Bet02] for a circle

with radius R which we will use,

$$f^{\circ}_{\boldsymbol{X},m}(r) = \frac{2}{\pi R^2}\left(1 - \frac{r^2}{R^2}\right) \tag{3.26}$$

Again the pdf shares all the same characteristics of the exact solution, with the density going to zero at the boundaries and maximum in the middle, whilst also being radially symmetric. Interestingly, in this case the curved boundary leads to linear decay near the border meaning the approximation is far better than the ones discussed previously. In Chapters 5,6 this is a special case of a more general distribution that is used[2].

Having looked at a range of different mobility models, both in this chapter and the literature review, we are well placed to compare how mobility impacts connectivity. Hopefully it is clear by now that we are motivated by doing network analysis that is both interesting and mathematically tractable. As a starting point we begin by comparing the performance of a range of SRGGs with non-uniform distributions, which are motivated by the RW and RWP models.

[2]In Chapters 5,6 we refer to the density in eq.(3.26) as "concave", whilst this is true for the approximate form it is not correct for the exact density.

Chapter 4

Mean degree

In the last chapter we discussed the RWP as a mobility model used to represent Mobile ad hoc networks (MANETs). In this chapter we use the RWP model, along with tools from stochastic geometry, to analyse the performance of MANETs in terms of the average number of connections. This chapter follows the work published in Ref [Pra16], of which I was a co-author; refer to Appendix A for more details on my contributions.

MANETs have been proposed as a model for environmental monitoring [Cho03], disaster relief [Kha16], military communications [Hel14] along with the next generation of mobile phone networks [Asa14, Teh14]. As such there has been a proliferation in research into MANETs over the past couple of decades as networks become increasingly mobile. As people, and therefore smart devices, move around, the spatial configuration evolves with time and the network properties fluctuate accordingly. For example, the number of users a base station serves may vary dramatically as people complete their daily commute to work. Much of the previous research is highly centralised and assumes a static architecture, which may not be able to cope with the expected increase in traffic demand, as it is not easily scalable as building further BSs is both costly and time consuming. By allowing smart devices to relay information through the network in a multi hop fashion can help alleviate the increases in traffic demands and reduce the end-to end delay, helping

to facilitate the transition into the next generation of wireless communication networks [Teh14, Tse05].

The question this chapter aims to address is *How does the spatial configuration of points, boundaries, the location of the user and the connection model impact upon network connectivity?*

To this end we analyse the average number of connections a user can make during a single time slot in a bounded domain, where the distribution of users is modelled by a non-uniform PPP. The density of nodes is chosen such that we can easily interpolate between a uniform, convex (more nodes near the boundary) and concave (more nodes near the centre) distribution of users, which have applications to real life scenarios; the uniform and concave distributions can can be used to approximate the RW and RWP models respectively. We further compare the mean degree for three different connection functions (Disk, Rayleigh and interference connection models) which represent different network scenarios, coupling this with our analysis of the non-uniform distribution of users. Finally, we use our results to discuss the scalability of finite MANETs and relating it to the field of percolation. We start by formally introducing the mean degree and system model.

4.1 Mean degree and system model

The mean degree is the average number of successful links a node at $\boldsymbol{x}_1$ can make, and is defined as,

$$\mu(\boldsymbol{x}_1) = \int_A \lambda(\boldsymbol{x})\mathcal{H}(|\boldsymbol{x}_1 - \boldsymbol{x}|)\mathrm{d}\boldsymbol{x} \tag{4.1}$$

where $\mathcal{H}(.)$ is the connection function, $\lambda(\boldsymbol{x})$ is the distribution of users in the region A, and $|\boldsymbol{x}_1 - \boldsymbol{x}|$ is the Euclidean distance between the user $\boldsymbol{x}_1$ and a transmitter $\boldsymbol{x}$.

In general we can discuss a range of distributions, but we focus on the stationary distribution of the RWP discussed previously and compare it with

the uniform and convex case. For tractability we assume that the distribution is modelled by two 1D processes, and generalise it such that we can interpolate between a uniform, convex (nodes are found near the corners predominately) and concave (RWP) distribution of devices. As such, let us define the distribution of points as,

$$\lambda(x,y) = \lambda_0 \left(c_x x^2 + 1 - \frac{c_x L_x^2}{3} \right) \left(c_y y^2 + 1 - \frac{c_y L_y^2}{3} \right) \tag{4.2}$$

where λ_0 is the average number of nodes per unit volume, the first bracket is a general 1D process in the x-direction, and the second is the same but in the y-direction. The constant c_x determines the profile of $\lambda(\boldsymbol{x})$ in the x-direction, whilst c_y does the same but for the y-direction. For simplicity, we consider only three cases of c_x, c_y: when $(c_x, c_y) = (0,0)$ we have the uniform distribution, $(c_x, c_y) = \left(-\frac{3}{2L_x^2}, -\frac{3}{2L_y^2} \right)$ is the RWP model and $(c_x, c_y) = \left(\frac{3}{L_x^2}, \frac{3}{L_y^2} \right)$ is the convex case. The latter refers to a model where the distribution is higher near the boundaries, particularly near the corners. This helps us compare between the standard case of the RW (uniform) and the more interesting stationary distribution of the RWP model (the distribution is higher in the middle of the domain), along with better isolating whether it is boundaries or the distribution of devices that influence network performance.

We now compute the mean degree for three different connection functions: the disk, Rayleigh and interference-limited connection models, as defined in Sec 2.2. We proceed by first discussing the Hard Disk and Rayleigh connection model.

4.2 Mean degree in the hard disk model

First recall the connection model is $\mathcal{H}(r) = \mathbb{1}_{r \leq r_0}$ for the hard disk connection model, as in the standard RGG. The mean degree in this case is simply the

mean number of points in the region $A \cap \mathcal{B}_{\boldsymbol{x}_1}(r_0)$,

$$\mu(\boldsymbol{x}_1) = \int_{A \cap \mathcal{B}_{\boldsymbol{x}_1}(r_0)} \lambda(\boldsymbol{x}) \mathrm{d}\boldsymbol{x} \tag{4.3}$$

Provided the ball, which defines the connection radius, does not intersect the boundary of the rectangle then the mean degree is given by,

$$\begin{aligned}
\mu(\boldsymbol{x}_1) = \pi r_0^2 \lambda_0 &+ \frac{c_y \pi r_0^2 \left(-4L_y^2 + 3\left(r_0^2 + 4y_1^2\right)\right) \lambda_0}{12} \\
&+ \frac{c_x \pi r_0^2 \left(-4L_x^2 + 3\left(r_0^2 + 4x_1^2\right)\right) \lambda_0}{12} \\
&+ \frac{c_x c_y \pi r_0^2 \lambda_0}{72 L_x L_y} \Bigg(8L_x^2 L_y^2 - 6L_y^2 r_0^2 + 3r_0^4 - 24 L_y^2 x_1^2 + 72 x_1^2 y_1^2 \\
&+ 18 r_0^2 \left(x_1^2 + y_1^2\right) - 6L_x^2 \left(r_0^2 + 4y_1^2\right) \Bigg)
\end{aligned} \tag{4.4}$$

Clearly for the uniform case, where the user is far from the boundary, then the mean degree is simply $\lambda_0 \pi r_0^2$. When either c_x or c_y are non-zero then there are spatial variations in the mean degree which correspond to those in the distribution of points, see Fig 4.2.

The introduction of boundaries creates further spatial variations in the mean degree, but often leads to a less tractable approach. For example, as the ball intersects (only) the right hand boundary of the rectangle the mean degree is written as,

$$\mu(\boldsymbol{x}_1) = \int_{x_1 - r_0}^{\min[L_x, x_1 + r_0]} \int_{y_1 - \sqrt{r_0^2 - (x - x_1)^2}}^{y_1 + \sqrt{r_0^2 - (x - x_1)^2}} \lambda(\boldsymbol{x}) \mathrm{d}\boldsymbol{x}, \tag{4.5}$$

and can only be solved in semi-analytic form for a general density $\lambda(\boldsymbol{x})$. Again, for the uniform case the mean degree is simply proportional to the size of the intersecting region, $\mu(\boldsymbol{x}_1) = \lambda_0 |\mathcal{B}_{\boldsymbol{x}_1}(r_0) \cap A|$. As such we only give the two extremal cases, that is when the receiver is located at the corner $\boldsymbol{x}_1 = (L_x, L_y)$ and the boundary $\boldsymbol{x}_1 = (L_x, 0)$.

$$\begin{aligned}\mu(L_x,0) = &\frac{\pi r_0^2\lambda_0}{2} + \frac{c_y r_0^2\left(-120L_y^2\pi + 90\pi r_0^2\right)\lambda_0}{720} \\ &+ c_x\frac{r_0^2\left(240L_x^2\pi - 960L_x r_0 + 90\pi r_0^2\right)\lambda_0}{720} \\ &+ \frac{c_x c_y r_0^2\lambda_0}{720}\Bigg(-80L_x^2L_y^2\pi + 320L_xL_y^2r_0 + 60L_x^2\pi r_0^2 \\ &- 30L_y^2\pi r_0^2 - 192L_x r_0^3 + 15\pi r_0^4\Bigg)\end{aligned} \tag{4.6}$$

$$\begin{aligned}\mu(L_x,L_y) = &\frac{\pi r_0^2\lambda_0}{4} + \frac{c_y r_0^2\left(240L_y^2\pi - 960L_y r_0 + 90\pi r_0^2\right)\lambda_0}{1440} \\ &+ \frac{c_x r_0^2\left(240L_x^2\pi - 960L_x r_0 + 90\pi r_0^2\right)\lambda_0}{1440} \\ &+ \frac{c_x c_y r_0^2\lambda_0}{1440}\Bigg(160L_x^2L_y^2\pi - 640L_xL_y\left(L_x+L_y\right)r_0 + 720L_xL_y r_0^2 \\ &+ 60\left(L_x^2+L_y^2\right)\pi r_0^2 - 192\left(L_x+L_y\right)r_0^3 + 15\pi r_0^4\Bigg)\end{aligned} \tag{4.7}$$

From the above two equations the role of boundaries acts to reduce the number of possible connections, with the mean degree being halved each time for the uniform case as it goes from the centre (eq. (4.4)), boundary (eq.(4.6)) and then the corner (eq.(4.7)). Furthermore, it is not difficult to see that the mean degree scales with λ_0, capturing the local behaviour of the network.

4.3 Mean degree in the Rayleigh model

To capture the effects of soft connectivity we use the Rayleigh connection model, $\mathcal{H}(r) = e^{-\frac{(\epsilon+r^\eta)}{r_0^\eta}}$. Through application of eq.(4.1) we can obtain closed form expressions for the mean degree in the square for particular parameters

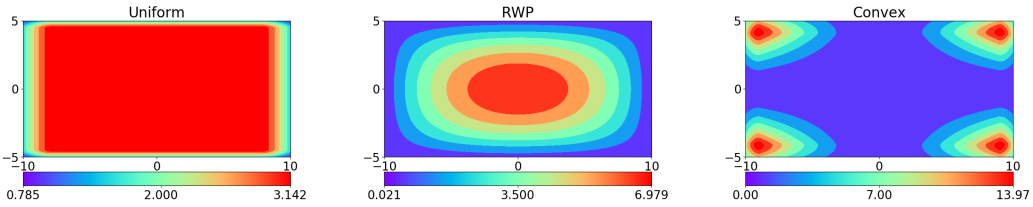

Figure 4.1: Surface plots of the mean degree for the Disk model, with parameters $r_0 = 1; L_x = 10, L_y = 5, \lambda_0 = 1$ and thus the average number of nodes is $\bar{N} = 200$.

of the path loss exponent η. For simplicity in our analysis we chose $\eta = 2$ (free space); we discuss the impact of different values of η later on in this chapter.

$$\begin{aligned}\mu(\boldsymbol{x}) &= \int_{-L_x}^{L_x}\int_{-L_y}^{L_y} e^{-\frac{\epsilon}{r_0^\eta}} e^{-\left(\frac{\sqrt{(x-x_0)^2+(y-y_0)^2}}{r_0}\right)^\eta} \lambda(x,y)\mathrm{d}x\mathrm{d}y \\ &= \frac{e^{-\frac{\epsilon+(L_x+x_1)^2+(L_y+y_1)^2}{r_0^2}} r_0^2\lambda_0}{144L_xL_y} Q(x_1,L_x,r_0,c_x)Q(y_1,L_y,r_0,c_y)\end{aligned} \tag{4.8}$$

where

$$\begin{aligned}Q(x,L_x,r_0,c_x) = -6c_xr_0 &\left(L_x - x_1 + e^{\frac{4L_xx_1}{r_0^2}}(L_x+x_1)\right) \\ &+ e^{\frac{\left(L_x^2+x_1^2\right)}{r_0^2}}\sqrt{\pi}\left(6 + c_x\left(-2L_x^2+3r_0^2+6x_1^2\right)\right) \\ &\times\left(\operatorname{erf}\left(\frac{L_x-x_1}{r_0}\right)+\operatorname{erf}\left(\frac{L_x+x_1}{r_0}\right)\right).\end{aligned}$$

Although a lengthy expressions, the important behaviour is that μ scales with λ_0, similar to the disk model. We can further simplify eq.(4.8) by considering

the uniform case,

$$\begin{aligned}\mu_(x_1, y_1) &= \frac{\pi r_0^2 \lambda_0}{4} e^{-\frac{\epsilon}{r_0^2}} \\ &\times \left(\operatorname{erf}\left[\frac{L_x + x_1}{r_0}\right] + \operatorname{erf}\left[\frac{L_x - x_1}{r_0}\right]\right)\left(\operatorname{erf}\left[\frac{L_y + y_1}{r_0}\right] + \operatorname{erf}\left[\frac{L_y - y_1}{r_0}\right]\right) \\ &\approx \pi r_0^2 \lambda_0 e^{-\frac{\epsilon}{r_0^2}}\end{aligned} \tag{4.9}$$

where the approximation is for when x_1, y_1 are not near the boundary, i.e $L_x \gg x$ and $L_y \gg y$. Notice that the average number of connections includes an additional factor $e^{-\epsilon r_0^{-2}}$. In fact we can generalise the approximation for a region with no boundaries and general η. Consider the integral over $\mathbb{R}^2$ instead, which yields the following simple expression

$$\mu_\infty^{\text{Rayleigh}} = 2\pi \int_0^\infty \lambda_0 e^{-\frac{(\epsilon + r^\eta)}{r_0^\eta}} r \mathrm{d}r = \lambda_0 \pi r_0^2 \Gamma\left[\frac{2+\eta}{\eta}\right] e^{-\left(\frac{\epsilon}{r_0}\right)^\eta} \tag{4.10}$$

To inspect the role of η let us compare $\mu_\infty^{\text{Rayleigh}}$ with the mean degree in the disk model (for a uniform PPP in $\mathbb{R}^2$), denoted as μ_∞^{Disk}. First recall that $\mu_\infty^{\text{Disk}} = \lambda_0 \pi r_0^2$. Comparing μ_∞^{Disk} and $\mu_\infty^{\text{Rayleigh}}$ highlights there is an extra factor $\Gamma\left[\frac{2+\eta}{\eta}\right] e^{-\left(\frac{\epsilon}{r_0}\right)^\eta}$ in $\mu_\infty^{\text{Rayleigh}}$, due to the long range nature of the connection functions. Therefore for the disk model to outperform the Rayleigh model ($\mu_\infty^{\text{Disk}} > \mu_\infty^{\text{Rayleigh}}$) then $\Gamma\left[\frac{2+\eta}{\eta}\right] e^{-\left(\frac{\epsilon}{r_0}\right)^2} < 1$ must hold. Since $\Gamma\left[\frac{2+\eta}{\eta}\right] e^{-\left(\frac{\epsilon}{r_0}\right)^2} \leq \Gamma\left[\frac{2+\eta}{\eta}\right] < 1$ then it follows that for all finite $\eta > 2$ then $\mu_\infty^{\text{Disk}} > \mu_\infty^{\text{Rayleigh}}$ regardless of the choice of ϵ[1]. As a result the mean degree only benefits from these "soft" connections when they are very soft, i.e. when $\eta <$ dimension as is the case in highly reflective media. Of course, allowing $\eta \to \infty$ means $\mu_\infty^{\text{Rayleigh}} \to \mu_\infty^{\text{Disk}} e^{-\left(\frac{\epsilon}{r_0}\right)^2}$, namely the Rayleigh model approaches the disk model scaled by the factor $e^{-\left(\frac{\epsilon}{r_0}\right)^2}$ which originates from the non-singular nature of the path loss model.

[1]For $\epsilon > 0$ then $\mu_\infty^{\text{Disk}} > \mu_\infty^{\text{Rayleigh}}$ can occur before $\eta >$ dimension

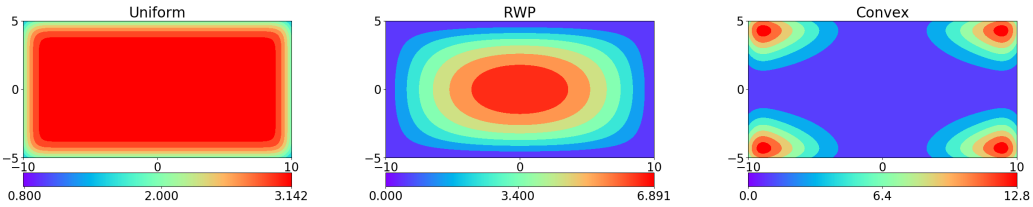

Figure 4.2: A surface plot of the mean degree for the Rayleigh connection function in the square with density given by eq(4.8), parameters: $L_x = 10, L_y = 5, \lambda_0 = 1; r_0 = 1$

It is difficult to interpret the mean degree via eq.(4.8) so instead we use use Fig 4.3. We can see that for the Rayleigh connection model (like the disk model) the mean degree roughly mirrors the spatial distribution of nodes, which is what we would expect; the more nodes there are nearby, the greater the number of connections. The far right panel of Fig 4.3 highlights the non-trivial interplay between boundaries and the node distribution, the maximum mean degree is found near, but not at, the boundary where the density is at its highest.

4.4 Mean degree in the interference model

The dependence on the underlying point process in the interference case means that the mean degree cannot be given in closed form when the domain is finite, even for the uniform case. In fact, closed form expressions for $\mathcal{H}(.)$, eq(2.17), can only be given for particular cases, for example in $\mathbb{R}^2$ or the centre of a circular domain. We can approximate a square domain by a circular one to investigate the behaviour of $\mathcal{H}(0,0)$, particularly since any interference from the boundaries will become increasingly negligible when $\eta > 2$. Let the radius of the disk be $R = \frac{2L_x}{\sqrt{\pi}}$, with $L_x = L_y$, and the distribution of users in the circle be $\lambda(r,\theta) = \lambda_0 \left(1 - \frac{bR^2}{2} + br^2\right)$ where $b = 0, -\frac{2}{R^2}, \frac{2}{R^2}$ are the uniform, RWP and convex case respectively. Then by

transforming the integral in eq.(2.17) to polar coordinates, and using the $\lambda(r)$, then the interference part of the connection probability at the centre can be written as

$$\begin{aligned}\mathcal{L}_{\circ}((0,0),r) &= \exp\left(-\int_0^{2\pi}\int_0^{R}\lambda(z,\theta)\frac{1}{1+\frac{g(r)}{q\gamma g(z)}}z\mathrm{d}z\mathrm{d}\theta\right)\\ &= \exp\Bigg(-\frac{q\gamma(r^{\eta}+\epsilon)R^2}{4(r^{\eta}q\gamma+\epsilon+\epsilon q\gamma)}\\ &\times\left((2-R^2)\,{}_2F_1\left(1,\frac{2}{\eta},1+\frac{2}{\eta},-\frac{R^{\eta}}{r^{\eta}q\gamma+\epsilon+q\gamma\epsilon}\right)\right.\\ &\left.+\,bR^2\,{}_2F_1\left(1,\frac{4}{\eta},1+\frac{4}{\eta},-\frac{R^{\eta}}{r^{\eta}q\gamma+\epsilon+q\gamma\epsilon}\right)\right)\Bigg)\end{aligned} \tag{4.11}$$

Here ${}_2F_1(.,.,.,.)$ is the Gauss hypergeometric function. The expression can be simplified further for specific values of η and /or ϵ. For example when $\eta = 4$,

$$\begin{aligned}\mathcal{H}(r) = \exp\left(-\frac{r^{\eta}+\epsilon}{r_0^{\eta}}\right)\exp\Bigg(-\lambda_0\pi\frac{q\gamma(r^4+\epsilon)}{2(\epsilon+q\gamma(r^4+\epsilon))}\Bigg(\\ (2-bR^2)\sqrt{\epsilon+q\gamma(r^4+\epsilon)}\arctan\left[\frac{R^2}{\sqrt{\epsilon+q\gamma(r^4+\epsilon)}}\right]\\ +\,b(\epsilon+q\gamma(r^4+\epsilon))\log\left[1+\frac{R^4}{q\gamma(r^4+\epsilon)+\epsilon}\right]\Bigg)\Bigg)\end{aligned} \tag{4.12}$$

Even for this (and others) simplified case only semi-analytic forms of the mean degree can be given, thus we generate surface plots for both the connection probability of $\mathcal{H}(.)$ in the domain, and the mean degree in python.

The top panel of Fig 4.3 represents the interference field in the rectangle for all three cases, which is $-\log$ of the interference part of the connection model given by eq.(2.17). Regions with high interference correspond to regions where the node density is highest. The effect a rectangular domain has on the connectivity is further highlighted by seeing that the side with the shortest length has a smaller portion of nodes and thus the impact of

interference is less.

Analysing Fig 4.3 we first note the boundaries reduce the interference field which increases $\mathcal{H}(\boldsymbol{x})$, but also increasing the average distance to other nodes in the network. For example, in Fig 4.3 we see that μ decreases at the border for a uniform density of nodes (left panel), with the maximal value being in the region located near the boundary (particularly the corner); μ is maximised by ensuring the interference field is at its lowest *and* the average distance to neighbouring nodes is not too high. The complicated interplay between boundaries and interference is well demonstrated by the convex case. We can see that the interference field is *not* maximised at the regions where the density is highest (i.e. at the corners), but instead in regions where the density is high but also away from the boundary. In addition, the mean degree is lowest in regions where the density is minimised. This demonstrates the balance between having too few nodes to connect and too many which causes outage due to interference. We also note that the mean degree is higher along the horizontal (longer) edge of the rectangle, as the number of nodes is higher compared with the interior and vertical sides of the domain. This is further demonstrated by the RWP case, where the mean degree is maximised in a ring between the regions with high and low node density.

These results were for $\lambda_0 = 10$, for a smaller average number of nodes we should expect the mean degree to mirror the profile of nodes, as the impact of interference becomes less. For larger values of γ the interference field will continue to dominate, and will act to decrease μ, see the discussion next on dense networks. Note that similar observations are expected to hold for the average achievable rate between nodes i and j given by $\mathbb{E}\left[\log[1 + SINR_{ij}]\right]$ (see Ref [Geo15]).

4.5 Dense Networks

An interesting limiting case is to study the performance when the average number of nodes $\bar{N}$ goes to infinity. First note that taking the mean number

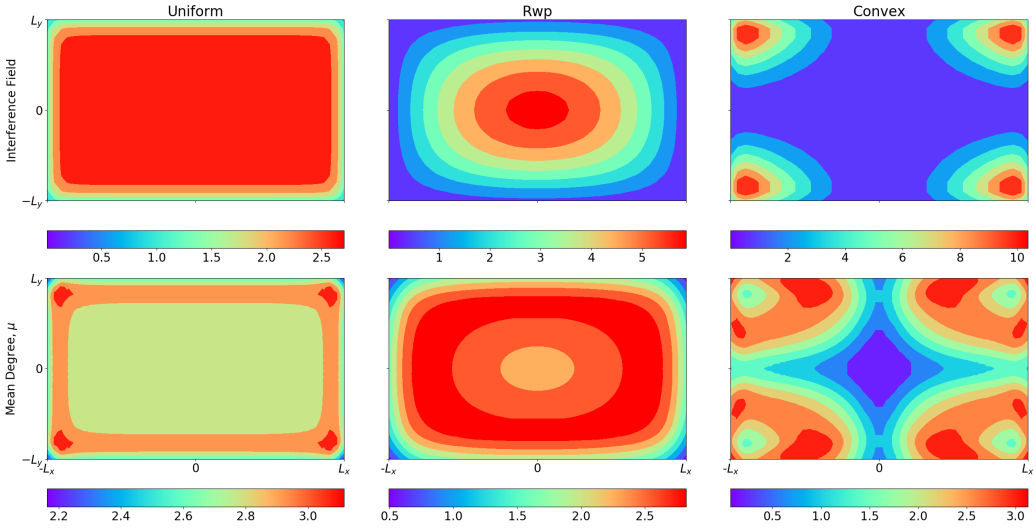

Figure 4.3: *Top panel*: The interference field in the rectangular domain for different distributions of users, assuming that the intended target is a distance $r = 0.5$ away. Bottom Panel: The mean degree in an interference-limited environment. Parameters: $\lambda_0 = 10, L_x = 5, L_y = 2.5; \eta = 4, \gamma = 0.1; q = r_0 = 1$ and $\epsilon = 0.01$.

of points to be infinite can be done by allowing $\lambda_0 \to \infty$ and fixing L_x, L_y, or fixing the density λ_0 but considering the PPP in $\mathbb{R}^2$. For simplicity we consider the case when $L_x, L_y \to \infty$, which results in $\lambda(\boldsymbol{x}) = \lambda_0$. Moreover, because we assume there will be a large proportion of interfering nodes, we neglect any noise in the channel and set $\sigma^2 = 0$ in eq.(2.17). Let us denote $\mu^*(\boldsymbol{x}) = \lim_{N\to\infty} \mu(\boldsymbol{x})$, the mean degree as the average number of nodes goes to infinity. Finally, we note for a PPP in the plane the mean degree is independent of the location of the receiver $\boldsymbol{x}_1$ due to motion invariance, where each node in the PP represents a *typical user*, therefore we can simply analyse the node at the origin. Focusing on the interference component of the connection probability given by eq.(2.17) (where r is the separation distance between a user and transmitter, and $d_{\mathcal{I}}$ is the distance between an interferer and user),

$$\begin{aligned} \mathcal{L}_{\mathcal{I}}\left(\frac{q\gamma}{g(r)}\right) &= \exp\left(-\int_A \frac{1}{1+\frac{g(r)}{q\gamma g(d_{\mathcal{I}})}}\lambda(\boldsymbol{X}_{\mathcal{I}})\mathrm{d}\boldsymbol{X}_{\mathcal{I}}\right) \\ &= \exp\left(-\int_0^{2\pi}\int_0^{\infty} \frac{\lambda_0}{1+\frac{g(r)}{q\gamma g(z)}} z\mathrm{d}z\mathrm{d}\theta\right) \end{aligned} \tag{4.13}$$

To analyse eq.(4.13) we consider the singular and non-singular path loss cases separately.

Singular path loss Model

The simplest path loss model is the singular one, which models how the signal decays with distance and is given by, $g(r) = r^{-\eta}$. By substituting $g(r)$ into eq.(4.13),

$$\begin{aligned} \mathcal{L}^*_{\mathcal{I}}\left(\frac{q\gamma}{g(r)}\right) &= \exp\left(-\frac{\pi\lambda_0 r^2\, {}_2F_1\left(1, \frac{2}{\eta}; 1+\frac{2}{\eta}; -\frac{r^\eta}{q\gamma r^\eta}\right)}{\eta-2}\right)\Bigg|_{r=0}^{\infty} \\ &= \begin{cases} \exp\left(-\frac{2\pi^2(q\gamma)^{\frac{2}{\eta}}\lambda_0 r^2 \csc\left(\frac{2\pi}{\eta}\right)}{\eta}\right) & \eta > 2, \\ 0 & \eta \leq 2. \end{cases} \end{aligned} \tag{4.14}$$

Some intuition behind this behaviour is given in Appendix D. Using the above expression for the connection probability and substituting it into eq.(4.1),

$$\begin{aligned}\mu^* &= 2\pi\lambda_0 \int_0^\infty \exp\left(-\frac{2\pi^2(q\gamma)^{\frac{2}{\eta}}\lambda_0 r^2 \csc\left(\frac{2\pi}{\eta}\right)}{\eta}\right) r\mathrm{d}r \\ &= \begin{cases} \frac{\eta \sin\left(\frac{2\pi}{\eta}\right)}{2\pi(q\gamma)^{\frac{2}{\eta}}} & \eta > 2, \\ 0 & \eta \leq 2. \end{cases}\end{aligned} \tag{4.15}$$

Since the uniform PPP in $\mathbb{R}^2$ is motion invariant, the coverage probability is independent of the users location and for $\eta > 2$ the mean degree is a constant. The intuition behind it is that adding nodes to the network seems to simultaneously scale the corresponding signal powers such that it preserves the mean degree of each node [Bac10b].

Non-singular path loss

Now consider the case $g(r) = (\epsilon + r^\eta)^{-1}$ with $\epsilon \neq 0$. Following a similar approach to before,

$$\mathcal{L}^*\left(\frac{q\gamma}{g(r)}\right) = \exp\left(-\frac{\pi\lambda_0 q\gamma(r^\eta+\epsilon)r^2\, {}_2F_1\left(1, \frac{2}{\eta}; 1+\frac{2}{\eta}; -\frac{r^\eta}{\epsilon+q\gamma(\epsilon+r^\eta)}\right)}{\epsilon + q\gamma(\epsilon + r^\eta)}\right)\Bigg|_{r=0}^{\infty} = 0 \tag{4.16}$$

Therefore, regardless of η, the mean degree tends to zero as $\lambda_0 \to \infty$. Essentially the interference from the additional nodes dominate causing every node in the network becoming isolated from every other node.

In Fig 4.4 we plot the mean degree at the centre, boundary and corner for a range of different densities, illustrating how for non-zero $\epsilon = 0$, $\mu \to 0$ under extreme densification, whilst for $\epsilon = 0$ the mean degree tends to a non-zero constant. Intuitively, this non-singular path loss model provides a greater insight into how we expect wireless communication networks to work; at low densities the mean degree is low since the total possible number of connections is also low, but as the density increases so does the mean degree.

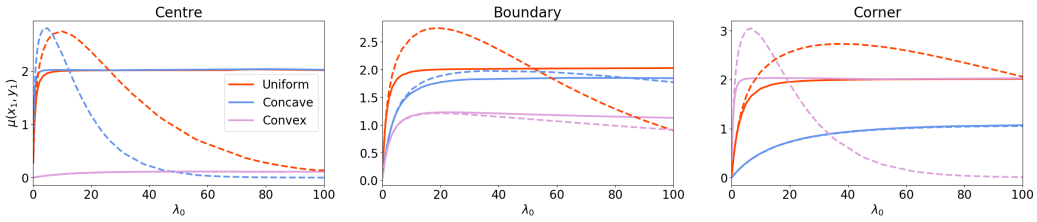

Figure 4.4: A plot of the mean degree as a function of density for three different locations in the domain for each different distribution. The dashed, solid lines are for $\epsilon = 0, 0.01$ respectively. Parameters: $L_x = 5, L_y = 2.5; \eta = 4; \gamma = 0.1, q = r_0 = 1$ and $\epsilon = 0.01$.

However, at some $\lambda_0 = \lambda_c$ the interference effects begin to dominate causing more and more link outages (smaller μ), even though there are more possible links available.

Interestingly, regardless of the value of ϵ, for $\gamma = 0.1$, the mean degree is small. Even for more advanced network protocols than ALOHA, such as carrier-sense multiple access with collision avoidance (CSMA/CA) which ensures an absence of traffic before transmission, these results are expected to hold, although the mean degree should increase (acts like a smaller value of γ). This highlights the need for effective interference management to ensure network connectivity.

4.6 Discussion

For both the disk and Rayleigh connection models the mean degree scales with λ_0. The former connection model captures the local behaviour of the network, where the mean degree can be a crude estimator of how network support nodes need to be deployed in real time. For example, if the mean degree is low at some particular location, then support nodes need to be deployed to act as a bridge between disconnected subsets to improve network connectivity, particular if we think about isolated nodes being the main obstacle to full connectivity [Pen91]. Conversely, the Rayleigh connection function captures

the long range behaviour and can become greater in more reflective environments (smaller values of η) and becomes more "local" for larger values of η ; with the limiting case being when $\eta \to \infty$ giving the disk model.

For all connection functions with no dependence on the underlying PP Φ we should expect similar behaviour; that is to say the mean degree is highest in regions with a high node density (or close by if the density is maximum near the boundary), and scales with λ_0.

A more interesting analysis is for a connection function that depends on the underlying PP Φ. For a singular path loss function the mean degree is non-decreasing with density λ_0. The mean degree increases with λ_0 to a maximum and then plateaus; whilst for $\epsilon > 0$ the mean degree is uni-modal, μ increases with λ_0 until some critical λ_c and then decays to zero. The latter reflects the percolation behaviour of the SIR graph in $\mathbb{R}^2$, where there is a critical range of densities in which there is a positive probability that the graph contains a component of infinite size [Dou06, Vaz12]. For the singular path loss model, from these results, we expect there to be a critical λ_c where for $\lambda_0 < \lambda_c$ the graph is disconnected and for $\lambda_0 > \lambda_c$ there is a positive probability that the SIR graph percolates; this remains an open problem since current results rely on $\int_0^\infty r g(r) \mathrm{d}r < \infty$ [Vaz12]. We also note that these results for the singular model are also very sensitive to the parameter η, in highly reflective mediums ($\eta \leq \dim$) where very long links can occur the aggregate interference causes outage, whilst for more local connections ($\eta > \dim$) then the mean degree is a constant.

This analysis provides insight into how connectivity of a node depends on its location and the underlying distribution of nodes in the network. Importantly, these results give us insight into the scalability of interference-limited networks under different channel conditions, and sophisticated network protocols need to be used to maximise connectivity when interference is accounted for, particular in the case of dense networks.

In the following chapter we look at how the next generation of 5G networks should be deployed to maximise user experience.

Chapter 5

Coverage in Ultra Dense Networks

In the previous chapter we discussed the *mean degree* as a metric to analyse global connectivity properties of MANETs and the interplay between mobility and boundaries. More specifically the mean degree helps to highlight areas where nodes are likely to be isolated, and we want to apply this insight into better understanding the next generation of wireless networks (5G). Here we discuss the work in Ref [Pra17] which was first posed as a problem by my co-author Dr Georgiou whilst he was working at Toshiba. Our aim here is to understand how mobility and boundaries will impact 5G networks, and ultimately use this insight to help optimise network performance in terms of user experience.

There is a general consensus that network densification, both spatially and over the frequency domain, can help cope with the expected 1000-fold increase in traffic demand over the coming decade whilst remaining cost effective [Bhu14,DR13]. By deploying smaller pico and femto cells (more generally referred to as Access Points (APs)), and making use of more diverse areas of the spectrum, a more heterogeneous network can help to improve network throughput, bring about higher data rates along with improving mobile user coverage [Bhu14]. One main advantage of utilizing a heterogeneous network

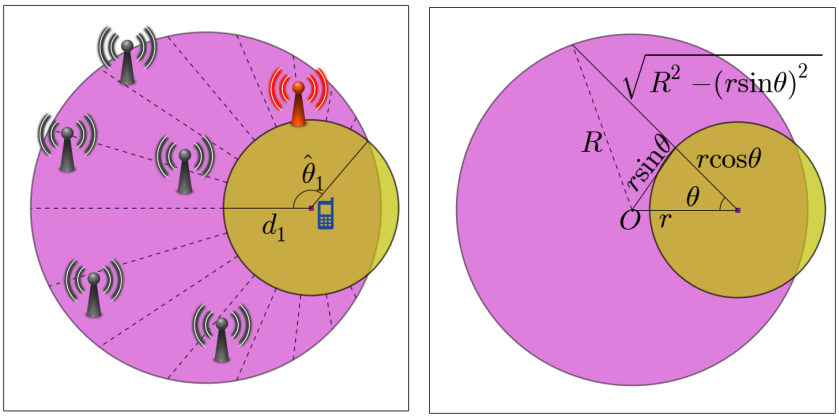

Figure 5.1: Left: A depiction of the coverage set up, with a user represented by a mobile phone connecting to its closest AP coloured red. Right: An illustration of the change of coordinates used in eq.(5.14)

is that it becomes far more scalable with network demand and has increased flexibility due to the size of APs. APs are easier to deploy since they have less restrictions both geographically and financially in comparison with BSs, whilst mobile APs (drones) can meet unusual peaks in network traffic such as during music festivals.

In general, these APs will have fewer antennas and network resources than typical BSs and thus transmit/receive data in a smaller region, to/from a smaller number of users. Moreover, location aware interference management techniques, such as making use of coordinated communication schemes (CoMP) are likely to be employed to minimise delays and improve user experience [DR13]. A typical assumption is that each AP serves the same number of users (i.e. smart devices), and since there are spatial variations in the Mobile User (MU) distribution due to mobility understanding how these APs should be deployed remains an important question. More specifically, the deployment of APs need to take into account the network traffic as a function of position, and be flexible enough to meet peak demand whilst saving resources when possible.

In this chapter we analyse how the probability a MU can connect to its

nearest AP in an ultra-dense network where the deployment of APs is non-uniform. Using this we then optimise the deployment of the APs for a given distribution of MU which can be achieved in real time networks through a thinning of the PPP. Much of this work is discussed in Ref [Pra17], with an additional analysis on dense regimes and coordinated transmission schemes.

5.1 Coverage model

We start by modelling the distribution of APs using a non-uniform PPP Φ with density $\lambda(\boldsymbol{t})$ in a circular disk $\mathcal{V} \in \mathbb{R}^2$ with radius R. For simplicity we assume that the density is given by the radially symmetric function,

$$\lambda(r) = \lambda_0 \left(1 - \frac{bR^2}{2} + br^2\right), \tag{5.1}$$

where t is the radial position, $\bar{N} = \lambda_0 \pi R^2 > 0$ is the density of APs and $b \in \left[-\frac{2}{R^2}, \frac{2}{R^2}\right]$ acts to interpolate between different distributions. A particular case of interest is when $b = -2/R^2$ which approximates the stationary distribution of the RWP in the disk [Bet03b], whilst $b = +2/R^2$ models the case when nodes are predominately found near the boundary (referred to as convex); a uniform distribution of APs is obtained by setting $b = 0$. This model provides a simple method to analyse the impact regions with high and low density, along with boundaries, have on coverage in finite domains.

The metric of focus is the K-coverage probability, the probability a MU can successfully download a message from its K nearest APs. For simplicity we neglect any interference from neighbouring MUs, and assume all interference arises from APs further away from the K^{th} nearest AP. Typically a MU will try to connect to the AP with the strongest signal, and we make the natural approximation that the strongest signal is from the closest AP to achieve a more tractable analysis[1]. For the large part we will aim to provide

[1]For a MU connecting to the AP with the strongest signal it requires the use of order statistics which often leads to a complicated approach that provides little insight. Also

any expressions in terms of a MU connecting to K APs, and discuss the special case when $K = 1$ separately. In order to proceed we first need to order all the APs in the network in terms of their distances from a MU of interest. As such let us denote the Euclidean distance between the i^{th} AP at $\boldsymbol{t}_i$ and a MU located at $\boldsymbol{r}$ as $d_i = |\boldsymbol{r} - \boldsymbol{t}_i|$ and order them such that $0 \leq d_1 \leq d_2 \leq ....$

We take the standard approach of modelling the signal from each AP as the product of the channel gain and path loss. As in Sec 2.2 we assume the channel gain is an exponential random variable with mean one, and for mathematical tractability we assume a singular path loss model and will use the insight gained from the previous chapter to discuss the qualitative changes a non-singular model would have in 5G networks at the end of this chapter. Once again we assume slotted ALOHA, which is controlled by the parameter $\gamma \in (0, 1]$ which thins the set of interfering signals.

We proceed by first calculating the nearest neighbour distribution for Φ in $\mathcal{V}$, and then the probability a MU can connect to its K nearest APs, both of which are later combined to compute the coverage probability in Sec 5.4.

5.2 Nearest neighbour distribution

The distribution to the K^{th} nearest neighbour is calculated through eq.(2.5) in Chapter2 [Sri10]. By exploiting the natural ordering of the points within our model, we only need the distribution of the K^{th} AP given the location of the $(K-1)^{\text{th}}$ AP, which we denote as $f^K_{NND}(\boldsymbol{x}, d_{K-1}, d_K)$. Recall, that this can be achieved through calculating the derivative of the contact distribution, which is the complement of the probability there are no nodes in the region. Thus, we can write the distribution of the K^{th} nearest neighbour, given the

note that this approximation is not valid for the uplink case, since in regions of higher density the AP may be closer but also be closer to other APs that may lead to outage. The directed nature of these SINR graphs make for an interesting analysis.

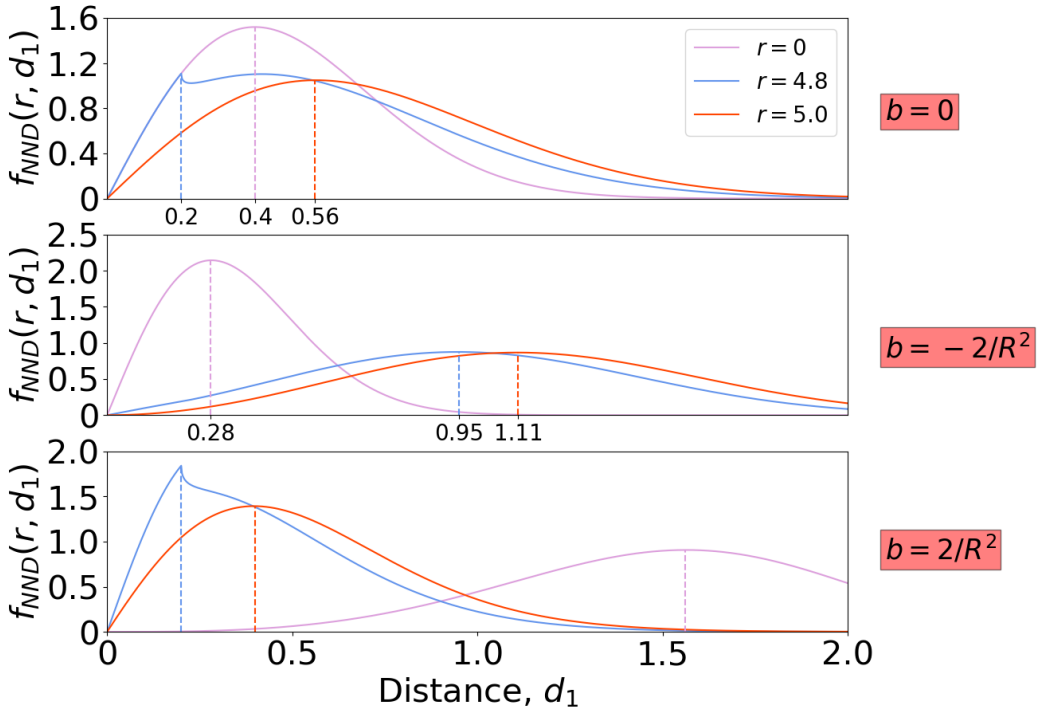

Figure 5.2: Plot of the nearest neighbour distribution given in eq.(5.10) for MUs at different distances $r \in [0, R]$ for different underlying distribution of APs: Uniform (top panel), Concave (middle), and Convex (bottom). Each plot has the same x-axis scale making for an easier comparison, with the dashed lines representing where the maximum for each case occurs. Parameters: $R = 5$ and $\lambda_0 = 1$.

location of its $K-1$ neighbours, as

$$\begin{aligned} f^K_{NND}(\boldsymbol{x}, d_{K-1}, d_K) &= -\frac{\mathrm{d}}{\mathrm{d}d_K} \exp\left(-\Lambda(\mathcal{A}_{\boldsymbol{x}}(d_{K-1}, d_K))\right), \\ &= -\frac{\mathrm{d}}{\mathrm{d}d_K} \exp\left(-\Lambda(\mathcal{B}_{\boldsymbol{x}}(d_K)) + \Lambda(\mathcal{B}_{\boldsymbol{x}}(d_{K-1}))\right), \end{aligned} \tag{5.2}$$

where $\mathcal{A}_{\boldsymbol{x}}(d_{K-1}, d_K))$ is the annulus centred at $\boldsymbol{x}$ with radius $r \in [d_{K-1}, d_K]$. In actual fact to solve the K-coverage problem we need the product, and once we cancel many of the exponential terms it can be written as,

$$\begin{aligned} f_{KNND}(\boldsymbol{x}, d_1, ..., d_K) &= f_{NND}(\boldsymbol{x}, d_1) f^2_{NND}(\boldsymbol{x}, d_1, d_2) ... f^K_{NND}(\boldsymbol{x}, d_1, ..., d_K) \\ &= \exp\Big(-\Lambda(|\mathcal{B}_{\boldsymbol{x}}(d_K) \cap \mathcal{V}|)\Big) \prod_{i=1}^{K} \frac{\mathrm{d}}{\mathrm{d}d_i} \Lambda(|\mathcal{B}_{\boldsymbol{x}}(d_i) \cap \mathcal{V}|). \end{aligned} \tag{5.3}$$

The measure of the region is a piecewise defined function dependent on $d_i, 1 \leq i \leq K$ due to the ball intersecting the boundary, see Fig 5.2 for the case $K = 1$. Explicit calculation of the mean number of points in $\mathcal{B}_{\boldsymbol{x}}(d_K) \cap \mathcal{V}$ is given below for the two cases when the ball does and does not intersect the boundary.

$$\Lambda(\mathcal{B}_{\boldsymbol{x}}(d_K) \cap \mathcal{V}) = \begin{cases} 2\pi \int_0^{d_K} \lambda(z) u \mathrm{d}u, & |\boldsymbol{x}| + d_K \leq R \\ 2 \int_{\hat{\theta}}^{\pi} \int_0^{d_K} \lambda(z) u \mathrm{d}u \mathrm{d}\theta + 2 \int_0^{\hat{\theta}} \int_0^{\hat{r}} \lambda(z) u \mathrm{d}u \mathrm{d}\theta, & \text{otherwise} \end{cases} \tag{5.4}$$

$$\Lambda(\mathcal{B}_{\boldsymbol{x}}(d_K)\cap\mathcal{V}) = \begin{cases} \pi\lambda_0 d_K^2\left(1+\frac{b}{2}d_K^2-\frac{bR^2}{2}+br^2)\right), & |\boldsymbol{x}|+d_K\le R \\ -\frac{\lambda_0}{8}\Bigg(d_K^2\big(5b\bar{d_K}+\pi\left(2b\left(R^2-2r^2\right)-4\right)\big) & \\ \quad +4bd_K^4\arctan\left[\frac{\bar{d_K}}{R^2-(d_K-r)^2}\right]-3\pi bd_K^4 & \\ \quad +2d_K^2b\left(d_K^2+4r^2-2R^2\right)\arctan\left[\frac{d_K^2+r^2-R^2}{\bar{d_K}}\right] & \text{otherwise} \\ \quad +(b(r^2-R^2)+4)\bar{d_K}-4\pi R^2 & \\ \quad +8d_K^2\arctan\left[\frac{d_K^2+r^2-R^2}{\bar{d_K}}\right] & \\ \quad +8R^2\arctan\left[\frac{-d_K^2+r^2+R^2}{\bar{d_K}}\right]\Bigg), & \end{cases} \tag{5.5}$$

where we define $\hat{\theta}=\pi-\arccos\left[\frac{r^2+d_K^2-R^2}{2d_Kr}\right]$;
$\hat{r}=-r\cos\theta+\sqrt{R^2-r^2\sin^2\theta}$; $z=\sqrt{u^2+r^2-2ru\cos(\theta)}$ and
$\bar{d_K}=\sqrt{(-d_K+r+R)\,(d_K+r-R)\,(d_K-r+R)\,(d_K+r+R)}$. The corresponding derivative of eq.(5.5) is,

$$\frac{\mathrm{d}}{\mathrm{d}d_K}\Lambda(\mathcal{B}_{\boldsymbol{x}}(d_K)\cap\mathcal{V}) = \begin{cases} \lambda_0\pi(2d_K(1+br^2)+2bd_K^3-bd_KR^2), & |\boldsymbol{x}|+d_K\le R \\ \frac{\lambda_0 d_K}{2}\Bigg(bd_K^2\left(3\pi-4\arctan\left[\frac{\bar{d_K}}{R^2-(d_K-r)^2}\right]\right) & \\ \quad -4b\bar{d_K}+\pi\left(2br^2-bR^2+2\right) & \text{otherwise;} \\ \quad -2b\left(d_K^2+2r^2-R^2\right) & \\ \quad -4\arctan\left[\frac{d_K^2+r^2-R^2}{\bar{d_K}}\right]\Bigg). & \end{cases} \tag{5.6}$$

The above two equations provide all we need to write the nearest neighbour distribution to the K^{th} neighbour given by eq.(5.3) which we will use later in calculating K-Coverage in cooperative transmission schemes[2].

[2]Remark: for the case when the ball intersects the boundary it is just as easy to work in Cartesian coordinates, particularly when calculating the derivative as we can use Leibniz's technique. Furthermore, for a large domain we can largely neglect the effect the curvature has on the disk, to simplify the above expressions; in fact, we can ignore boundaries

5.3 Probability of connection to the K^{th} nearest neighbour

We now introduce a slightly modified version of the interference-limited connection function used in Chapter 4. For this model we need to condition on the set of interferers being further away from the K^{th} nearest transmitter, which means that we also need to condition on the PP having at least $N > K$ points, namely the BPP discussed in 2.1.2.

The signal in a CoMP system is modelled as the sum of the K nearest signals, and the interference comes from all other nodes, which can be written as,

$$\begin{aligned}
\mathcal{H}(r, d_1,..., d_K) &= \mathbb{P}[\mathrm{SINR}_K \geq q | d_1, ..., d_K, \Phi(A) = N] \\
&= \mathbb{P}\left[\frac{\sum_{i=1}^{K} |h_i|^2 g(d_i)}{\sigma^2 + \gamma \sum_{j=K+1}^{N} |h_j|^2 g(d_j)} \geq q \middle| d_1, ...d_K, \Phi(A) = N \right] \\
&\overset{(1)}{=} \mathbb{E}_{\mathcal{I}_K}\left[\mathbb{P}\left[\sum_{i=1}^{K} |h_i|^2 g(d_i) \geq q(\sigma^2 + \mathcal{I}_K) \middle| d_1, ...d_K, \Phi(A) = N, \mathcal{I}_K \right] \right] \\
&\overset{(2)}{=} \mathbb{E}_{\mathcal{I}_K}\left[\sum_{m=1}^{K} \prod_{\substack{l=1 \\ l \neq m}}^{K} \left(\frac{g(d_m)}{g(d_m) - g(d_l)} \right) \exp\left(-\frac{q(\sigma^2 + \mathcal{I}_K)}{g(d_l)} \right) \right] \\
&= \sum_{m=1}^{K} \prod_{\substack{l=1 \\ l \neq m}}^{K} \left(\frac{g(d_m)}{g(d_m) - g(d_l)} \right) \exp\left(-\frac{q\sigma^2}{g(d_m)} \right) \\
&\quad \times \mathbb{E}_{|h_s|^2, g(d_s)}\left[\prod_{s=K+1}^{\bar{N}} \exp\left(-\frac{\gamma q |h_s|^2 g(d_s)}{g(d_m)} \right) \right]
\end{aligned} \tag{5.7}$$

altogether provided we are far enough away.

$$\mathcal{H}(r, d_1,..., d_K) \overset{(3)}{=} \sum_{m=1}^{K} \prod_{\substack{l=1 \\ l\neq m}}^{K} \left(\frac{g(d_m)}{g(d_m) - g(d_l)} \right) \exp\left(-\frac{q\sigma^2}{g(d_m)} \right) \mathbb{E}_{g(d_s)} \left[\frac{1}{1 + \frac{\gamma q g(d_s)}{g(d_m)}} \right]$$

$$\overset{(4)}{=} \sum_{m=1}^{K} \prod_{\substack{l=1 \\ l\neq m}}^{K} \left(\frac{g(d_m)}{g(d_m) - g(d_l)} \right) \exp\left(-\frac{q\sigma^2}{g(d_m)} \right)$$

$$\times \exp\left(-2 \int_0^{\hat{\theta}} \int_{d_K}^{\hat{R}} \frac{\lambda(z)}{1 + \frac{g(d_m)}{\gamma q g(d_s)}} d_s \mathrm{d}d_s \mathrm{d}\theta \right), \tag{5.8}$$

where (1) we make the substitution $\mathcal{I}_K = \gamma \sum_{j=K+1}^{\bar{N}} |h_j|^2 g(d_j)$, in (2) we have calculated the inner probability noticing $\sum_{i=1}^{K} |h_i|^2 g(d_i)$ can be treated as a sum of K independent exponential random variables with different means $\frac{1}{g(d_i)}$ [Bib13] and in (3) we take the expectation of $|h_s|^2$. In (4) we approximate the BPP as PPP to use the PGFL to compute the final expectation since we assume the network to be very dense. The integration region in eq.(5.8) is over the whole volume excluding the ball $\mathcal{B}_{\boldsymbol{x}}(d_K)$, and the density has been translated using the cosine rule, where $z = \sqrt{r^2 + d_s^2 - 2 r d_s \cos\theta}$, $\hat{R} = r\cos\theta + \sqrt{R^2 - r^2 \sin^2\theta}$ and $\hat{\theta} = \min\left[\arccos\left[\frac{r^2 + d_K^2 - R^2}{2 r d_K} \right], \pi \right]$. We now introduce the K-coverage probability metric.

5.4 Coverage probability

The most important metric in this chapter is the *K-Coverage probability*, that is the probability a user located at $\boldsymbol{r}$ can successfully decode the sum of the signals from its K closest APs. Namely, a user is in coverage if the $SINR$ measured at the receiver is greater than the threshold parameter q. As a result, the coverage probability can be written as averaging over all possible locations of the K intended transmitters, once again assuming the natural ordering of points with d_1 being the closest.

$$C_K(\boldsymbol{r}, b, \lambda_0 \pi R^2) = \int_0^{d_{\max}} ... \int_{d_{K-1}}^{d_{\max}} \mathcal{H}(r, d_1, ..., d_K) f_{\text{KNND}}(\boldsymbol{r}, d_1, ..., d_K) \mathrm{d}d_K ... \mathrm{d}d_1, \tag{5.9}$$

where $d_{\max} = r + R$ is the maximum separation between a MU and an AP, C_K is the coverage probability for the K nearest APs and $\mathcal{H}$ is given in eq.(5.8) and f_{KNND} in eq.(5.3). The K-Coverage probability is radially symmetric, since the distribution of APs is also radially symmetric, and as a result is governed by the radial position of the MU, the parameter b and average number of nodes in the network ($\lambda_0 \pi R^2$). In general this can only be solved numerically, even for the case when $K = 1$, with the exception when the domain is $\mathbb{R}^2$ and $\eta > 2$, which we will see later in Sec.5.5. As a result let us first consider the special case of $K = 1$, where a user connects only to its closest AP, i.e. there is no cooperative transmission scheme and all other APs (may) act as interferers.

5.4.1 Coverage in non-cooperative networks

We first begin with the nearest neighbour distribution. The nearest neighbour distribution, f_{NND} (where we drop $K = 1$ in the notation for simplicity), is obtained through eq.(5.3), by substituting the in eq.(5.5) and eq.(5.6). As an example we give the case when the distribution of users is uniform below.

$$f_{\text{NND}}(r, d_1, b = 0) = \begin{cases} 2 d_1 \lambda_0 \pi \lambda_0 \exp(-\pi \lambda_0 d_1^2) & r + d_1 \leq R, \\ \lambda_0 d_1 \left(\pi - 2 \arctan \left[\frac{d_1^2 + r^2 - R^2}{\bar{d}_1} \right] \right) & \\ \quad \times \exp\left(\frac{\lambda_0}{8} \left(\bar{d}_1 - \pi (d_1^2 + R^2) \right. \right. & \text{otherwise.} \\ \quad + 2 d_1^2 \arctan \left[\frac{d_1^2 + r^2 - R^2}{\bar{d}_1} \right] & \\ \quad \left. \left. + 2 R^2 \arctan \left[\frac{-d_1^2 + r^2 + R^2}{\bar{d}_1} \right] \right) \right) & \end{cases} \tag{5.10}$$

As before, the case when the ball does not intersect the boundary can be given in a nice compact form, when boundaries need to be accounted the expression becomes more complicated. We plot the pdf of nearest neighbour distribution for different locations $\boldsymbol{x} = (r, 0)$ in the circular domain, for a range of different parameters b in Fig.5.2.

For a node not at the centre, the pdf is a piecewise function since as the ball of radius d_1 grows, it will eventually intersect the boundary of the domain. Furthermore, both the boundary effects and the underlying distribution impact the average distance to the nearest neighbour. It is not hard to see that for a uniform PPP the average distance from a user to the nearest neighbour is much smaller compared with a user at the boundary. This behaviour indicates that you have to receive a message from an AP further away on average near the boundary; an effect which is amplified in the concave case, and mitigated somewhat in the convex case where the density of nodes near the border increases. As such the NND depends on both the location of the MU and the distribution of APs modelled by Φ, with boundary effects acting to increase it.

The remaining piece of the jigsaw is the connection probability for $K = 1$. Fortunately eq.(5.8) reduces to a much simpler form in this case,

$$\begin{aligned}\mathcal{H}(r, d_1) &= \exp\left(-\frac{q\sigma^2}{g(d_1)}\right)\exp\left(-2\int_0^{\hat{\theta}}\int_{d_1}^{\hat{R}}\frac{\lambda(z)}{1+\frac{g(d_1)}{\gamma q g(d_s)}}d_s\mathrm{d}d_s\mathrm{d}\theta\right)\\ &= \exp\left(-\frac{q\sigma^2}{g(d_1)}\right)\exp\left(-\lambda_0\int_0^{\hat{\theta}_1}\zeta(\hat{R})-\zeta(d_1)\mathrm{d}\theta\right),\end{aligned} \tag{5.11}$$

where $\hat{R} = r\cos\theta + \sqrt{R^2 - r^2\sin^2\theta}$ we define the function $\zeta(x)$ as,

$$\begin{aligned}\zeta(x) = \frac{x^2}{6}\Bigg(&6(1-\frac{bR^2}{2}+br^2)\,{}_2F_1\left(1,\frac{2}{\eta};\frac{2}{\eta}+1;-\frac{x^\eta}{d_1^\eta q\gamma}\right)\\ &+3x^2 b\,{}_2F_1\left(1,\frac{4}{\eta};1+\frac{4}{\eta};-\frac{x^\eta}{q\gamma d_1^\eta}\right)-8brx\cos\theta\,{}_2F_1\left(1,\frac{3}{\eta};1+\frac{3}{\eta};-\frac{x^\eta}{q\gamma d_1^\eta}\right)\Bigg).\end{aligned} \tag{5.12}$$

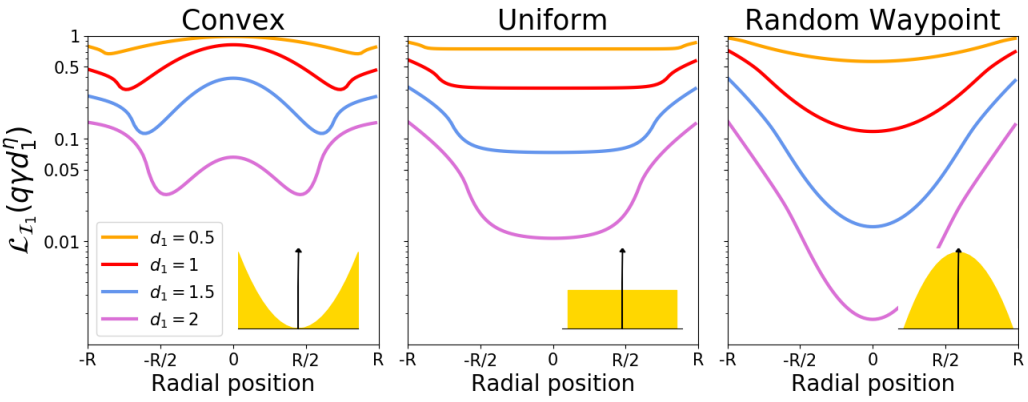

Figure 5.3: The Laplace functional from eq.(5.11) plotted as a function of radial position r for a range of fixed separation distances d_1. From left to right the value of b that determines the distribution of points in the disk are $2/R^2, 0, -2/R^2$ with the profiles of the AP distribution plotted in the lower right of each subplot. Parameters: $\eta = 6, q = 1, \gamma = 1, \lambda_0 = 1$.

In general we are left with a semi-analytic form of eq.(5.11) except at the centre where

$$\mathcal{H}(r, d_1) = \exp\left(-\frac{q\sigma^2}{g(d_1)}\right) \exp\Bigg(\frac{2d_1^2 q\gamma(2 + bd_1^2 - bR^2)}{4(1 + q\gamma)} - 4R_2^2 {}_2F_1\left(1, \frac{2}{\eta}, +\frac{2}{\eta}\frac{R^\eta}{q\gamma\, d_1^\eta}\right) + bR_2^4 {}_2F_1\left(1, \frac{4}{\eta}, 1 + \frac{4}{\eta}, \frac{R^\eta}{q\gamma\, d_1^\eta}\right)\Bigg). \tag{5.13}$$

The first term in eq.(5.11) is the usual noise term for a Rayleigh channel and does not depend to the location of the MU. The second term is the Laplace transform of the random variable $\mathcal{I}_K$ which depends on the location of the MU, the network geometry and the underlying spatial distribution of APs.

As in Sec 4 the connection probability increases when the MU is located near the boundary due to a decrease in the interference field, regardless of the underlying distribution of APs. For a nearest neighbour communication

model the impact of boundaries can have a greater impact on the connection probability since it is conditions on all other j interferers being further away than $d_1(\leq d_j)$. Conditioning on longer range communications (larger d_1) results in a reduction in the connection probability even though the interfering nodes are also further away. Intuitively this is a result of conditioning on the closest AP being d_1 away. Firstly, by conditioning on d_1 being further away, the set of interferes are a PPP restricted to the region $\mathcal{B}_{\boldsymbol{x}}(d_1)\cap\mathcal{V}$. If, say, the nearest interferer's distance can be expressed as $d_2 = d_1 + c$ for some $c > 0$ then the area of the annular region in which the nearest interferer can be is an increasing function of d_1. Therefore, the ratio d_2/d_1 is stochastically decreasing with respect to d_1 which results in the connection probability decaying to zero. Finally, in densely populated regions the connection probability drops due to interference, for example at the centre of the domain for the concave case, while the converse is also true.

Having computed both the NND and the connection probability we are in a position to calculate the coverage probability. We first re-write eq.(5.9) as

$$C(\boldsymbol{r}, b, \lambda_0\pi R^2) = \int_0^{d_{\max}} \mathcal{H}(r, d_1) f_{\mathrm{NND}}(\boldsymbol{r}, d_1)\mathrm{d}d_1, \tag{5.14}$$

where we drop the K notation for simplicity. Although the distributions and connection probability are much simpler a closed form expression still remains out of reach, so we analyse it through Fig 5.4.1.

From Fig 5.4.1 we observe that the coverage probability drops at the boundary, even though the interference field is reduced. Simply put, at the border the nearest neighbour is further away on average (see Sec.2.1.1), and the ratio of $\frac{d_k}{d_1}$ for $d_2, d_3, ...$ is closer to one, so the intended and interfering signals have a similar strength leading to outage. Near (but not at) the boundary the AP distribution can either amplify the border effects creating a *sweet spot* that maximises the coverage probability (convex) or mitigate them (concave), again which is related to ratio of the expected distances between

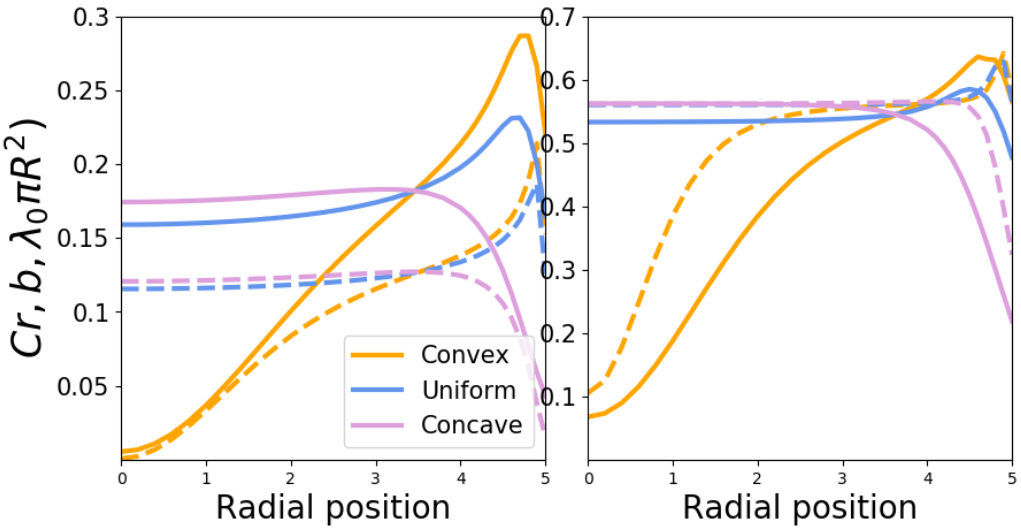

Figure 5.4: The coverage probability, eq. (5.14), as a function of radial position r from the centre to the boundary, with $\sigma^2 = q = \gamma = 1, R = 5$ and $\eta = 2, 4$ for the left and right panels respectively. The solid lines are for $\lambda_0 = 1$ and the dashed lines are for $\lambda_0 = 10$.

the transmitters and nearest interferes. This phenomenon also applies when considering the distribution of points. For example, the convex case performs extremely poorly at the centre, even though this is where the interference field is minimised, whilst the concave cases outperforms the others near the centre, even as the density increases. Therefore, even away from the boundaries it is beneficial to be closer to your nearest AP, regardless of the increased interference field in this model.

As expected from the previous chapter, for a larger path loss exponent the coverage probability increases since the signal decays more quickly therefore only nodes that are close to d_1 contribute to any meaningful interference effects. In addition, for a non-singular path loss function we should also expect that as the density increases, users in regions where the density of APs is high (e.g. centre of the concave case) will become unable to connect (they are in outage).

5.5 Dense network limits

Since this model is based on very dense networks, it is interesting to understand what happens to the location dependent coverage probability as $\bar{N} = \lambda_0 \pi R^2 \to \infty$. First note that taking the mean number of points to be infinite can be done by allowing $\lambda_0 \to \infty$ and fixing R, or $R \to \infty$ and λ_0 fixed. For simplicity we consider the case when $R \to \infty$, which results in $\lambda(r) = \lambda_0$. Moreover, because we assume there will be a large proportion of interfering nodes, we neglect any noise in the channel, setting $\sigma^2 = 0$. Let us denote $C^*(r, b, \lambda_0 \pi R^2) = \lim_{\bar{N} \to \infty} C(r, b, \lambda_0 \pi R^2)$, or in words the coverage probability as the mean number of APs goes to infinity. Recall that we use * to denote some limit as the number of nodes goes to infinity.

To compute $C^*(r, b, \lambda_0 \pi R^2)$ we need both the nearest neighbour distribution and connection probability in the dense network limit. Since we allow $R \to \infty$, this means that $b \to 0$ which allows us to use the nearest neighbour

distribution model for a uniform PPP in $\mathbb{R}^2$, given by,

$$f^*_{\text{NND}}(d_1) = 2\pi\lambda_0 d_1 e^{-\lambda_0 \pi d_1^2} \tag{5.15}$$

For the coverage probability we also need the nearest neighbour connection probability, recalling that $\hat{R} = r\cos\theta + \sqrt{R^2 - r^2\sin^2\theta}$, where we start from eq.(5.11).

$$\begin{aligned}
\mathcal{H}^*(r, d_1) &= \exp\left(-\frac{q\sigma^2}{g(d_1)}\right)\exp\left(-\int_0^{\hat{\theta}}\int_{d_1}^{\hat{R}} \frac{\lambda(z)}{1+\frac{g(d_1)}{\gamma q g(d_s)}} d_s \mathrm{d}d_s \mathrm{d}\theta\right) \\
&\underset{R\to\infty}{\longrightarrow} \exp\left(-\frac{q\sigma^2}{g(d_1)}\right)\exp\left(-\int_0^{2\pi}\int_{d_1}^{\infty} \frac{\lambda_0}{1+\frac{g(d_1)}{\gamma q g(d_s)}} d_s \mathrm{d}d_s \mathrm{d}\theta\right) \\
&= \exp\left(-\frac{q\sigma^2}{g(d_1)}\right)\exp\left(-\pi\lambda_0 d_s^2\, {}_2F_1\left(1, \frac{2}{\eta}; 1+\frac{2}{\eta}; -\frac{d_s^\eta}{q\gamma d_1^\eta}\right)\Bigg|_{d_s=d_1}^{d_s=\infty}\right) \\
&= \begin{cases} \exp\left(-\frac{q\sigma^2}{g(d_1)}\right)\exp\Bigg(-\frac{2d_1^2\pi^2\lambda_0(q\gamma)^{\frac{2}{\eta}}\csc\left(\frac{2\pi}{\eta}\right)}{\eta} \\ \qquad -\pi\lambda_0 d_1^2\, {}_2F_1\left(1, \frac{2}{\eta}; \frac{2+\eta}{\eta}; -\frac{1}{q\gamma}\right)\Bigg) & \eta > 2, \\ 0 & \eta \le 2. \end{cases}
\end{aligned} \tag{5.16}$$

Now all that remains is to combine f^*_{NND} and $\mathcal{H}^*(r, d_1)$ into eq.(5.14) to obtain $C^*(r, b, \lambda_0\pi R^2)$. Through direct application of eq.(5.14) we obtain,

$$\begin{aligned}
C^*(r, b, \lambda_0\pi R^2) &= \int_0^{\infty} f^*_{\text{NND}}(d_1, r)\mathcal{H}^*(r, d_1)\mathrm{d}d_1 \\
&= \begin{cases} 0 & \text{for } \eta \le 2, \\ \frac{1}{1+\frac{2q\gamma\, {}_2F_1\left(1,1-\frac{2}{\eta};2-\frac{2}{\eta};-q\gamma\right)}{\eta-2}} & \text{for } \eta > 2. \end{cases}
\end{aligned} \tag{5.17}$$

Some interesting particular cases include when $q = \gamma = 1, \eta = 4$, $C^*(r, b, \lambda_0\pi R^2) =$

$\frac{4}{4+\pi}$ and $\eta = 6$, $C^*(r, b, \lambda_0 \pi R^2) = \frac{9}{9+\sqrt{3}\pi \log[8]}$. A similar result can be found by taking $\lambda_0 \to \infty$ and taking R to be fixed. In this case, by using the average spacing between points scales like $\frac{1}{\sqrt{\lambda_0}}$, and making the approximation that boundary effects only matter *at* the boundary, one can show a similar result. This approach takes far more steps, but does allow for the coverage probability to be zero at points where the density is zero for $\eta >$ dimension.

From the numerics shown in Fig 5.5 we see that for $\eta = 2$, $C^*(r, b, \lambda_0 \pi R^2) \to 0$. This is again an example of when the path loss exponent is equal to or less than the dimension the global behaviour dominates and the interference field diverges. However, for $\eta > 2$, $C^*(r, b, \lambda_0 \pi R^2) \to$ constant since only a smaller neighbourhood of nodes contribute to the interference and thus it encapsulates the more local behaviour of the network. The bottom panel of Fig 5.5 shows some variation in regions near where the distribution of APs goes to zero; for the path loss exponent less than or equal to the dimension the coverage goes to zero much faster. As more nodes get added to the network, the additional interference counteracts the increased proximity of the transmitting node. For non-singular path loss model we should expect the coverage probability to tend to zero everywhere for $\lambda_0 \pi R^2 \to \infty$.

5.6 Optimal Coverage Probability

An interesting question that arises from this work, is *what is the optimal distribution of APs to meet network demands?* Provided we have some prior knowledge to the distribution of MUs at a particular instant, then we should be able to optimise how we deploy the APs. For simplicity we model the distribution of APs in a similar fashion to users so we can interpolate between the two cases when APs are predominantly near the boundary (convex) or centre (convex). Therefore, let the distribution of MUs be given by,

$$\rho(r) = \rho_0(1 + \frac{\hat{b}R^2}{2} - \hat{b}r^2) \tag{5.18}$$

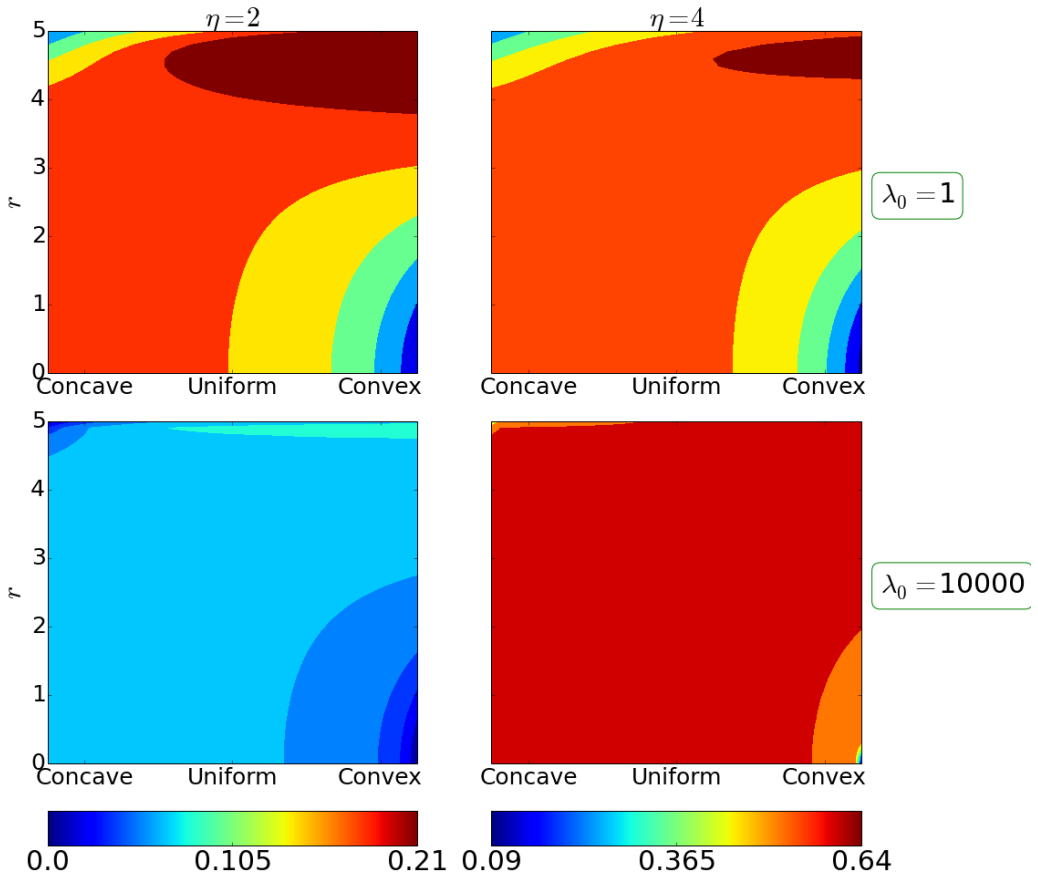

Figure 5.5: Surface plot of the coverage probability as function of radial position r (vertical) and AP distribution b (horizontal) as expressed in eq.(5.17). The system is assumed to be Noise free, or alternatively the interference from neighbouring nodes dominates. The left and right panels show the coverage probability for different path loss exponents $\eta = 2, 4$, whilst the top and bottom panel have different densities $\lambda_0 = 1, 10000$ respectively. The disk has radius $R = 5$ and the constant in the bottom right panel (dark red region away from regions where the density is zero) is $\frac{4}{4+\pi}$.

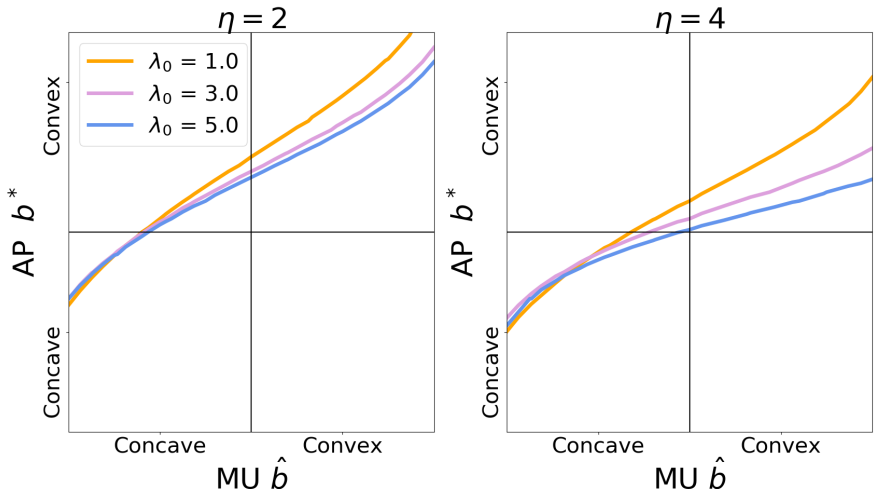

Figure 5.6: The optimal distribution of AP given a deployment of MU for different λ_0 with $R = 5$, and $\eta = 2, 4$ for the left and right panel respectively.

where $\hat{b}$ plays much the same role as b does in eq.(5.1), whilst ρ_0 is the density of APs. The average coverage, denoted as $\bar{C}$, is obtained by averaging over the distribution of MUs

$$\bar{C}(b, \hat{b}, \lambda_0 \pi R^2) = \frac{2}{R^2} \int_0^R \rho(r) C(r, b, \lambda_0 \pi R^2) r \mathrm{d}r \tag{5.19}$$

We can maximise eq. (5.19) to give the optimal value of b

$$b^*(\eta, \hat{b}, \lambda_0 \pi R^2) = \arg\max_b \bar{C}(b, \hat{b}, \lambda_0 \pi R^2), \tag{5.20}$$

conditioned on $\eta, \hat{b}$ and density of APs λ_0 in $\mathcal{V}$.

When the spatial distribution of MUs is convex (representing the demand of data in the downlink), the network architecture (in terms of the distribution APs) should also be convex (representing the supply of data in the downlink). However, when the MUs are located near the boundaries of the domain, then the AP distribution should be closer to uniform. This is

again a consequence of the trade-off between interference and boundary effects. The role of η also plays an important role, the performance of a 5G network with a uniform deployment of APs improves as η increases. One can see this by considering the limiting case as $\eta \to \infty$, which is simply the disk connection model, and provided the density of APs is dense enough, each MU should easily be served. Finally, as the network becomes increasingly dense, the optimal distribution of APs can be achieved through a uniform deployment, as we would expect from eq.(5.17).

These results highlight how the spatial densification of networks can bring about improved network performance, particularly with 5G in mind. For instance, in a city such as New York where $\eta \approx 6$ [3]then a uniform deployment of APs would meet network demands well, although the density of APs would need to be higher due to the increased network traffic. For areas where η is typically smaller then a more intelligent network needs to be deployed, in order to meet demand and not waste resources. For example, a real time thinning of the APs could be used to optimise network resources as the distribution of MUs goes from concave during work-hours to convex at night time.

We now return to the CoMP network, and aim to compare its performance with the non-cooperative case.

5.7 Cooperative Multi Point Network

In general when there are K cooperative APs, the coverage probability is given by eq.(5.14). Even for the simplified case when $K = 2$ for the K-coverage probability in $\mathbb{R}^2$, provided $\eta > 2$, then the connection function

[3]The large path loss is a result of the large number of high-rise buildings obstructing signal propagation.

remains a complicated expression.

$$\begin{aligned}\mathcal{H}(r,d_1,d_2) &= \sum_{m=1}^{2}\prod_{\substack{l=1\\l\neq m}}^{2}\left(\frac{g(d_m)}{g(d_m)-g(d_l)}\right)\exp\left(-\frac{q\sigma^2}{g(d_m)}\right)\\ &\times\exp\left(-\int_0^{\hat{\theta}}\int_{d_2}^{\hat{R}}\frac{\lambda(z)}{1+\frac{g(d_m)}{\gamma q g(d_s)}}d_s\mathrm{d}d_s\mathrm{d}\theta\right)\\ &= \left(\frac{d_2^{\eta}}{d_2^{\eta}-d_1^{\eta}}\right)\exp\left(-\frac{q\sigma^2}{g(d_1)}\right)\\ &\times\exp\left(-\frac{\lambda_0 q\gamma 2\pi d_2^{2-\eta}d_1^2\,{}_2F_1\left(1,\frac{\eta-2}{\eta};2-\frac{2}{\eta};-q\gamma\left(\frac{d_1}{d_2}\right)^{\eta}\right)}{\eta-2}\right)\\ &+\left(\frac{d_1^{\eta}}{d_1^{\eta}-d_2^{\eta}}\right)\exp\left(-\frac{q\sigma^2}{g(d_2)}\right)\\ &\times\exp\left(-\frac{\lambda_0 q\gamma 2\pi d_2^2\,{}_2F_1\left(1,\frac{\eta-2}{\eta};2-\frac{2}{\eta};-q\gamma\right)}{\eta-2}\right)\end{aligned}\tag{5.21}$$

which when substituted in eq.(5.14) leads to an intractable solution. As a result we rely on numerical integration and simulations to analyse the performance of K cooperative networks. From Fig 5.7 we see that, as we might expect, the coverage probability improves under a cooperative transmission scheme, with some of the more significant improvements coming for convex case.

Next let us discuss the case when the user connects to its nearest AP, and the remaining $K-1$ APs turn off to reduce the impact of interference. In this case, the connection probability is the same as that expressed in eq.(5.11) except the radial integral is from d_K to $\hat{R} = r\cos\theta + \sqrt{R^2 - r^2\sin^2\theta}$.

$$\mathcal{H}_g(r,d_1,d_K) = \exp\left(-\frac{q\sigma^2}{g(d_1)}\right)\exp\left(-2\int_0^{\hat{\theta}}\int_{d_K}^{\hat{R}}\frac{\lambda(z)}{1+\frac{g(d_1)}{\gamma q g(d_s)}}d_s\mathrm{d}d_s\mathrm{d}\theta\right),\tag{5.22}$$

where $z = \sqrt{d_s^2 + r^2 - 2d_s r\cos\theta}$. The coverage probability in this case is

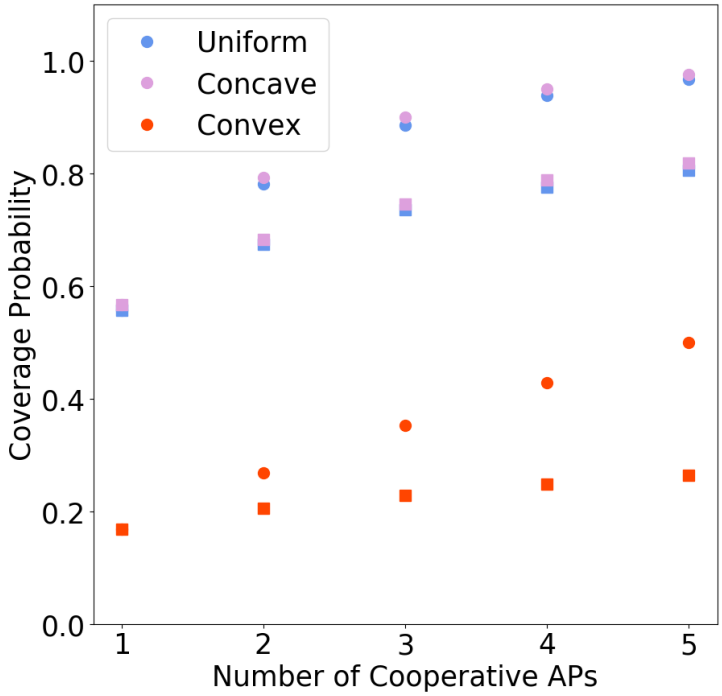

Figure 5.7: The coverage probability for a CoMP scheme, with parameters : $R = 5$, $\lambda_0 = 1$, $\eta = 4$ and $\gamma = q = 1$. The circle markers are the K-coverage probability while the square markers are the nearest neighbour AP coverage probability with the next $K - 1$ AP turned off.

calculated by averaging over the possible locations of the K^{th} AP, and then averaging over the locations of d_1 as before. Here we use the the distribution of the K^{th} AP conditioned on the location of d_1 which is given by eq.(5.2). This allows us to write the coverage probability as,

$$C(r,b,\lambda_0\pi R^2)=\int_0^{R_{\max}}\int_{d_1}^{R_{\max}} f_{NND}(d_1,r)f_{KNND}(d_K,d_1,r)\mathcal{H}_g(r,d_1,d_K)\mathrm{d}d_K\mathrm{d}d_1. \tag{5.23}$$

As before we analyse the above equation numerically and plot the results in Fig 5.7, where we focus on the case when a MU is located at the centre of the circular domain. First, the coverage probability for the uniform case (blue) improves for higher larger values of K, as the set of interferers are now further away on average compared with our initial model ($K = 1$), a similar result is observed for the concave case (purple). Interestingly the coverage probability improves very little for large K in the convex case, largely due to the main obstacle in connecting being the nearest AP being so far away rather than the interference field.

5.8 Discussion

In order for the next generation of wireless networks to deliver the anticipated improvements in network performance it is likely to be ultra dense and have many network tiers. The network demand is likely to be non-uniform as is the distribution of users. We explore how a simple adaptive transmission scheme should be used to achieve the necessary network flexibility, by a simple thinning of APs to ensure optimal coverage. In highly populated regions, such as city centres during work/shopping hours, there also needs to be a large number of APs to serve users, with additional nodes being activated to meet demand during peak times. Conversely, when the population tends to disperse, for example in the evenings as people return home, a more uniform approach is sufficient, with only an increased number of APs needed

in densely populated areas like tower blocks etc. This can be viewed as having multiple smaller disks with a concave distribution of APs in a larger area which outside these hotspots is uniform. Alternatively, APs near the boundary, of in sparsely populated regions should increase their transmission power, and thus their radius of coverage.

In addition we also discuss the limiting values of the coverage probability in ultra dense networks in terms of the path loss exponent, observing a transition when the path loss exponent η equals the dimension. We should expect our analysis for the optimal distribution of APs to still hold for different path loss models, but the coverage probability may be much less. For example, from the previous chapter we saw that for the non-singular path loss then we should expect the coverage to decay to zero regardless of η, and both [AlA17] and [Zha15] show under different path loss models (stretched exponential and multi-slop path loss respectively) the coverage goes to zero in the dense network limit.

Naturally, by using a collaborative transmission scheme the coverage probability increases, whilst we should also expect improvements in network performance with more sophisticated interference management techniques.

Chapter 6

Low Power Wide Area Networks

In this chapter we explore an open problem that has recently seen a rapid growth in interest since Ref [Geo17] where they show that Long Range (LoRa) networks, which is an example of the more general Low Power Wide Area Network (LPWAN), do not scale with the number of devices. A LoRa network consists of a NetServer, gateways and end devices forming a star of star network with the leaves being the end devices [Geo17], an illustrative example is given in Fig 6.1. Devices within these networks connect to a gateway if they meet both a noise condition, and the signal is four times the maximum interfering signal. This connection model differs from the ones previously considered in two key ways: firstly it is in the uplink, so we know the location of the receiver but not necessarily the transmitter, and secondly, instead of a product of signals, we are only concerned with the maximum interfering one.

In this chapter we first model a LoRa network with a single gateway, and discuss how our calculations can be further generalised to multiple gateways. For the single gateway model we consider a set of mobile wireless devices (transmitters) trying to connect to a single gateway (receiver) located at the centre of a circular domain and analyse the connection probability and

SF	**Packet air-time ms**	**Transmits per hour**	**SNR** q_{SF} dBm
7	36.6	98	-6
8	64	56	-9
9	113	31	-12
10	204	17	-15
11	372	9	-17.5
12	682	5	-20

Table 6.1: A table taken from [Geo17] on some features on the spreading factors in LoRa networks

coverage probability in the uplink case. One of the main reasons why LoRa networks are so popular in the deployment of smart technologies is due to them having variable data rates which help to improve network coverage and/or energy consumption [Geo17]. That is to say, the further away you are from the gateway the slower the data rate is which helps to improve the probability of its success [Geo17]. The length of the transmission is determined by the spreading factor (SF) and each increment in spreading factor doubles the length of time needed to transmit the same amount of data [Fia18]. To summarise, MUs that are far from the gateway in which they wish to communicate have a high spreading factor resulting in the time for data transmission being much longer, allowing communication over larger distances. For the finer details on how end devices associate and transmit to their nearest gateway in these networks the reader is referred to Ref [Raz17, Van15, Aug16, Fia18],. We depict these variable data rates with the different coloured annuli in Fig. 6.1, with the furthest annulus having the highest SF.

The following work was done during a three month placement at Toshiba in collaboration with the authors of Ref [Geo17] to extend previous work to networks with non-uniform deployments of end devices and multiple gateways.

6.1 Single Gateway System Model

Consider a PPP Φ with intensity $\lambda(\boldsymbol{x})$ in a circular domain $\mathcal{V}$ with radius R, with mean number of points $\bar{N} = \Lambda(\mathcal{V})$, let the distance from the closest node be denoted as $d_1, d_2, ...$ Assume $\boldsymbol{x} = (x, 0)$ (in polar coordinates) is not part of Φ, and is located in the annulus

$$\mathcal{A}(\boldsymbol{x}) = \{l_{\min}(x) \leq x \leq l_{\max}(x), \theta \in [0, 2\pi) : \{x, \theta\}\} \tag{6.1}$$

which has mean number of points given by $\Lambda(\mathcal{A}_{\boldsymbol{x}}(l_{\min}, l_{\max}))$. For simplicity we relax the notation for the annulus and write it as $\mathcal{A}(x)$ in the subsequent analysis. Consider the gateway to be at the centre of the domain, with m different regions each with an assigned different q_{SF}, see Fig 6.1. To make it easier analysing the q_{SF} we use a modified version of the path loss function $g_L(r) = (\psi/(4\pi r))^{\eta}$, where ψ is the carrier wavelength, and we use the subscript L to differentiate it from the normalised model before. Finally, let γ be a thinning on Φ, which is usually observed to be small ($\gamma \approx 0.01$) [Geo17].

6.2 Connection Probability for a single gateway

An end device can connect to a particular gateway if and only if the following two criteria are satisfied [Geo17]:

1. The received $SNR \geq q_{SF}$ at the gateway where q_{SF} is a threshold parameter that depends on the location of the end user.

2. The received signal is four times stronger than the maximum interfering node with the same spreading factor (SF).

The first criterion describes the quality of the channel and is independent of the underlying distribution of points and we denote this probability $\mathcal{H}_0$.

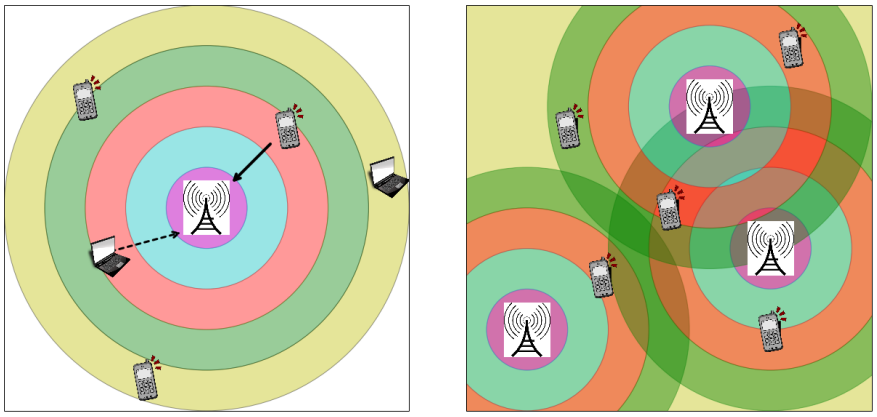

Figure 6.1: Left: An example of a LoRa network with a single gateway, where the different colour annuli represent different spreading factors q_{sf} increasing with r, the solid line the intended uplink of a device, and the dashed line the maximum interfering signal. Right: An example of a situation of multiple gateways, where again the colours represent different spreading factors.

The spreading factor is determined on the separation distance between the end user and gateway. A higher q_{SF} means a lower receiver sensitivity (a gateway and end user can transmit over longer distances) but at the cost of a longer packet air-time and the number of transmits per hour, see Table 6 taken from [Geo17]. Assuming a Rayleigh channel model then we obtain an identical expression to that in Table 2.1.

$$\mathcal{H}_0(x) = \mathbb{P}\left[SNR \geq q_{SF} \middle| x\right] = \exp\left(-\frac{q_{SF}\sigma^2}{\mathcal{P}_1 g_L(x)}\right). \tag{6.2}$$

We note however, that q_{SF} does depend on the location of the end-user in relation to the gateway.

The second criterion, denoted $\mathcal{H}_1$ gives a far more involved expression, and unlike previous models, the signal only needs to be four times that of the maximum interfering signal.

$$\mathcal{H}_1(x) = \mathbb{P}\left[\frac{|h_x|^2 g_L(x)}{\max_{k\in\Phi(\mathcal{A}(x))}|h_k|^2 g_L(d_k)} \geq 4 \middle| \Phi(\mathcal{A}(x)) \neq 0\right] + 1 \cdot \mathbb{P}\left[\Phi(\mathcal{A}(x)) = 0\right] \tag{6.3}$$

$$\begin{aligned}\mathcal{H}_1(x) &= \mathbb{E}_{d_k^*,|h_k^*|^2}\left[\exp\left(-\frac{4|h_k^*|^2 g(d_k^*)}{g_L(d_1)}\right)\right]\cdot(1-e^{-\gamma\Lambda(\mathcal{A}(x))})+e^{-\Lambda(\gamma\mathcal{A}(x))} \\ &= \mathbb{E}_{Z_k^*}\left[\exp\left(-\frac{4Z_k^*}{g_L(d_1)}\right)\right]\cdot(1-e^{-\gamma\Lambda(\mathcal{A}(x))})+e^{-\gamma\Lambda(\mathcal{A}(x))},\end{aligned} \tag{6.4}$$

where k^* denotes the node with the maximum signal, and Z_k^* denotes the maximum interfering signal and has distribution $F_{Z_k}(z)$. The second term is the probability that the annulus which the end user is in is empty; in this case it does not have to compete with any interfering signals and always connects. To calculate $F_{Z_k}(z)$ we follow a similar approach to that in Ref [Geo17], and outline it below for completeness. The pdf of the distance to a user located at d_i within the same annulus as the end user can be written as

$$f_{d_i}(x) = 2\pi d_i \lambda_{d_i}(x), \tag{6.5}$$

where $\lambda_{d_i}(x)$ is the original distribution of end users in the domain that is normalised according to the annulus in which x lies, i.e $\lambda_0 = \frac{\bar{N}}{\Lambda(\mathcal{A}(\boldsymbol{x}))}$where $l_{\min}, l_{\max}$ are the minimum and maximum of the radius of the annuli in which $\boldsymbol{x}$ lies. Transforming this pdf in terms of the path loss function $g_L(.)$ gives

$$\begin{aligned}f_{g_L}(y) &= 2\pi\lambda_0\left(1-\frac{bR^2}{2}+b\left(\frac{\psi}{4\pi}\right)^2 y^{-\frac{2}{\eta}}\right)\left(\frac{\psi}{4\pi}\right)y^{-\frac{1}{\eta}}\frac{-1}{\eta}\left(\frac{\psi}{4\pi}\right)y^{-\frac{1}{\eta}-1} \\ &= \frac{2\pi\lambda_0}{\eta}\left(1-\frac{bR^2}{2}+b\left(\frac{\psi}{4\pi}\right)^2 y^{-\frac{2}{\eta}}\right)\left(\frac{\psi}{4\pi}\right)^2 y^{-\frac{2}{\eta}-1}.\end{aligned} \tag{6.6}$$

Calculating the pdf of the product of $f_g(\cdot)$ and the channel gain is done by

using the standard expression for multiplying continuous random variables.

$$\begin{aligned}
f_Z(z) &= \int_{-\infty}^{\infty} f_X(x) f_Y\left(\frac{z}{x}\right) \frac{1}{|x|} \mathrm{d}x \\
&= \int_{g_L(l_{\min}(x))}^{g_L(l_{\max}(x))} \lambda_{g_L}(x,y) e^{-\frac{z}{y}} \frac{1}{|y|} \mathrm{d}y \\
&= \int_{g_L(l_{\min}(x))}^{g_L(l_{\max}(x))} -\frac{2\pi\lambda_0}{\eta} \left(1 - \frac{bR^2}{2} + b\left(\frac{\psi}{4\pi}\right)^2 y^{-\frac{2}{\eta}}\right) \left(\frac{\psi}{4\pi}\right)^2 y^{-\frac{2+2\eta}{\eta}} e^{-\frac{z}{y}} \mathrm{d}y \\
&= \frac{2\pi\lambda_0}{\eta} \left(\frac{\psi}{4\pi}\right)^2 \left[\left(1 - \frac{bR^2}{2}\right) \Gamma\left[\frac{\eta+2}{\eta}, \frac{z}{y}\right] z^{-\frac{2}{\eta}-1} \right. \\
&\quad \left. + b\left(\frac{\psi}{4\pi}\right)^2 \Gamma\left[\frac{\eta+4}{\eta}, \frac{z}{x}\right] z^{-\frac{4}{\eta}-1}\right]_{y=g_L(l_{\max}(x))}^{y=g_L(l_{\min}(x))}.
\end{aligned} \tag{6.7}$$

Integrating with respect to z once more to obtain the CDF, we obtain

$$\begin{aligned}
F_Z(z) &= \frac{2\pi\lambda_0}{\eta} \left(\frac{\psi}{4\pi}\right)^2 \left[\left(1 - \frac{bR^2}{2}\right) \frac{\eta}{2} \left(y^{-\frac{2}{\eta}}(e^{-\frac{z}{y}} - 1) - \Gamma\left[\frac{\eta+2}{\eta}, \frac{z}{y}\right] z^{-\frac{2}{\eta}}\right) \right. \\
&\quad \left. + b\left(\frac{\psi}{4\pi}\right)^2 \frac{\eta}{4} \left(y^{-\frac{4}{\eta}}(e^{-\frac{z}{y}} - 1) - \Gamma\left[\frac{\eta+4}{\eta}, \frac{z}{y}\right] z^{-\frac{4}{\eta}}\right)\right]_{y=g_L(l_{\max}(x))}^{y=g_L(l_{\min}(x))} \\
&= \pi\lambda_0 \left(\frac{\psi}{4\pi}\right)^2 \left[\left(1 - \frac{bR^2}{2}\right) \mathcal{Q}(y,2) + \frac{b}{2}\left(\frac{\psi}{4\pi}\right)^2 \mathcal{Q}(y,4)\right]_{y=g_L(l_{\max}(x))}^{y=g_L(l_{\min}(x))},
\end{aligned} \tag{6.8}$$

where we have defined $\mathcal{Q}(y,\alpha) = \left(y^{-\frac{\alpha}{\eta}}(e^{-\frac{z}{y}} - 1) - \Gamma\left[\frac{\eta+\alpha}{\eta}, \frac{z}{y}\right] z^{-\frac{\alpha}{\eta}}\right)$. The number of points in a particular annulus is a Poisson random variable with mean $\gamma\Lambda(\mathcal{A}(x)) = \gamma\lambda_0|\mathcal{A}(x)|$ (recall γ is a thinning of Φ). Furthermore, the cumulative density function (CDF) of the maximum of n i.i.d. random

variables is the product of n CDFs. That is,

$$\begin{aligned} F_{Z_k^*}(z) &= \sum_{k=1}^{\infty} [F_Z(z)]^k \frac{(\gamma\Lambda(\mathcal{A}(z)))^k e^{-\gamma\Lambda(\mathcal{A}(z))}}{k!} \frac{1}{1-\exp(-\gamma\Lambda(\mathcal{A}(z)))} \\ &= \frac{1}{1-\exp(-\gamma\Lambda(\mathcal{A}(z)))} e^{-\gamma\Lambda(\mathcal{A}(z))} \left(e^{\gamma\Lambda(\mathcal{A}(z))F_Z(z)} - 1\right), \end{aligned} \tag{6.9}$$

where $F_{Z_k^*}(z)$ is the CDF of the *maximum* interfering signal. Substituting this into eq.(6.4) gives,

$$\begin{aligned} \mathcal{H}_1(x) &= \mathbb{E}_{Z_k^*}\left[\exp\left(-\frac{4Z_k^*}{g_L(x)}\right)\right] + e^{-\gamma\Lambda(\mathcal{A}(x))} \\ &= \exp\left(-\frac{4z}{g_L(d_1)}\right) F_{Z_k^*}(z)\Big|_0^{\infty} \\ &+ \frac{4}{g_L(x)} \int_0^{\infty} \exp\left(-\frac{4z}{g_L(x)}\right) F_{Z_k^*}(z)\mathrm{d}z + e^{-\gamma\Lambda(\mathcal{A}(x))} \\ &=^{(1)} \int_0^{\infty} \exp\left(-\hat{z}\right) F_{Z_k^*}\left(\frac{g_L(x)\hat{z}}{4}\right) \mathrm{d}\hat{z} + e^{-\gamma\Lambda(\mathcal{A}(x))}. \end{aligned} \tag{6.10}$$

In (1) we use the definition of the CDF and make the substitution $\hat{z} = \frac{g_L(x)}{4} z$, which matches that in [Geo17] when the density is uniform. Clearly this connection function is far more complicated than the one given previously by averaging over the interference from all users, and as such any further calculations like the mean degree or coverage would be intractable using eq.(6.10). As such, we now focus on trying to approximate the connection function with interference below.

6.2.1 A Sparse approximation

For low densities, or else small γ as is often the case, we approximate node closest to the gateway to have the strongest interfering signal.

$$\mathcal{H}_1(x) \approx \mathbb{E}_{d_k^*}\left[\frac{1}{1+\frac{4g_L(d_k^*)}{g_L(x)}}\right] \cdot (1-e^{-\Lambda(\mathcal{A}(x))}) + e^{-\Lambda(\mathcal{A}(x))} \tag{6.11}$$

$$\mathcal{H}_1(x) = \int_{\mathcal{A}(x)} \frac{1}{1+\frac{4g_L(z)}{g_L(x)}} f_{NND}(z)\mathrm{d}z \cdot (1-e^{-\gamma\Lambda(\mathcal{A}(x))}) + e^{-\gamma\Lambda(\mathcal{A}(x))}, \tag{6.12}$$

where $f_{NND}(x)$ denotes the nearest neighbour distribution in the corresponding annulus and is calculated by differentiating the void probability and taking its absolute value. We observe $f_{NND}(x)$ is given by,

$$f_{NND}(x) = \frac{2\pi\lambda_0\gamma}{\Lambda(\mathcal{A}(x))}\left(\left(1-\frac{bR^2}{2}\right)x - bx^3\right) e^{-\pi\lambda_0\gamma\left(\left(1-\frac{bR^2}{2}\right)(x^2-l_{\min}^2(x))+\frac{b}{2}\left(x^4-l_{\min}^4(x)\right)\right)}. \tag{6.13}$$

The expression is a good approximation when the value of γ is small due to the sparsity of interfering nodes. This yields an approximation for $\mathcal{H}_1$,which can be written as,

$$\mathcal{H}_1(x) \approx -\int_{\mathcal{V}(x)} \frac{1}{1+\frac{4g(z)}{g(x)}} \frac{\mathrm{d}}{\mathrm{d}z} e^{-\Lambda(A(x,z))}\mathrm{d}z \cdot (1-e^{-\Lambda(\mathcal{A}(x))}) + e^{-\Lambda(\mathcal{A}(x))}, \tag{6.14}$$

where $V(l_{\min}(x), z)$ is the reduced annulus with radial limits $[l_{\min}(x), x]$, and $\Lambda(\cdot)$ represents the intensity measure for a general non-uniform PPP in V. It turns out this approximation works well for small $\wp$, particularly when the end user is close to the gateway.

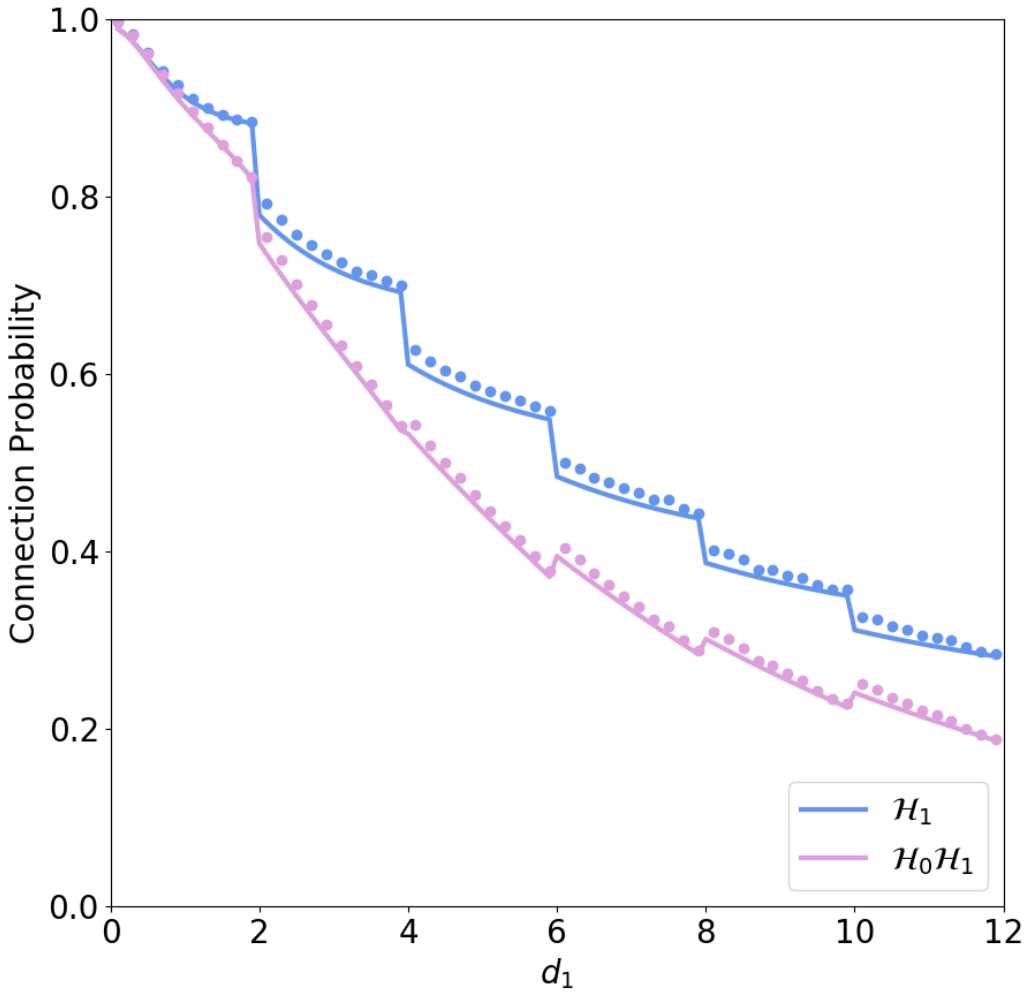

Figure 6.2: The connection probability $\mathcal{H}_0(x), \mathcal{H}_1(x)$. The parameters are chosen identical to those in Ref [Geo17]: $g_L(x) = \left(\frac{\psi}{4\pi x}\right)^{\eta}; \eta = 2.7; b = 0; \gamma = 0.01; P_1 = 19dBm; \sigma^2 = -174 + 6 + \log_{10}[125000], R = 12km$ and $\psi = \left(\frac{3\times10^5}{868\times10^6}\right) km$. Note that the wavelength ψ is expressed in the ratio of the speed of light in km/s and the frequency of the carrier wave. The markers are simulated points and the lines are approximations given in eq.(6.14).

6.2.2 Coverage

As in Sec 5 we can define the coverage probability that an end device is in coverage, which is now the uplink case,

$$C_1(\lambda_0 \pi R^2, b) = \frac{2\lambda_0}{R^2} \int_0^R \mathcal{H}(x) \left(1 - \frac{bR^2}{2} + bx^2\right) x \mathrm{d}x. \tag{6.15}$$

The number of end devices increases, the coverage probability decreases, as is shown in Fig 6.3 . For a fixed annulus assignment where the spacing between annuli is fixed, the coverage probability is better for those networks where the density is highest near the boundaries.

6.3 Discussion

Ref [Geo17] gives a semi-analytic expression for the connection probability and a crude approximation for the coverage using a first order expansion.

Looking at the problem in detail, it appears that when the thinning of the point process is high, the network becomes very sparse and we can approximate the strongest interferer as the closest one within the corresponding annulus. This method provides some initial insight into the problem with a far more tractable solution.

For non-sparse networks, the connection probability can only be given in semi-analytic form, as was shown in [Geo17]. Adding increased complexity in terms of a non-uniform density of users comes at little cost, since everything remains semi-analytic and the numerical computation is very similar.

We should expect by adding more gateways and increasing the network diversity, the coverage probability should improve. For the case where the gateways are identical then this problem follows the analysis done in this section, however a more interesting problem would be where the gateways are different and have different spreading factors at different distances. This would mean an end user wouldn't associate to its nearest gateway but one

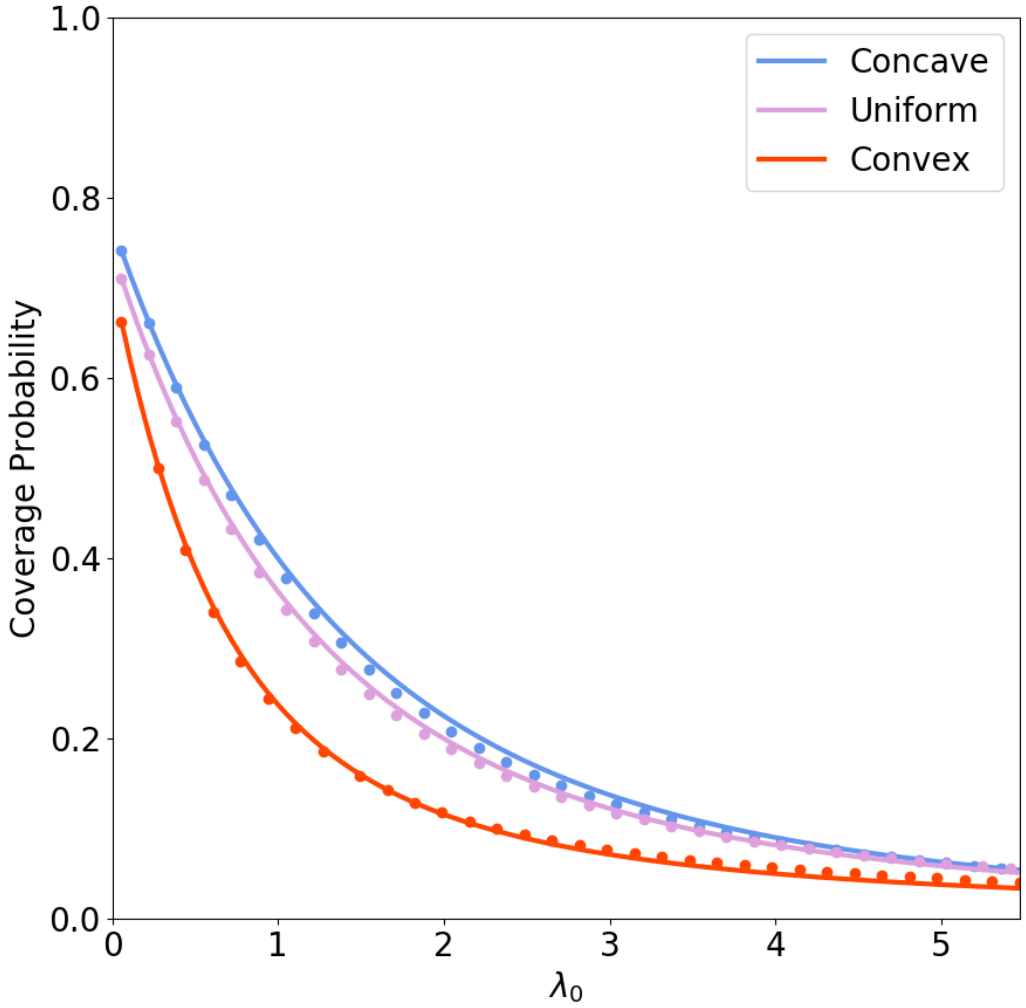

Figure 6.3: The coverage probability for a range of different densities for different distributions of end users. The convex, concave and uniform refer to the distribution used in the previous chapter, with $b = 2/R^2, 0, -2/R^2$ respectively. The markers are simulated data points after 10000 trials, and the solid lines are approximations of the coverage probability using equations eq. (6.15) and eq.(6.14) Parameters:$g_L(x) = \left(\frac{\psi}{4\pi x}\right)^{\eta}; \eta = 2.7, \gamma = 0.01; P_1 = 19\text{dBm}, \sigma^2 = -174 + 6 + \log_{10}[125000], R = 12km, \psi = \left(\frac{3\times10^5}{868\times10^6}\right) km.$

which maximises the spreading factor whilst ensuring the interference is not too high to cause outage.

Chapter 7

Spatio-temporal Networks

As of this far we have only analysed a snapshot of the network at a particular instance in time. However, even with a fixed topology, SRGGs experience temporal fluctuations due to random link failures [Kar08], which are often spatially correlated [Kar10]; or even as nodes turn off from the networks, the local and global connectivity properties of the network can drastically change. Mobility can help to mitigate the impact of random link failures in these dynamic networks, as nodes continually cross paths [Gup00,Gro01]. As a consequence, we extend our model to the connectivity in mesh networks and analyse connectivity over multiple time slots, referred to as a spatio-temporal network. This chapter is taken from the paper "Temporal connectivity in finite networks with non-uniform measures", see Ref [Pra18], of which I was an author with Carl Dettmann and Woon Hau Chin.

To date there has been little focus on spatio-temporal networks where the dynamics on the network are caused by the probabilistic nature of links, node mobility or both. One approach is to assume the nodes have infinite mobility resulting in no spatial correlation between time slots, or alternatively fix the underlying distribution of nodes and assume information diffuses quickly through the network; either way this has largely been focused on the uniform case [Hae13, Det18a]. When the node locations are fixed, uniformly distributed on the torus (mitigating edge effects by using periodic boundary

conditions) and links are drawn during each time slot, connectivity is determined by those nodes which are "highly isolated" [Det18a]. When the nodes are mobile, and follow a RW in $\mathbb{R}^d$, Ref [Per13] obtained asymptotic results for how long a node takes to connect to any other node in the graph when the connection model is that of the RGG.

Previously we discussed how isolated nodes are the obstacle to full connectivity in uniform SRGGs, Refs [Pen97, Mao13, Hsi05, Iye12]. In addition, in finite uniform SRGGs boundaries play a key role in P_{fc} [Coo12a, Det16], whilst the approximation of P_{fc} occurring when there are no isolated nodes improves in networks with a fractal nature [Det18a]. Furthermore, we have seen from the previous chapters that mobility can greatly impact network performance, with sparse regions more likely to cause outage, particularly when near boundaries. Motivated by this body of work, we ask the question, how does all this change (if at all) when considering spatio-temporal networks.

More specifically, we explore the probability that a spatio-temporal network is fully connected through the isolation probability of a single node located near a boundary. Since multiple transmissions occur on a much smaller time scale when compared with human mobility, we can assume the nodes/users have a fixed, non-uniform, distribution. Furthermore, comparing these results with the case when users have infinite mobility, we are able to give bounds on the impact mobility has on these finite spatio-temporal networks.

7.1 Network Model

The aim is to understand how boundaries and non-uniformity impact on the global connectivity properties of spatio-temporal networks. With this in mind we use a non-uniform PPP in a triangular region to model the random locations of users in the MANET. More formally, let Φ be a non-uniform

PPP with density $\lambda(r, \theta)$ in a triangular region

$$A = \{(x, y) : 0 \leq x \leq L, 0 \leq y \leq x \tan \phi\}. \tag{7.1}$$

To clarify we assume that once we realise the PP, the points remain fixed for all time slots as we assume the time to realise links is on a much smaller time scale than for nodes to move. The density of points grows away from the corner of interest, described by,

$$\lambda(r, \theta) = \bar{N} c r^{\alpha} g_{\phi}(\theta), \;\; \alpha \geq 0 \tag{7.2}$$

where $\bar{N}$ is the mean number of nodes in Φ, c is a normalisation constant such that $\int_A \lambda(r, \theta) r \mathrm{d}r \mathrm{d}\theta = \bar{N}$ and $g_{\phi}(\theta)$ models the angular variation in the density. Often we will choose $g_{\phi}(\theta)$ such that it goes to zero when $\theta = 0, \phi$ or both. The motivation for this particular density is that we would expect in a real world spatio-temporal network with mobile nodes the proportion of nodes near a corner/boundary would be less compared with that in the bulk. An example is for the RWP model where the density grows linearly away from the corner and is zero along the boundaries, as discussed in Chapter 3. The case we will mainly focus on however is when $\alpha = 2$ and $g_{\phi}(\theta) = \sin(\theta) \sin(\phi - \theta)$ which can be thought of modelling a mobility model where MUs spend a lot of time within the bulk of the domain, making the boundaries even sparser in terms of node density.

In particular we focus on a point $\boldsymbol{\xi}$ located near the corner of the region and study how long it remains isolated from the rest of the network[1]. In the Cartesian coordinate system we denote $\boldsymbol{\xi} = (\xi_x, \xi_y)$, whilst in polar coordinates and $\boldsymbol{\xi} = (r, \theta)$. Moreover, we study these isolation probabilities in terms of a wide range of connection functions, including: Rayleigh, Waxman, MIMO, SD, SA, QD and an SIR model, all of which are discussed in

[1] $\boldsymbol{\xi}$ is not in the point process since this would break some of our later assumptions. For example, we will sometimes want to choose $\boldsymbol{\xi}$ such that it is on the boundary, but often we will also choose the density such that it goes to zero at the boundary

Sec 2.2, summarised in Table 2.1 (the SIR model is obtained from the SINR model here by setting $\sigma^2 = 0$) and illustrated in Fig 2.2. Furthermore, we assume the node locations remain fixed throughout the process; this can be interpreted as the system having two different time scales: that of human mobility, and that of sending a wireless packet, with the latter being assumed to be much smaller. The final assumption is that there is no temporal dependence between time slots, that is to say the event that a node is isolated at time T is independent from the past, given the point process.

With the model outlined we are well placed to analyse network connectivity, in terms of isolated nodes located near a vertex. Thus, the main object of study will be the probability a node is isolated at time T, denoted as $\mathbb{P}^T_{\text{iso}}(\boldsymbol{\xi})$, which is the complement of the connection probability $\mathbb{P}^T_{\text{iso}}(\boldsymbol{\xi}) = 1 - \mathbb{P}_{C_T}(\boldsymbol{\xi})$. We note that somewhat related work has been done in one dimension, and it was shown that for $\alpha > 0$ the expected number of isolated nodes is finite, whilst this is not necessarily true for $\alpha \leq 0$ [Det18a]. In our model however, we are concerned with the probability a node near the corner is isolated, and how this determines the global properties of connectivity in spatio-temporal networks.

7.2 Isolation Probabilities

We provide three methods for computing the probability a node $\boldsymbol{\xi}$ is isolated for T consecutive time slots near a corner. First we write the probability that a node, not in the point process, cannot connect to any point in Φ after T time steps, using both the PGFL and that the sets of edges are independent across time. We then diverge into three different methods for different connection functions, with the general intuition being that pairs of nodes that are closer are more likely to connect. The first method is applied to connection functions with compact support, whilst the other two are used for connection functions with global support. The last two methods can also be applied to those connection functions with compact support and the corresponding

discontinuities can be handled separately although these contributions can often be ignored in the small parameter expansions [Det18a]. We proceed by giving the initial formulation of the analysis, and then consider each method separately in the subsequent sections.

The probability that a user $\boldsymbol{\xi}$ is isolated from all other points in Φ, conditioned on Φ, for T consecutive time steps is,

$$\begin{aligned} \mathbb{P}_{\text{iso}}^{T}(\boldsymbol{\xi}|\Phi) &= \prod_{\boldsymbol{y}\in\Phi} \left(1-\mathcal{H}\left(|\boldsymbol{\xi}-\boldsymbol{y}|\right)\right)^{T} \\ \mathbb{P}_{\text{iso}}^{T}(\boldsymbol{\xi}) &= \exp\left(-\int_{A}\left(1-\left(1-\mathcal{H}\left(|\boldsymbol{\xi}-\boldsymbol{y}|\right)\right)^{T}\right)\Lambda(\mathrm{d}\boldsymbol{y})\right) \end{aligned} \tag{7.3}$$

where we have computed the expectation with respect to Φ using the PGFL for PPPs, the integral is over the triangular region, and $\Lambda(\cdot)$ is the intensity measure of Φ. For a single time slot eq. (7.3) reduces to,

$$\mathbb{P}_{\text{iso}}^{T=1}(\boldsymbol{\xi}) = \exp\left(-\int_{A}\mathcal{H}\left(|\boldsymbol{\xi}-\boldsymbol{y}|\right)\lambda(\boldsymbol{y})\mathrm{d}\boldsymbol{y}\right) = e^{-M(\boldsymbol{\xi})}, \tag{7.4}$$

where $M(\boldsymbol{\xi})$ is the usual connectivity mass [Coo12a, Det16].

Due to the nature of the PPP, this model never guarantees $\boldsymbol{\xi}$ is connected, which can be seen through eq.(7.3). Consider the limit as $T\to\infty$ for $\mathcal{H}(r)=1$ with infinite support, in a finite domain A,

$$\lim_{T\to\infty}\mathbb{P}_{\text{iso}}^{T}(\boldsymbol{\xi}) = \exp\left(-\int_{A}\lambda(y,\theta)y\mathrm{d}y\mathrm{d}\theta\right) = e^{-\Phi(A)} = e^{-\bar{N}} > 0 \tag{7.5}$$

Therefore, since there is a positive probability that the point process Φ is empty, the probability $\boldsymbol{\xi}(\notin\Phi)$ is isolated is also positive.

We proceed by using eq.(7.3) to calculate the isolation probabilities for different connection functions expressed in Sec 2.2, starting with those with compact support.

7.3 Isolation probabilities for connection functions with compact support

The method used for calculating the isolation probability (and thus connection probability) for $\boldsymbol{\xi}$ is very similar for all connection models with compact support (with the exception of the QD model case which is discussed separately in Sec 7.5) so we proceed by deriving it for the Soft Disk model, and give the results for the SA model in Table 7.1.

Recall that for the SD model the connection probability is $\mathcal{H}(r) = \wp \mathbb{1}_{r \leq r_0}$. From eq.(7.3) it is not possible to obtain an explicit expression for $\mathbb{P}_{\text{iso}}^T$ when $\boldsymbol{\xi}$ is located at an arbitrary location in $\mathcal{V}$. However, we focus our analysis on the particular case when $\boldsymbol{\xi} = (r, \omega)$ is isolated near the corner, and $r_0 \geq r$ which guarantees that the ball centred at $\boldsymbol{\xi}$ with radius r_0, $B_{\boldsymbol{\xi}}(r_0)$, intersects both boundaries and includes the vertex at the origin. From these assumptions, and eq.(7.3) we have,

$$\begin{aligned} \mathbb{P}_{\text{iso}}^T(r, \omega) &= \exp\left(-\left(1-(1-\wp)^T\right) \int_0^{\phi} \int_0^z \lambda(y, \theta) y \mathrm{d}y \mathrm{d}\theta \right) \\ &= \left(\exp\left(-\int_0^{\phi} \int_0^z \lambda(y, \theta) y \mathrm{d}y \mathrm{d}\theta \right) \right)^{\left(1-(1-\wp)^T\right)} \\ &= V_{\mathcal{B}_{\boldsymbol{\xi}}}(r_0)^{\left(1-(1-\wp)^T\right)}, \end{aligned} \tag{7.6}$$

where $z = \sqrt{r_0^2 + r^2 - 2 r_0 r \cos(\theta - \omega)}$, and $V_{\mathcal{B}}(\boldsymbol{\xi}, r_0)$ is the void probability. For the uniform case the inner integral in eq.(7.6) is proportional to the size of the region. For the general case we expand the integrand of eq.(7.3) for small r to provide a closed form approximation:

$$\mathbb{P}_{\text{iso}}^T(\boldsymbol{\xi}) = \exp\left(-\bar{N} c (1 - (1 - \wp)^T) \int_0^{\phi} \int_0^z y^{\alpha+1} g_{\phi}(\theta) \mathrm{d}y \mathrm{d}\theta \right) \tag{7.7}$$

$$
\begin{aligned}
\mathbb{P}^{T}_{\text{iso}}(\boldsymbol{\xi}) &= \exp\Bigg(-\bar{N}c(1-(1-\wp)^{T})\int_{0}^{\phi}\Bigg(\frac{r_0^{\alpha+2}}{\alpha+2} \\
&\quad - \cos(\theta-\omega)r_0^{\alpha+1}r + \frac{1+\alpha\cos^2(\theta-\omega)}{2}r_0^{\alpha}r^2 + ...\Bigg)g_{\phi}(\theta)\mathrm{d}\theta\Bigg) \\
&\approx \exp\Bigg(-\bar{N}c(1-(1-\wp)^{T}) \\
&\quad \times \left(\frac{r_0^{\alpha+2}}{\alpha+2}G_{\phi} - G_c(\omega)r_0^{\alpha+1}r + G_2(\omega)r_0^{\alpha}r^2\right)\Bigg),
\end{aligned}
\tag{7.8}
$$

where

$$
\begin{aligned}
G_{\phi} &= \int_{0}^{\phi} g_{\phi}(\theta)\mathrm{d}\theta, \\
G_c(\omega) &= \int_{0}^{\phi} g_{\phi}(\theta)\cos(\theta-\omega)\mathrm{d}\theta, \\
G_2(\omega) &= \int_{0}^{\phi} \frac{1}{2}g_{\phi}(1+\alpha\cos^2(\theta-\omega))\mathrm{d}\theta.
\end{aligned}
\tag{7.9}
$$

At the corner the above reduces to just taking the leading order term. See Table 7.1 for a similar expression for the soft-annulus model.

In the limit as $T \to \infty$ we return to the original void probability, for the SA model it converges to the probability the annulus $V_{\mathcal{A}_{\boldsymbol{\xi}}}(r_-, r_+)$ is empty. We notice that this type of connection function with compact support results in no guarantee that $\boldsymbol{\xi}$ connects, even if the PP is non-empty as the relevant connection region might be; trivially this *all or nothing* type of connection means we need at least the average number of nearest neighbours to be greater than one [Gil61].

7.4 User Isolation - Method I

In this section we focus on connection functions with global support, and provide a method based on translating the distance between points. Since

local behaviour will dominate (very long connections are unlikely) we approximate the domain to be infinite for tractability. We first start by writing eq.(7.3) in polar coordinates.

$$\mathbb{P}_{\text{iso}}^{T}(\boldsymbol{\xi}) = \exp\left(-\int_0^{\phi}\int_0^{\frac{L}{\cos\theta}}\left(1-(1-\mathcal{H}(z))^{T}\right)\lambda(y,\theta)y\mathrm{d}y\mathrm{d}\theta\right), \tag{7.10}$$

where the node $\boldsymbol{\xi}$ is located (in polar coordinates) at (r,ω) and $z = \sqrt{r^2+y^2-2ry\cos(\theta-\omega)}$ is the corresponding transformation using the cosine rule. We can expand the integrand using the binomial theorem, expand for small radial component x and assume the contributions come from near by so the domain is assumed to be infinite to give,

$$\mathbb{P}_{\text{iso}}^{T}(\boldsymbol{\xi}) = \exp\left(-c\bar{N}\sum_{k=1}^{T}(-1)^{k+1}\binom{T}{k}\left(\mathcal{H}_{k,\alpha+1}G_{\phi} - \frac{k}{r_0}G_c(\omega)\mathcal{H}'_{k-1,\alpha+1}r + O(r^2)\right)\right), \tag{7.11}$$

where $G_{\phi}, G_c(\omega)$ are as before, $\mathcal{H}_{k,\alpha}^{(n)} = \int_0^{\infty}\mathcal{H}^{(n)}\left(\frac{y}{r_0}\right)\mathcal{H}^{k}\left(\frac{y}{r_0}\right)y^{\alpha}\mathrm{d}y$ and $^{(n)}$ corresponds to n^{th} derivative. As an illustrative example we calculate the isolation probabilities for the Rayleigh and Interference connection functions outlined in chapter 2.2 through direct application of eq.(7.11).

Example I: Rayleigh Connection Model

First we consider the Rayleigh connection function defined in Sec 2.2 where we need the following integrals,

$$\begin{aligned}
\mathcal{H}_{k,\alpha+1} &= \int_0^{\infty}\exp\left(-k\left(\frac{y}{r_0}\right)^{\eta}\right)y^{\alpha+1}\mathrm{d}y = \frac{r_0^{2+\alpha}}{\eta}\Gamma\left[\frac{2+\alpha}{\eta}\right]k^{\frac{2+\alpha}{\eta}} \\
\mathcal{H}'_{k,\alpha+1} &= \int_0^{\infty}\exp\left(-k\left(\frac{y}{r_0}\right)^{\eta}\right)y^{\alpha+1}\frac{\mathrm{d}}{\mathrm{d}y}\exp\left(-\left(\frac{y}{r_0}\right)^{\eta}\right)\mathrm{d}y \\
&= -r_0^{1+\alpha}\Gamma\left[\frac{1+\alpha+\eta}{\eta}\right](1+k)^{\frac{\eta+\alpha-1}{\eta}}.
\end{aligned} \tag{7.12}$$

Substituting the above into eq.(7.11), we get the following expression

$$\begin{aligned}\mathbb{P}_{\text{iso}}^{T}(\boldsymbol{\xi}) = \exp\Bigg(&-c\bar{N}\frac{r_0^{\alpha+2}}{\eta}\Gamma\left[\frac{2+\alpha}{\eta}\right]H_{T,1}^{\frac{2+\alpha}{\eta}}G_\phi \\ &- c\bar{N}r_0^{\alpha+1}\Gamma\left[\frac{1+\alpha}{\eta}+1\right]H_{T,1}^{\frac{1+\alpha}{\eta}}rG_c(\omega)+O(r^2)\Bigg),\end{aligned} \tag{7.13}$$

where $H_{T,\beta}^{\frac{\alpha+2}{\eta}} = \sum_{k=1}^{T}(-1)^{k+1}\binom{T}{k}k^{-\frac{\alpha+2}{\eta}}\beta^k$ is the generalised Roman harmonic number given in [Rom92, Det18a]. Note that we include the constant β for the Waxman case, the result of which is given in Table 7.1, and for brevity later on we will often use $s = \frac{\alpha+2}{\eta}$.

To find an asymptotic approximation for large values of T for eq.(7.13) and begin by taking the natural logarithm of both sides.

$$\begin{aligned}-\log\mathbb{P}_{\text{iso}}^{T}(\boldsymbol{\xi}) &= \int_0^{\phi}\int_0^{\infty}\left(1-\left(1-e^{-\left(\frac{y}{r_0}\right)^{\eta}}\right)^{T}\right)\lambda(y,\theta)y\mathrm{d}y\mathrm{d}\theta \\ &= c\bar{N}G_\phi\int_0^{\infty}\left(1-\left(1-e^{-\left(\frac{y}{r_0}\right)^{\eta}}\right)^{T}\right)y^{\alpha+1}\mathrm{d}y \\ &=^{z=\left(\frac{y}{r_0}\right)^{\eta}} \frac{c\bar{N}G_\phi r_0^{\alpha+2}}{\eta}\int_0^{\infty}\left(1-\left(1-e^{-z}\right)^{T}\right)z^{\frac{\alpha+2}{\eta}-1}\mathrm{d}z \\ &=^{s=\frac{\alpha+2}{\eta}} \frac{c\bar{N}G_\phi r_0^{\alpha+2}}{\eta}\Bigg(\int_0^{\log\beta T}\left(1-\left(1-e^{-z}\right)^{T}\right)z^{s-1}\mathrm{d}z \\ &+ \int_{\log\beta T}^{\infty}\left(1-\left(1-e^{-z}\right)^{T}\right)z^{s-1}\mathrm{d}z\Bigg) \\ &= \frac{c\bar{N}G_\phi r_0^{\alpha+2}}{\eta}(I_1+I_2)\end{aligned} \tag{7.14}$$

where we have split up the integral at $\log\beta T$ and will analyse both separately, starting with I_1.

$$I_1 = \int_0^{\log\beta T}\left(1-\left(1-\beta e^{-z}\right)^{T}\right)z^{s-1}\mathrm{d}z \tag{7.15}$$

$$
\begin{aligned}
I_1 &= \frac{(\log \beta T)^s}{s} - \int_0^{\log \beta T} \exp\left(T \log\left(1-\beta e^{-z}\right)\right) z^{s-1} \mathrm{d}z \\
&\overset{y=\log \beta T - z}{=} \frac{(\log \beta T)^s}{s} - \int_0^{\log \beta T} \exp\Bigg(T \log\left(1-\beta e^{-(\log \beta T - y)}\right) \\
&\quad + (s-1)\log[\log[\beta T]-y]\Bigg)\mathrm{d}y \\
&= \frac{(\log \beta T)^s}{s} - \int_0^{\log \beta T} \exp\Bigg(T \log\left(1-\beta \frac{1}{\beta T} e^{y}\right) \\
&\quad + (s-1)\log[\log[\beta T]-y]\Bigg)\mathrm{d}y \\
&\overset{\text{expand } e^y}{=} \frac{(\log T)^s}{s} - \int_0^{\log[\beta T]} \exp\Bigg(-T \log\left[1 - \frac{1+y+\frac{y^2}{2}+\frac{y^3}{6}+...}{T}\right] \\
&\quad + (s-1)\left(\log[\log[\beta T]] - \frac{y}{\log[\beta T]} - \frac{y^2}{2(\log[\beta T])^2} - \frac{y^3}{3(\log[\beta T])^3} + ...\right)\Bigg)\mathrm{d}y \\
&\overset{\text{expand for large } T}{=} \frac{(\log \beta T)^s}{s} - (\log[\beta T])^{s-1} \int_0^{\log[\beta T]} \exp\Bigg(-\left(1+y+\frac{y^2}{2}+\frac{y^3}{6}+...\right) \\
&\quad - \frac{1}{2T}\left(1+y+\frac{y^2}{2}+\frac{y^3}{6}+...\right)^2 - \frac{1}{6T^2}\left(1+y+\frac{y^2}{2}+\frac{y^3}{6}+...\right)^3 \\
&\quad + O(T^{-3})\Bigg) e^{-\frac{(s-1)}{\log[\beta T]}y + O(\log[\beta T]^{-}2)}\mathrm{d}y \\
&\approx \frac{(\log \beta T)^s}{s} - (\log[\beta T])^{s-1} \int_0^{\log[\beta T]} \exp\Big(-e^y + O(T^{-1})\Big) \\
&\quad \times e^{-\frac{(s-1)}{\log[\beta T]}y + O(\log[\beta T]^{-}2)}\mathrm{d}y \\
&= \frac{(\log \beta T)^s}{s} - (\log[\beta T])^{s-1} \int_0^{\log[\beta T]} \exp\Big(-e^y\Big) e^{-\frac{(s-1)}{\log[\beta T]}y}\mathrm{d}y \\
&\overset{u=e^y}{=} \frac{(\log[\beta T])^s}{s} - (\log[\beta T])^{s-1} \int_1^{\beta T} e^{-u} u^{-\frac{s-1}{\log[\beta T]}-1}\mathrm{d}u \\
&= \frac{(\log[\beta T])^s}{s} - (\log[\beta T])^{s-1}\left(\Gamma\left[-\frac{(s-1)}{\log T}, 1\right] - \Gamma\left[-\frac{(s-1)}{\log[\beta T]}, \beta T\right]\right)
\end{aligned}
\tag{7.16}
$$

Leaving I_1 in this form for now and turning our attention to I_2 yields the following.

$$
\begin{aligned}
I_2 &= \int_{\log[\beta T]}^{\infty} \left(1-\left(1-\beta e^{-z}\right)^T\right) z^{s-1}\mathrm{d}z \\
&=^{(1)} \int_0^{\infty} \left(1-\left(1-\beta e^{-(y+\log[\beta T])}\right)^T\right) (y+\log[\beta T])^{s-1}\mathrm{d}y \\
&=^{(2)} \int_0^{\infty} \exp\Bigg(\log\left[1-\sum_{k=0}^{T}(-1)^k\binom{T}{k}\beta^k e^{-k(y+\log[\beta T])}\right] \\
&+ (s-1)\left(\log[\log[\beta T]]+\frac{y}{\log[\beta T]}-\frac{y^2}{2(\log[\beta T])^2}+...\right)\mathrm{d}y \\
&= (\log[\beta T])^{s-1}\int_0^{\infty}\exp\Bigg(\log\left[\sum_{k=1}^{T}(-1)^{k+1}\binom{T}{k}T^{-k}e^{-ky}\right]\Bigg) \\
&\times \exp\left(\frac{(s-1)}{\log[\beta T]}y\right)\mathrm{d}y \\
&= (\log[\beta T])^{s-1}\int_0^{\infty}\exp\left(1-\left(1-\frac{e^{-y}}{T}\right)^T\right)\exp\left(\frac{(s-1)}{\log[\beta T]}y\right)\mathrm{d}y \\
&=^{(3)} (\log[\beta T])^{s-1}\int_1^{\infty}\exp\Bigg(\log\left[\sum_{k=1}^{T}(-1)^{k+1}\binom{T}{k}x^{-k}T^{-k}\right]\Bigg)x^{\frac{(s-1)}{\log[\beta T]}-1}\mathrm{d}x \\
&= (\log[\beta T])^{s-1}\int_1^{\infty}\left(1-\left(1-\frac{1}{Tx}\right)^T\right)x^{\frac{(s-1)}{\log[\beta T]}-1}\mathrm{d}x \\
&= \frac{(\log[\beta T])^s}{(s-1)}\left({}_2F_1\left(-\frac{(s-1)}{\log[\beta T]},-\beta T;1-\frac{(s-1)}{\log[\beta T]};\frac{1}{\beta T}\right)-1\right)
\end{aligned}
\tag{7.17}
$$

where in (1): Substitute in $y = z - \log[\beta T]$ (2): Using the binomial theorem, and expanding the second term for small y. (3): Using another substitution of $y = \log x$ and the last integral is only true provided $\frac{s-1}{\log[\beta T]} < 1$.

The integral I_2 is now left in terms of a Gauss Hypergeometric function which is quick and easy to implement numerically in standard libraries, as opposed to the Roman Harmonic sum which needs to be done more carefully for large T due to the alternating signs. The above approximation holds for

$\frac{s-1}{\log[\beta T]} < 1$, and holds in all the reasonable cases for α, η we study later. For $s \leq 1$, I_2 can be approximated further ; starting from point (3) in the above,

$$
\begin{aligned}
I_2 &= (\log[\beta T])^{s-1} \int_0^{\infty} \exp\left(\log \left[\sum_{k=1}^{T} (-1)^{k+1} \binom{T}{k} T^{-k} e^{-ky} \right] \right) \exp\left(\frac{(s-1)}{\log[\beta T]} y \right) \mathrm{d}y \\
&= (\log[\beta T])^{s-1} \int_0^{\infty} \exp\left(\log \left[e^{-y} - \frac{T-1}{2T} e^{-2y} + \frac{(T-1)(T-2)}{6T^2} e^{-3y} + ... \right] \right) \\
&\times \exp\left(\frac{(s-1)}{\log[\beta T]} y \right) \mathrm{d}y \\
&=^{(4)} (\log[\beta T])^{s-1} \int_0^{\infty} \exp\left(\log \left[1 - e^{-e^{-y}} + O\left(\frac{1}{T} \right) \right] e^{\frac{(s-1)}{\log[\beta T]} y} \mathrm{d}y \right. \\
&=^{u=e^{-y}} (\log[\beta T])^{s-1} \int_0^{1} \left(1 - e^{-u} \right) u^{-\frac{(s-1)}{\log[\beta T]} - 1} \mathrm{d}u \\
&= (\log[\beta T])^{s-1} \left(-\frac{\log[\beta T]}{(s-1)} - \Gamma\left[-\frac{(s-1)}{\log[\beta T]}, 0, 1 \right] \right)
\end{aligned}
\tag{7.18}
$$

(4): We use the definition of the exponential function and neglect terms of $O(T^{-1})$. Notice now that both I_1, and I_2 are given as incomplete Gamma functions, when they are combined the expression can be simplified and further approximated by large T.

$$
\begin{aligned}
I_1 + I_2 &= \frac{(\log[\beta T])^s}{s} - (\log[\beta T])^{s-1} \left(\Gamma\left[\frac{(1-s)}{\log[\beta T]}, 1 \right] - \Gamma\left[\frac{(1-s)}{\log[\beta T]}, \beta T \right] \right) \\
&+ (\log[\beta T])^{s-1} \left(-\frac{\log[\beta T]}{(s-1)} - \Gamma\left[-\frac{(s-1)}{\log[\beta T]}, 0, 1 \right] \right) \\
&=^{\Gamma[s,\beta T] \approx \Gamma[s]} \frac{(\log[\beta T])^s}{s} \\
&- (\log[\beta T])^{s-1} \left(\Gamma\left[-\frac{(s-1)}{\log[\beta T]}, 1 \right] + \frac{\log[\beta T]}{(s-1)} + \Gamma\left[-\frac{(s-1)}{\log[\beta T]}, 0, 1 \right] \right)
\end{aligned}
\tag{7.19}
$$

$$
\begin{aligned}
I_1 + I_2 &= \frac{(\log[\beta T])^s}{s} - (\log[\beta T])^{s-1}\left(\Gamma\left[-\frac{(s-1)}{\log[\beta T]}\right] + \frac{\log[\beta T]}{(s-1)}\right) \\
&=^{(1)} \frac{(\log[\beta T])^s}{s} \\
&- (\log[\beta T])^{s-1}\left(-\frac{\log[\beta T]}{(s-1)} - \gamma_c - \frac{1}{12}(\pi^2 + 6\gamma_c^2)\frac{(s-1)}{\log[\beta T]}\right. \\
&\left. + \frac{(s-1)^2}{6(\log[\beta T])^2}\left(\gamma_c^3 + \frac{\gamma_c \pi^2}{2} - \psi^{(2)}(1)\right) + O\left((\log[\beta T])^{-3}\right) + \frac{\log[\beta T]}{(s-1)}\right) \\
&= \frac{(\log[\beta T])^s}{s} + \gamma_c(\log[\beta T])^{s-1} + \frac{(s-1)}{12}(\pi^2 + 6\gamma_c^2)(\log[\beta T])^{s-2} \\
&+ \frac{(s-1)^2}{6}\left(\gamma_c^3 + \frac{\gamma_c \pi^2}{2} - \psi^{(2)}(1)\right)(\log[\beta T])^{s-3} + O\left((\log[\beta T])^{s-4}\right)
\end{aligned}
\tag{7.20}
$$

where $^(1)$ we expand the Gamma function for large T, $\psi^{(n)}(1)$ is the n^{th} derivative of the digamma function[2] and $\gamma_c = 0.557215...$ is the Euler-Mascheroni constant. This result is consistent with that in Ref [Det18a], with the added generality of also being applicable to the Waxman case by including the constant β. Furthermore, the above analysis highlights which regime the approximation is valid, and gives an alternative approximation in terms of hypergeometric functions when η is small, or α is large resulting in $\frac{\alpha+2}{\eta} > 1$.

As a result, we can approximate the isolation probabilities for large T by

$$
H_T^s \approx \frac{(\log[\beta T])^s}{s} + \gamma_c(\log[\beta T])^{s-1} + \frac{(6\gamma_c^2 + \pi^2)(s-1)}{12}(\log[\beta T])^{s-2} + O\left((\log[\beta T])^{s-3}\right)
\tag{7.21}
$$

[2]Digamma function is defined as: $\psi^{(n)}(x) = \frac{\mathrm{d}}{\mathrm{d}x}\log\left[\Gamma[x]\right]$

A special case of the above is when $s = \frac{\alpha+2}{\eta} = 1$.

$$\begin{aligned}\int_0^\infty (1-(1-e^{-x})^T)\mathrm{d}x &= \int_0^1 \frac{1-u^T}{1-u}\mathrm{d}u = \int_0^1 \sum_{k=1}^{T} u^{k-1}\mathrm{d}u \\ &= \sum_{k=1}^{T}\int_0^1 u^{k-1}\mathrm{d}u = H_T\end{aligned} \tag{7.22}$$

In the first equality we use the substitution $u = 1 - e^{-x}$, and the second we use the definition of the geometric series. Namely, for $s = 1$, the expression in eq.(7.10) is the integral representation of the classical Harmonic number H_T with corresponding asymptotic representation Ref [Gra89].

$$H_T = \log T + \gamma_c + \frac{1}{2T} - \frac{1}{12T^2} + O(T^{-4}) \tag{7.23}$$

Conversely, for the case when α is large then we can approximate the integral in terms of a gamma function,

$$\int_0^\infty (1-(1-e^{-z})^T) z^{\frac{\alpha+2}{\eta}-1}\mathrm{d}z \sim \int_0^\infty T e^{-z} z^{\frac{\alpha+2}{\eta}-1}\mathrm{d}z = T\Gamma\left[\frac{\alpha+2}{\eta}\right] \tag{7.24}$$

This is a useful approximation for a very inhomogeneous network (or a highly reflective environment) and suggests the isolation of nodes after time T slots behaves like $\exp(-\text{constant}T)$. For the Waxman model the above provides a good approximation, particularly for the RWP distribution, see Fig 7.2.

Interference

In Sec.2.2 we introduce the interference-limited connection function for a node with a general location in A. A tractable form of $\mathcal{H}$ (not expressed in terms of hyper geometric functions) is only possible for the specific case when $\boldsymbol{\xi}$ is located at the corner and the domain is assumed to be infinite.

$$\begin{aligned}\mathcal{H}(r) &= \exp\left(-\int_0^{\phi}\int_0^{\frac{L}{\cos\theta}}\left(1-\frac{1}{1+\frac{q\gamma r^{\eta}}{z^{\eta}}}\right)\lambda(z,\theta)z\mathrm{d}z\mathrm{d}\theta\right)\\ &=^{(*)}\frac{c\bar{N}s^{\frac{2+\alpha}{\eta}}\pi}{\eta}\csc\left(\frac{(2+\alpha)\pi}{\eta}\right)G_{\phi}\\ &= c\bar{N}G_{\phi}c_{\mathcal{I}}r^{2+\alpha},\end{aligned} \tag{7.25}$$

where $*$ denotes we have assumed an infinite wedge, $c_{\mathcal{I}} = \frac{(q\gamma)^{\frac{2+\alpha}{\eta}}\pi}{\eta}\csc\left(\frac{(2+\alpha)\pi}{\eta}\right)$ and we require $\alpha+2<\eta$ to hold. The condition that $\alpha+2<\eta$ ensures that there is indeed positive probability of connection; recall that there exists a phase transition when η equals the dimension such that when η is less than or equal to the dimension the global behaviour begins to dominate and the aggregate interference causes disconnection. Since we assume an infinite domain, which has an infinite number of nodes, we need to ensure the *local behaviour* dominates, hence $\alpha+2<\eta$. Consequently, for the RWP case we need $\eta>3$; a reasonable assumption in any large town or city where there are multiple obstructions. Alternatively we can make the approximation that all non-negligible interference comes from all those devices within a distance $r_{\mathcal{I}}$ which allows for the relaxation of the $\alpha+2<\eta$ restriction; but yields a connection function in terms of hypergeometric functions which leads to an intractable calculation later; see [DR16] amongst others on approximating interference.

When the node is located near the corner we can compute the approximation through method I or II (outlined in the next subsection). For method I we approximate the connection probability at x to be the same as at the vertex at the origin such that we can apply eq.(7.11), noting $r_0=1$, to get

$$\begin{aligned}-\log\mathbb{P}^{T}_{\mathrm{iso}}(\boldsymbol{\xi}) &= \frac{H_T}{(2+\alpha)c_{\mathcal{I}}}\\ &\quad+\frac{(c\bar{N})^{\frac{1}{2+\alpha}}}{(c_{\mathcal{I}}G_{\phi})^{\frac{1+\alpha}{2+\alpha}}}\Gamma\left[\frac{3+2\alpha}{2+\alpha}\right]H_T^{\frac{1+\alpha}{2+\alpha}}rG_c(\omega)+O(r^2).\end{aligned} \tag{7.26}$$

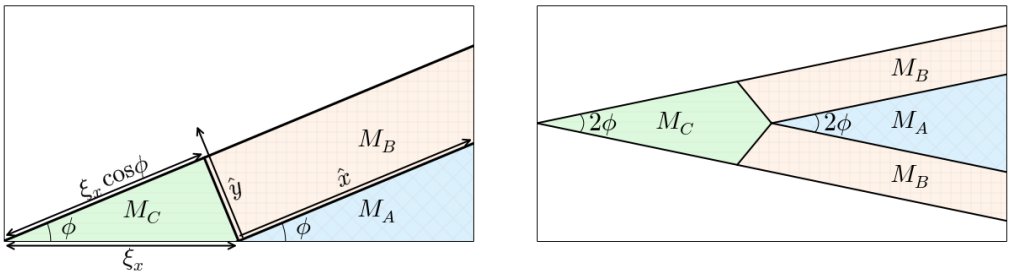

Figure 7.1: (Left): Schematic of the wedge and the regions M_A, M_B and M_C. The $\hat{x}, \hat{y}$ correspond to the translated and rotated coordinate system discussed in Sec 7.5.2. (Right) By combining two wedges together, along the boundary where the density is non-zero, we can calculate the probability that a single user is isolated from the network near the corner.

The leading order term in eq.(7.26) is independent of the density of users and the angle of the wedge. This is consistent with the results in [And11] which highlights how any increase in signal power due to proximity is counterbalanced by an increase in the interference field.

However, the second term (first order correction term) scales like $\bar{N}^{\frac{1}{2+\alpha}}$ and does in fact depend on both the geometry of the wedge and the density of users, ultimately leading to $\lim_{\bar{N}\to\infty} \mathbb{P}^T_{\text{iso}}(\boldsymbol{\xi}) \to \mathbb{P}^T_{\text{iso}}(\underline{0})$. Intuitively this is because in the high density limit[3], the local picture for each node looks the same due to the scaling of power and interference which means connections are dominated by the local neighbourhood.

7.5 User Isolation - Method II

In this section our aim is to give an alternative approach to Method I which provides greater tractability and is more suited to more complicated connection functions such as MIMO or those outlined in [Det16] where closed form expressions cannot be obtained via method I. For a non-increasing connection function $\mathcal{H}(r)$ with global support the approximation can be expressed

[3]This is only true for the singular path loss model, as discussed in Sec 4.5

as a combination of one-dimensional integrals which are quick to compute numerically. In this analysis we require the density to go to zero along the top border, which is akin to the RWP case or other mobility models where boundaries are left largely unexplored.

In this section we will consider the user located on the bottom boundary, $\boldsymbol{\xi} = (\xi_x, 0)$, and divide the domain into three regions M_A, M_B and M_C, see Fig7.1. This allows us to consider the probability the node at $\boldsymbol{\xi}$ is isolated as the exponential of the sum of the contributions from each region, and is written as,

$$\mathbb{P}^T_{\text{iso}}(\boldsymbol{\xi} = (\xi_x, 0)) = \exp\left(-(M_A + M_B + M_C)\right).$$

To obtain an expression for a user located near the corner, but not on either boundary, we can combine two triangular domains together along the non-zero boundaries. In general the two triangular regions need not be identical, but we assume so merely for brevity. We now proceed to calculate each of the contributions from these sub-regions using eq.(7.3), starting with M_A .

7.5.1 Conectivity in the region M_A

The region M_A, as shown by the purple region in Fig 7.1, has a transformed polar coordinate system centred at $(\xi_x, 0)$. For this case we use the cosine rule to make the necessary transformation of the density.

$$\begin{aligned} M_A &= \int_0^{\phi} \int_0^{\frac{(L-\xi_x)}{\cos\theta}} \left(1 - (1 - \mathcal{H}(y))^T\right) \lambda(z, \hat{\omega}) y \mathrm{d}y \mathrm{d}\hat{\theta} \\ &= \int_0^{\infty} \left(1 - (1 - \mathcal{H}(y))^T\right) \left(y^{\alpha+1} G_{\phi} + (\alpha+1)\, y^{\alpha} G_c(0) \xi_x + ...\right) \mathrm{d}y \\ &= G_{\phi} I(\alpha+1) + (\alpha+1) G_c(0) I(\alpha) \xi_x + O(\xi_x^2), \end{aligned} \tag{7.27}$$

where $z = \sqrt{y^2 + \xi_x^2 - 2y\xi_x \cos(\pi - \hat{\theta})}$, $\hat{\omega} = \arcsin\left[\frac{y \sin\hat{\theta}}{\sqrt{y^2 + \xi_x^2 + 2y\xi_x \cos\theta}}\right]$ and $I(s) = \int_0^{\infty} (1 - (1 - \mathcal{H}(y))^T) y^s \mathrm{d}y$.

In the above, we have expanded for small ξ_x and assumed the domain to be large allowing us to take the upper limit of the radial integral to be infinite. The remaining expression is now given as a sum of the integrals $I(s)$, reducing the number computations needed. In fact,we will subsequently see that the main contribution arises from the region M_A since the contributions from other regions are of order ξ_x^2.

7.5.2 Conectivity in the region M_B

The region M_B, see Fig 7.1, has a translated and rotated coordinate system $(\hat{x}, \hat{y})$. Since the function $g_\phi(\theta)$ goes to zero near the top boundary, we can approximate $\hat{y}$ to be small. Following this, the connection function can therefore be approximated as,

$$\mathcal{H}\left(\sqrt{\hat{x}^2+\hat{y}^2}\right)^k \approx \mathcal{H}^k\left(\hat{x}\right)+\frac{k}{\hat{x}}\mathcal{H}\left(\hat{x}\right)^{k-1}\mathcal{H}'\left(\hat{x}\right)\hat{y}^2+... \tag{7.28}$$

We also need to translate the function $g_\phi(\theta)$ in terms of $\hat{x}, \hat{y}$. By applying the cosine rule we can write $g_\phi(\hat{\theta}) = g_\phi\left(\arccos\left[\frac{-\hat{x}^2-\hat{y}^2+\xi_x^2+d^2}{2d\xi_x}\right]\right)$ where $\hat{\theta}$ is the angular component in the transformed coordinate system and then we can approximate it for small $\xi_x, \hat{y}$.

$$\begin{aligned}
g_\phi(\hat{\theta}) = g_\phi(\hat{\theta})\big|_{\xi_x=\hat{y}=0} &+ g'_\phi(\hat{\theta})\left(\xi_x\frac{\mathrm{d}}{\mathrm{d}\xi_x}\hat{\theta}+\hat{y}\frac{\mathrm{d}}{\mathrm{d}y}\hat{\theta}\right)\big|_{\xi_x=\hat{y}=0} \\
&+\left(g''_\phi(\hat{\theta})\left(\frac{\mathrm{d}}{\mathrm{d}\xi_x}\hat{\theta}\right)^2+g'_\phi(\hat{\theta})\frac{\mathrm{d}^2}{\mathrm{d}\xi_x^2}\hat{\theta}\right)\big|_{\xi_x=\hat{y}=0}\xi_x^2 \\
&+\left(g''_\phi(\hat{\theta})\left(\frac{\mathrm{d}}{\mathrm{d}\hat{y}}\hat{\theta}\right)\left(\frac{\mathrm{d}}{\mathrm{d}\xi_x}\hat{\theta}\right)+g'_\phi(\hat{\theta})\frac{\mathrm{d}^2}{\mathrm{d}\xi_x\hat{y}}\hat{\theta}\right)\big|_{\xi_x=\hat{y}=0}\xi_x\hat{y} \\
&+\left(g''_\phi(\hat{\theta})\left(\frac{\mathrm{d}}{\mathrm{d}\xi_x}\hat{\theta}\right)\left(\frac{\mathrm{d}}{\mathrm{d}\hat{y}}\hat{\theta}\right)+g'_\phi(\hat{\theta})\frac{\mathrm{d}^2}{\mathrm{d}\hat{y}\xi_x}\hat{\theta}\right)\big|_{\xi_x=\hat{y}=0}\xi_x\hat{y} \\
&+\left(g''_\phi(\hat{\theta})\left(\frac{\mathrm{d}}{\mathrm{d}\hat{y}}\hat{\theta}\right)^2+g'_\phi(\hat{\theta})\frac{\mathrm{d}^2}{\mathrm{d}\hat{y}^2}\hat{\theta}\right)\big|_{\xi_x=\hat{y}=0}\hat{y}^2+...
\end{aligned} \tag{7.29}$$

$$
\begin{aligned}
g_\phi(\hat{\theta}) = & \frac{g'_\phi(\phi)}{\hat{x}}\left(\xi_x \sin\phi - \hat{y}\right) \\
& + \frac{1}{\hat{x}^2}\Bigg(\left(\xi_x^2 \sin^2\phi + \hat{y}^2 + 2\xi_x\hat{y}\sin\phi\right) g''_\phi(\phi) \\
& + \left(\xi_x^2 \sin(2\phi) - 2\xi_x\hat{y}\cos\phi\right) g'_\phi(\phi)\Bigg) + ...
\end{aligned}
\tag{7.30}
$$

where $g_\phi(\phi) = 0$ by construction. By applying the aforementioned approximations, and rewriting the integrand as a sum, the contribution from the region M_B is given by,

$$
\begin{aligned}
M_B &= \int_{M_B} \left(1 - \left(1 - \mathcal{H}\left(|\boldsymbol{\xi} - \boldsymbol{y}|\right)\right)^T\right) \lambda(y,\theta) y \mathrm{d}y\mathrm{d}\theta \\
&= \sum_{k=1}^{T} (-1)^{k+1} \binom{T}{k} \int_0^{\xi_x \sin\phi} \int_0^{\infty} \mathcal{H}^k\left(\sqrt{\hat{x}^2 + \hat{y}^2}\right) \lambda(\hat{x},\hat{y}) \mathrm{d}\hat{x}\mathrm{d}\hat{y} \\
&=^{(1)} \bar{N}c \sum_{k=1}^{T} (-1)^{k+1} \binom{T}{k} \int_0^{\xi_x \sin\phi} \int_0^{\infty} \left(\mathcal{H}^k\left(\hat{x}\right) + \frac{k}{\hat{x}} \mathcal{H}\left(\hat{x}\right)^{k-1} \mathcal{H}'\left(\hat{x}\right) \hat{y}^2\right) \\
&\times \left(x^\alpha + \alpha\xi_x(\cos(\phi)\hat{x}^{\alpha-1} - \hat{y}\sin(\phi))\right) \left(\frac{g'_\phi(\phi)}{\hat{x}} \sin\phi \left(\xi_x \sin\phi - \hat{y}\right)\right) \mathrm{d}\hat{x}\mathrm{d}\hat{y} \\
&= \frac{\bar{N}c g'_\phi(\phi)}{2} \sum_{k=1}^{T} \binom{T}{k} (-1)^{k+1} \left(\xi_x^2 \sin^3\phi \mathcal{H}_{k,\alpha-1} + o(\xi_x^2)\right)
\end{aligned}
\tag{7.31}
$$

Notice that we have expressed the sum in terms of the previously defined integrals $\mathcal{H}_{k,\alpha}$. We notice immediately that the leading order term is of order ξ_x^2 which we can later neglect from our final approximation.

7.5.3 Conectivity in the region M_C

For the M_C region, neighbouring nodes are close by so we approximate $\mathcal{H}(r) \approx 1$, and we observe that the contribution is proportional to the size of

the region,

$$M_C = \int_0^{\phi}\int_0^{\frac{\xi_x\cos\phi}{\cos(\phi+\theta)}} \left(1-\left(1-\mathcal{H}\left(r\right)\right)^T\right)\lambda(r,\theta)r\mathrm{d}r\mathrm{d}\theta$$
$$\approx \int_0^{\phi}\int_0^{\frac{\xi_x\cos\phi}{\cos(\phi+\theta)}} \lambda(r,\theta)r\mathrm{d}r\mathrm{d}\theta = \bar{N}c\frac{\xi_x^{2+\alpha}}{2+\alpha}\int_0^{\phi} g_\phi(\theta)(\cos\phi\sec(\theta-\phi))^{2+\alpha}\mathrm{d}\theta \tag{7.32}$$

In fact the best case scenario (in this particular model) is for the uniform distribution,where $\alpha = 0$, and $g_\phi(\theta) = 1$ leaving,

$$M_C = \bar{N}c\frac{\sin(2\phi)}{4}\xi_x^2.$$

By combining the contributions from each region and taking terms up to order ξ_x the probability a point located along the border is isolated can be written in terms of the following simplified 1-dimensional integral,

$$\begin{aligned} -\frac{\log\mathbb{P}_{\mathrm{iso}}^T[(\xi_x,0)]}{c\bar{N}} &\approx \int_0^{\infty}\bar{\mathcal{H}}^T\left(r^{\alpha+1}G_\phi+(\alpha+1)G_c r^{\alpha}\xi_x+...\right)\mathrm{d}r \\ -\frac{\log\mathbb{P}_{\mathrm{iso}}^T[(\xi_x,0)]}{c\bar{N}} &\approx I(\alpha+1)G_\phi+(\alpha+1)G_c(0)I(\alpha)\xi_x+... \end{aligned} \tag{7.33}$$

where $I(s) = \int_0^{\infty}\left(1-\left(1-\mathcal{H}\left(r\right)\right)^T\right)r^s\mathrm{d}r$. For the asymptotic approximations we need only expand once for large T now and we are done. This method provides a greater tractability since it involves computing only one integral (albeit with different parameters s), and for large times often an asymptotic approximation can be found.

We now proceed by computing the isolation probabilities for the MIMO and Quasi-disk connection functions.

Example: MIMO

For the MIMO connection function we apply eq. (7.33) directly.

$$-\frac{\log \mathbb{P}_{\text{iso}}^{T}(\boldsymbol{\xi})}{\bar{N}c} = \frac{r_0^{\alpha+2}G_\phi}{\eta}\int_0^\infty \bar{\mathcal{H}}^T(r)r^{\alpha+1}\mathrm{d}r + \frac{(\alpha+1)r_0^{\alpha+1}G_c\xi_x}{\eta}\int_0^\infty \bar{\mathcal{H}}^T(r)r^{\alpha}\mathrm{d}r$$
$$= \frac{r_0^{\alpha+2}G_\phi}{\eta}I_{\text{MIMO}}\left(\frac{\alpha+2}{\eta}\right) + \frac{(\alpha+1)r_0^{\alpha+1}G_c\xi_x}{\eta}I_{\text{MIMO}}\left(\frac{\alpha+1}{\eta}\right), \tag{7.34}$$

where $I_{\text{MIMO}}(s) = \int_0^\infty (1-(1-e^{-x}(2+x^2-e^{-x})^T)x^{s-1}\mathrm{d}x$. We now provide approximations for the integral $I_{\text{MIMO}}(s)$ for large s or large T and $s \leq 1$. When s is large, this implies that the connection function is "very soft" (a small value of η) and/or the majority of nodes are found away from the corner (large α). When α is large, it is preferable that the signal decays relatively quickly else sophisticated network protocols would need to be utilised to avoid outage, hence it is reasonable to assume $s \leq 1$.

First we consider the case when s is large, such that the x^{s-1} term in the integrand dominates, to obtain a simple asymptotic form of the integral in terms of gamma functions.

$$\begin{aligned} I_{\text{MIMO}}(s) &= \int_0^\infty \left(1-\left(1-e^{-x}(2+x^2-e^{-x})\right)^T\right)x^{s-1}\mathrm{d}x \\ &\sim \int_0^\infty Te^{-x}(2+x^2-e^{-x})x^{s-1}\mathrm{d}x \\ &= 2T\Gamma\left[s\right] + T\Gamma\left[s+2\right] - T2^{-s}\Gamma\left[s\right]. \end{aligned} \tag{7.35}$$

For "small" s and large T we can do a similar asymptotic expansion to that of the Roman Harmonic number by splitting the integral up at $c\log T$, with $c \geq 1$.

$$\begin{aligned} I_{\text{MIMO}}(s) &= \frac{c\log^s T}{s} + (\log[T^{1-c}(c\log[T])^2] + \gamma)(c\log[T])^{s-1} \\ &+ \left(6\gamma^2 + \pi^2 + 12\gamma\log[T^{1-c}(c\log[T])^2]\right. \\ &\left. + 6(\log[T^{1-c}(c\log[T])^2])^2\right)\frac{(s-1)}{12}(c\log[T])^{s-2} + ... \end{aligned} \tag{7.36}$$

There is an additional constant c in this approximation, since the point in which the integral is split up is sensitive to the choice of α and η. To approximate the integral we first split it up at $c\log[T]$, where c depends on s and T, and $I_L(s), I_R(s)$ being the integral I_{MIMO} with the limits $[0, c\log[T]], [c\log[T], \infty]$ respectively. Starting with $I_L(s)$.

$$
\begin{aligned}
I_L(s) &= \int_0^{c\log[T]} \left(1 - \left(1 - e^{-x}(2 + x^2 - e^{-x})\right)^T\right) x^{s-1}\mathrm{d}x \\
&= \frac{(c\log[T])^s}{s} - \int_0^{c\log[T]} \Bigg(\left(1 - e^{y - c\log[T]}(2 + (c\log[T] - y)^2 - e^{y-c\log[T]})\right)^T \\
&\exp\left((s-1)\log[c\log[T] - y]\right)\Bigg)\mathrm{d}y \\
&= \frac{(c\log[T])^s}{s} - (c\log[T])^{s-1} \\
&\times \int_0^{c\log[T]} \left(1 - e^y T^{-c}(2 + (c\log[T] - y)^2 - e^y T^{-c})\right)^T \exp\left(\frac{(1-s)}{c\log[T]}y\right)\mathrm{d}y \\
&\overset{1}{\approx} \frac{(c\log[T])^s}{s} - (c\log[T])^{s-1} \\
&\times \int_0^{c\log[T]} \left(1 - e^y T^{-c}(c\log[T])^2\right)^T \exp\left(-\frac{(s-1)}{c\log[T]}y\right)\mathrm{d}y \\
&= \frac{(c\log[T])^s}{s} - (c\log[T])^{s-1} \\
&\times \int_0^{c\log[T]} \sum_{k=0}^{T} (-1)^k \binom{T}{k} e^{ky} T^{-kc} (c\log[T])^{2k} \exp\left(-\frac{(s-1)}{c\log[T]}y\right)\mathrm{d}y,
\end{aligned}
\tag{7.37}
$$

where in (1) we have taken the leading order behaviour for large T. Now as $c \geq 1$,

$$
\begin{aligned}
S_1 &= \sum_{k=0}^{T} (-1)^k \binom{T}{k} e^{ky} T^{-kc} (c\log[T])^{2k} \\
&= 1 - e^y T^{(1-c)} (c\log[T])^2 + \frac{T(T-1)}{2} T^{-2c} e^{2y} (c\log[T])^4 + \ldots
\end{aligned}
\tag{7.38}
$$

$$
\begin{aligned}
S_1 = 1 - e^y T^{(1-c)}(c\log[T])^2 + \frac{1}{2}T^{2(1-c)}e^{2y}(c\log[T])^4 + ... \\
\exp\left(-\exp(y)T^{1-c}(c\log[T])^2 + O\left(T^{1-2c}(c\log[T])^4\right)\right).
\end{aligned}
\tag{7.39}
$$

This allows us to write $I_L(s)$ as,

$$
\begin{aligned}
I_L(s) &= \frac{(c\log[T])^s}{s} \\
&\quad - (c\log[T])^{s-1}\int_0^{c\log[T]} \exp\left(-\exp(y)T^{1-c}(c\log[T])^2\right)\exp\left(\frac{(1-s)}{c\log[T]}y\right)\mathrm{d}y \\
&\overset{e^y=u}{=} \frac{(c\log[T])^s}{s} - (c\log[T])^{s-1}\int_0^{T^c} \exp\left(-uT^{1-c}(c\log[T])^2\right)u^{-\frac{(s-1)}{c\log[T]}y-1}\mathrm{d}u \\
&= \frac{(c\log[T])^s}{s} - (c\log[T])^{s-1}\mathrm{EI}\left[1+\frac{s-1}{c\log[T]}, T^{1-c}(c\log[T])^2\right].
\end{aligned}
\tag{7.40}
$$

Here, $\mathrm{EI}[n,z]$ is the exponential integral defined as, $\mathrm{EI}[n,z] = \int_1^\infty e^{-zt}t^{-n}\mathrm{d}t$. Let's leave this for now and turn our attention to the right hand side integral. For the RHS we have,

$$
\begin{aligned}
I_R(s) &= \int_{c\log[T]}^\infty \left(1-\left(1-e^{-x}(2+x^2-e^{-x})\right)^T\right)x^{s-1}\mathrm{d}x \\
&\overset{(1)}{=} \int_0^\infty \sum_{k=1}(-1)^{k+1}\binom{T}{k}\exp(-y)T^{-c}(c\log[T])^2 \\
&\quad \times \exp\left((s-1)\log[c\log[T]+y]\right)\mathrm{d}y \\
&\overset{(2)}{=} (c\log[T])^{s-1}\int_0^\infty \exp\left(\frac{(s-1)}{c\log[T]}y\right)\mathrm{d}y \\
&\quad - (c\log[T])^{s-1}\int_0^\infty \exp\left(-\exp(-y)T^{1-c}(c\log[T])^2\right)\exp\left(\frac{(s-1)}{c\log[T]}y\right)\mathrm{d}y
\end{aligned}
\tag{7.41}
$$

$$I_R(s = (c\log[T])^{s-1}\Bigg(\mathrm{EI}\left[1+\frac{s-1}{c\log[T]}, T^{1-c}(c\log[T])^2\right] - \frac{c\log[T]}{s-1} - \Gamma\left[-\frac{s-1}{c\log[T]}\right](T^{1-c}(c\log[T])^2)^{\frac{s-1}{c\log[T]}}\Bigg), \tag{7.42}$$

where in (1) we have made the change of variables $x = y - c\log[T]$, written the x^{s-1} term as an exponential, approximated $e^{-y}T^{-c}(2 + (y + c\log[T])^2 - e^{-y}T^{-c}) \sim e^{-y}T^{-c}(c\log[T])^2$ and used the binomial theorem; (2) using the approximation of S_1, and expanding the logarithm in terms of small y .

Therefore, we can use the above to approximate the MIMO connection function when T becomes large.

$$\begin{aligned} I_{\mathrm{MIMO}}(s) &\approx \frac{(c\log[T])^s}{s} - (c\log[T])^{s-1}\Bigg(\frac{c\log[T]}{s-1} \\ &\quad + \Gamma\left[-\frac{s-1}{c\log[T]}\right](T^{1-c}(c\log[T])^2)^{\frac{s-1}{c\log[T]}}\Bigg) \\ &= \frac{c\log^s T}{s} + (\log[T^{1-c}(c\log[T])^2] + \gamma)(c\log[T])^{s-1} \\ &\quad + \left(6\gamma^2 + \pi^2 + 12\gamma\log[T^{1-c}(c\log[T])^2] + 6(\log[T^{1-c}(c\log[T])^2])^2\right) \\ &\quad \times \frac{(s-1)}{12}(\log[T])^{s-2} + ... \end{aligned} \tag{7.43}$$

The accuracy of this approximation depends on the choice of c which itself depends on the parameters α and η, however in typical urban environments choosing $c \approx 2$ works well, see Fig 7.2 for a demonstration of this. Alternatively, c can easily be found on a case by case basis if α and η are known through inspection of the integrand, which is far more convenient than numerically computing the original integral for all values of T[4].

[4] The main point of this approach is to highlight that the problem can be decomposed into solving one integral, which often itself can be given in a more convenient form saving lengthy computations. For example, having a good approximation of the isolated

Example II: Quasi Disk Model

The quasi-disk model is a piecewise connection function which can model a change in channel conditions; for example transitioning from a clutter free environment to a cluttered one. In general, assuming a SD model transitioning to one which decays with distance at r_-, through application of eq.(7.3) we obtain,

$$\begin{aligned} -\frac{\log \mathbb{P}_{\text{iso}}^{T}(\boldsymbol{\xi})}{\bar{N}c} &= \left(1-(1-\wp)^{T}\right)\int_{\mathcal{V}\cap B_{\boldsymbol{\xi}}(r_-)} y^{\alpha+1} g_\phi(\theta)\mathrm{d}y\mathrm{d}\theta \\ &+ \int_{\mathcal{V}\cap \mathcal{A}_{\boldsymbol{\xi}}(r_-r_+)} \left[\left(1-\left(1-\wp+\wp\left(\frac{y-r_-}{r_+-r_-}\right)^{\mu}\right)^{T}\right)\right] y^{\alpha+1}\mathrm{d}y g_\phi(\theta)\mathrm{d}\theta. \end{aligned} \tag{7.44}$$

We can use the previous result for the soft-disk model (see Table 7.1) for the first term on the right hand side in eq(7.44). The second term, (denoting the inner radial integral as I_{Quasi}) can only be given in semi-analytic form using the previously outlined methods when $\boldsymbol{\xi} \neq 0$. That is to say we are left with an integral of the form $\int_0^{\phi} g_\phi(\theta)(..{}_2F_1\left(a,b;c;\xi\cos\theta\right))\mathrm{d}\theta$, where ${}_2F_1\left(a,b;c;z\right)$ is the Gauss hypergeometric function, which cannot be computed. From method II we need to compute the radial integral where we let $r_+ = \kappa r_-$.

$$I_{\text{Quasi}}(\alpha+1) = \int_{r_-}^{\kappa r_-}\left[\left(1-\left(1-\wp+\wp\left(\frac{y-r_-}{r_+-r_-}\right)^{\mu}\right)^{T}\right)\right] y^{\alpha+1}\mathrm{d}y \tag{7.45}$$

For general values of μ we can only approximate the integrand, but for $\mu = 1$ we can express the integral in terms of the Gauss hypergeometric function,

$$\begin{aligned} I_{\text{Quasi}}(\alpha+1) = \frac{r_-^{2+\alpha}}{2+\alpha}\Bigg[\kappa^{2+\alpha} - 1 + \left(\frac{1}{\Delta(1-\kappa)}\right)^{T}\Bigg(&{}_2F_1\left(-T,\alpha+2,\alpha+2\wp\Delta\right) \\ &- \kappa^{2+\alpha}\,{}_2F_1\left(-T,\alpha+2,\alpha+2\kappa\wp\Delta\right)\Bigg)\Bigg], \end{aligned} \tag{7.46}$$

probability would greatly speed up computations of the mean number of isolated clusters.

where $\Delta = \frac{1}{1-\kappa(1-\wp)}$ and $\kappa \neq \frac{1}{1-\wp}$ so $\Delta \neq 0$.

For the case when $\kappa = \frac{1}{1-\wp}$ we use the following limit,

$$\lim_{c\to 0} c^T (-1)^T {}_2F_1\left(-T, a, b, \frac{1}{c}\right) = \frac{\Gamma[b]\Gamma[a+T]}{\Gamma[a]\Gamma[b+T]} \tag{7.47}$$

We now directly use the above result to give I_{radial} when $\kappa = \frac{1}{1-\wp}$,

$$I_{\text{Quasi}}(\alpha+1) = r_-^{2+\alpha}\left(\frac{\kappa^{2+\alpha}-1}{2+\alpha} + \frac{\wp^T(1-\kappa^{2+\alpha+T})}{(2+T+\alpha)(\kappa-1)^T}\right) G_\phi \tag{7.48}$$

Finally from method II we have a general approximation in terms of $I_{\text{Quasi}}(\alpha+1)$

$$\begin{aligned} -\frac{\log \mathbb{P}_{\text{iso}}^T(\xi_x, \xi_y)}{c\bar{N}} =& (1-(1-\wp)^T)\left(\frac{r_0^{\alpha+2}}{\alpha+2} G_\phi + G_c\left(\arctan\left[\frac{\xi_y}{\xi_x}\right]\right) r_0^{\alpha+1}\sqrt{\xi_x^2+\xi_y^2}\right) \\ &+ I_{\text{Quasi}}(\alpha+1) G_\phi + (\alpha+1) I_{\text{Quasi}}(\alpha) G_c(0)\xi_x \end{aligned} \tag{7.49}$$

In the limit as $T \to \infty$ the probability of connection converges to the void probability for the ball of radius κr_-.

$$\lim_{T\to\infty} \mathbb{P}_{\text{iso}}^T(\boldsymbol{\xi}) \to V_{\mathcal{B}}(\boldsymbol{\xi}, \kappa r_-) \tag{7.50}$$

The QD model can be defined such that it has an exponential decay function and the analysis is very similar to that above, the major difference being that the integral $I_{\text{QD}}(\alpha)$ is expressed in terms of Roman harmonic numbers rather than hypergeometric functions.

Table 7.1:

Model	Approximations for the probability a node $\boldsymbol{\xi}$ is isolated at time T
SD	$\exp\left(-\bar{N}c(1-(1-\wp)^T)\left(\frac{r_0^{\alpha+2}}{\alpha+2}G_\phi + G_c(\omega)r_0^{\alpha+1}r + r_0^\alpha G_2(\omega)r^2\right)\right)$
SA	$\exp\left(-\bar{N}c(1-(1-\wp)^T)\left(\frac{(r_+^{\alpha+2}-r_-^{\alpha+2})}{\alpha+2}G_\phi + G_c(\omega)(r_+^{\alpha+1}-r_-^{\alpha+1})r + G_2(\omega)(r_+^\alpha - r_-^\alpha)r^2\right)\right)$
QD	$\exp\left(-\bar{N}c\left((1-(1-\wp)^T)\left(\frac{r_0^{\alpha+2}}{\alpha+2}G_\phi + G_c\left(\arctan\left[\frac{\xi_y}{\xi_x}\right]\right)r_0^{\alpha+1}\sqrt{\xi_x^2+\xi_y^2}\right) + I_{\mathrm{r}}(\alpha+1)G_\phi + (\alpha+1)I_{\mathrm{r}}(\alpha)G_c(0)\xi_x\right)\right)$
Rayleigh	$\exp\left(-\bar{N}c\left(\frac{r_0^{\alpha+2}}{\eta}\Gamma\left[\frac{2+\alpha}{\eta}\right]H_{T,1}^{\frac{2+\alpha}{\eta}}G_\phi + r_0^{\alpha+1}\Gamma\left[\frac{1+\alpha}{\eta}+1\right]H_{T,1}^{\frac{1+\alpha}{\eta}}rG_c(\omega) + ...\right)\right)$
Waxman	$\exp\left(-\bar{N}c\left(r_0^{2+\alpha}\Gamma[2+\alpha]\bar{H}_{T,\beta}^{2+\alpha}G_\phi + r_0^\alpha\Gamma\left[\alpha+1\right]\bar{H}_{T,\beta}^{1+\alpha}G_c(\omega)r + ...\right)\right)$
Interference	$\exp\left(-\bar{N}c\left(\frac{H_T}{(2+\alpha)c_{\mathcal{I}}} + \frac{(c\bar{N})^{\frac{1}{2+\alpha}}}{(c_{\mathcal{I}}G_\phi)^{\frac{1+\alpha}{2+\alpha}}}\Gamma\left[\frac{3+2\alpha}{2+\alpha}\right]H_T^{\frac{1+\alpha}{2+\alpha}}rG_c(\omega) + O(r^2)\right)\right)$
MIMO	$\exp\left(-\bar{N}c\left(\frac{r_0^{\alpha+2}G_\phi}{\eta}I_1\left(\frac{\alpha+2}{\eta}\right) + \frac{(\alpha+1)r_0^{\alpha+1}G_c(0)}{\eta}I_1\left(\frac{\alpha+1}{\eta}\right)\xi_x\right)\right)$

Table of approximations for a range of different connection functions $\mathcal{H}$ calculated from eq.(7.3), see Table 2.1 and Sec 2.2 for definition of connection functions and symbols. Recall that $\boldsymbol{\xi} = (\xi_x, \xi_y)$ is in Cartesian coordinates while $\boldsymbol{\xi} = (r, \omega)$ is in polar coordinates.

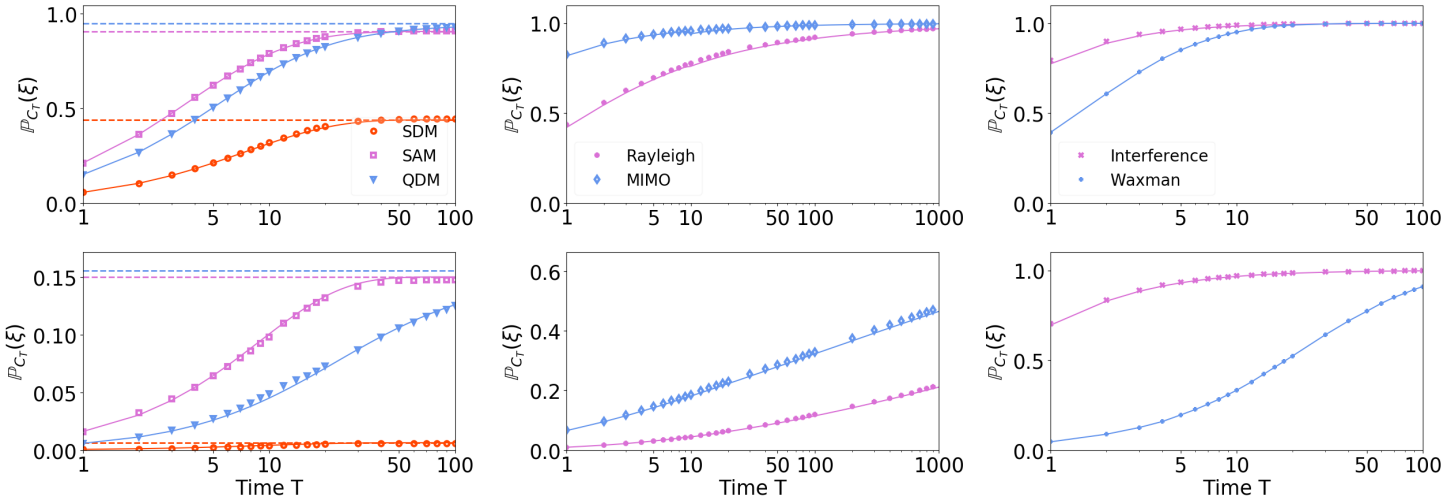

Figure 7.2: The probability that a node located near the corner at $\boldsymbol{\xi} = (0.2, \phi/2)$ is connected for different connection functions. The top panel and bottom panels have parameter $\alpha = 0, 2$ respectively, comparing the impact the spatial distribution of nodes in the network has on connectivity. The dashed lines represent the void probabilities, the solid thin lines are the approximations (given in Table 7.1) and the circle markers are simulated points. For the SD and SA models the approximations are found from translating the densities (Sec 7.3); the Rayleigh, Waxman and Interference case use Method I (Sec 7.4) and the relevant asymptotic approximations, whilst the MIMO case uses method II (Sec 7.5). Parameters $\wp = 0.1, \phi = \frac{\pi}{4}, \eta = 6, \beta = 0.5, r_0 = 1.0; r_- = 1.0, r_+ = 2.5, L = 10$.

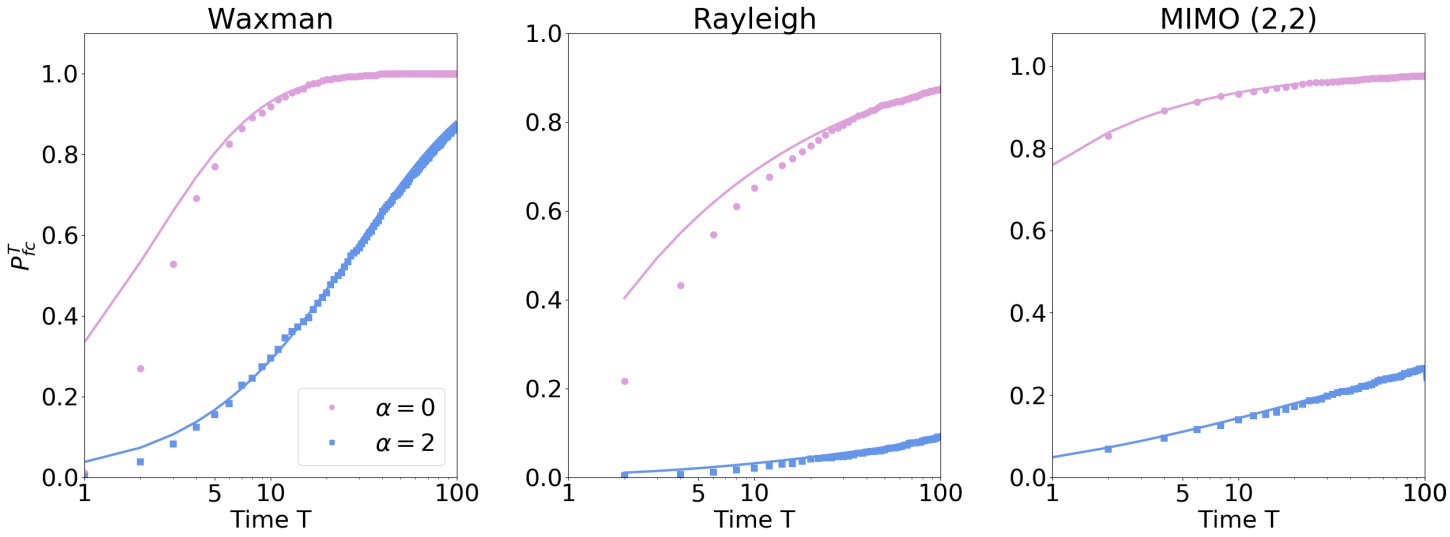

Figure 7.3: The approximate form of the probability that a node located near the corner is connected at time T (solid line) compared with a simulation of the probability every node in the network is connected at time T (circle markers). The figure, certainly for large T and/or large α, the simulated points and expressions match well, suggests that the probability every node is connected at time T is determined by if the one near the corner is connected or not. Parameters used: $L = 10$, $\phi = \pi/4$, $\eta = 2$, $\beta = 0.5$, $\boldsymbol{\xi} = (0.2, \phi/2)$ and $r_0 = 1$.

7.6 Discussion

Firstly, the approximations provided in the previous chapters, included in Table 7.1, are a good fit for the simulated data points, see Fig 7.2. One general observation (all connection functions except for the interference case) is that the probability of connection tends to its maximum much faster for larger $\bar{N}$ (similarly for larger r_0 or smaller α) as the local neighbourhood becomes increasingly dense. For the interference model the change in connection probability as the density changes is much smaller since only the second term depends on $\bar{N}$, a result of the trade-off between connectivity and interference, and as nodes are added to the network the probability of connections are counter balanced by the increase in interference field.

7.6.1 Connection functions with compact support

For connection functions with compact support the probability $\boldsymbol{\xi}$ has connected by time T as $T \to \infty$ tends to the complement of the void probability and is represented by the dashed lines in Fig 7.2. That is to say, the limiting behaviour is restricted to there existing a node within the connection range, i.e the void probability which is characterised by the PPP Φ and r_0, r_-, r_+. Such connection functions are employed in the modelling of wireless sensor networks, and an easy way to ensure connectivity is to enforce an underlying structure to the network (lattice) so that the maximum distance between any two sensors is at most r_0. However, in dense networks (or equivalently when the typical connection range is large) where devices are located predominately within the bulk, it is likely that a lattice structure is not needed and will only waste resources. Our results highlight how the boundaries, along with inhomogeneities, significantly decrease the connection probability. For example, if $r_0 = 1; L = 10; \phi = \pi/2$ then the mean degree when $\alpha = 0$ is ≈ 0.407 compared with ≈ 0.003 when $\alpha = 2$. As a result, in networks that exhibit such behaviour it is likely nodes need only need be added near the boundary to ensure connectivity.

7.6.2 Connection functions with global support

For connection functions with infinite support we see that the probability approaches the complement of the probability the PPP is non-empty and does so faster for a larger $r_0, \bar{N}$ and smaller α. This behaviour is a finite domain effect, and if we condition on there being at least one point in the PPP (or else use a Binomial Point Process), then $\mathbb{P}[C_T] \to^{T\to\infty} 1$. For both the Rayleigh and MIMO cases the asymptotic expansions work well for large T, and improve when the path loss exponent η increases (the signal decays faster), or the distribution of points becomes more uniform. For the MIMO case a better approximation can be provided for specific α, η but it is unclear how to improve it for the general case. However, as the probability for long links increases, such as in the Waxman case, the usefulness of the large T approximation is limited to the uniform case, but for the non-uniform case the approximation for very inhomogeneous networks works well.

The connectivity of infinite networks are obstructed by corner nodes, provided some assumptions on the density that it grows away from the corner, $\alpha > 0$. If however, the PP is uniform, or even if $\alpha < 0$ then the network may never connect and you may have infinitely many isolated nodes [Det18a].

7.6.3 Infinite Mobility Model

In a network where nodes have mobility we should expect an improvement in terms of how long individual nodes remain isolated for due to the self configuring nature of MANETs [Gro01]. This behaviour is highlighted by the extremal case where each node in Φ has infinite mobility which removes the spatial correlation of nodes from one time step to another. In this case, the probability a node is isolated for T consecutive time steps is simply

$$\mathbb{P}^T_{\text{iso}}(\boldsymbol{\xi}) = e^{-TM(\boldsymbol{\xi})}, \tag{7.51}$$

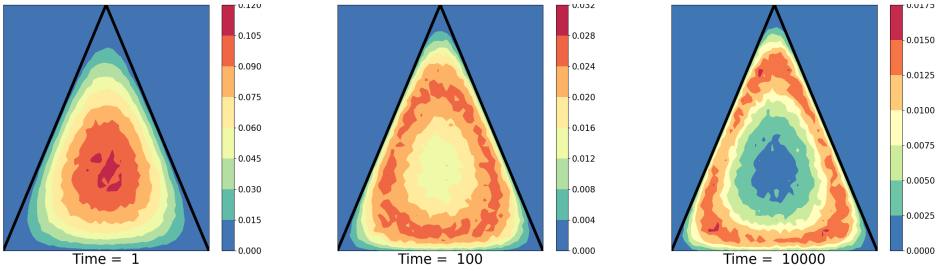

Figure 7.4: The distribution of isolated nodes in a spatio-temporal random graph at time $T = 1, 100, 10000$, for the RWP model. The connection function is the stretched exponential $\mathcal{H}(r) = e^{-\left(\frac{r}{r_0}\right)^{\eta}}$. Parameters: $L = 10, \lambda_0 = 5, \phi = \pi/3, r_0 = 0.1$ and $\eta = 2$.

since a new realisation of Φ happens at each time slot. Hence, the probability $\boldsymbol{\xi}$ is connected at time T is the CDF of a geometric random variable with mean $M(\boldsymbol{\xi})$, therefore $\boldsymbol{\xi}$ can always transmit in finite time provided $M(\boldsymbol{\xi}) > 0$. In this model the number of points varies during each time slot as a new PPP is realised, which can be thought of as modelling devices turning on and off, or alternatively you could condition on the number of points in Φ (BPP).

7.6.4 Full connectivity

In static networks with no temporal component P_{fc} is defined as there existing a multi-hop path between any two nodes in the network. In a temporal network this is more complicated since there exists a network with directional (causal) paths between nodes. We introduce a weaker sense of full connectivity, that is the probability that every node in the network has made at least one link to some other at, or prior to, time slot T; we will denote this as P_{fc}^{T}. Analogous to other work, we want to make use of there being no isolated nodes to approximate that of P_{fc}^{T}[5]. Indeed, focusing on the idea that boundary nodes are likely to be "more isolated" we see that nodes near

[5]Remark: this notion only makes sense for connection functions with long links.

the corner are the last to connect when links are independent,see Fig 7.3, as we saw in previous chapters. In addition to this we plot the distribution of isolated nodes at different times in Fig 7.4, for a SRGG in a triangle with the distribution given by eq.(3.23) and $\mathcal{H}(r) = e^{-r^2}$. Initially the isolated nodes are focused more toward the bulk, as that is where the higher proportion of nodes are. As time elapses the isolated nodes in the bulk form links as there neighbours are on average closer resulting in the remaining isolated nodes being located near the boundaries. Clearly, the distribution of isolated nodes can no longer be modelled by a limiting Poisson distribution as in the uniform case. From this we should expect that the nodes that take the longest to connect are located near the boundary. Naturally, when considering interference this behaviour is not necessarily true since nodes near the bulk may be in outage if the interference field is to high; in fact the boundary may help connectivity due to a decreased interference field. Essentially, we have shown in Fig 7.3 that the time for every node in the network to form a link is determined by how long the highly isolated nodes take to form a link, which are those nodes near the corners. Furthermore, provided the network is dense enough and $\alpha \gtrapprox 1$ then it is likely the first causal path occurs from any node in the network to a boundary node when the boundary node makes a single connection.

For infinite networks with non-uniform measure isolated nodes are likely be play a more significant role for P_{fc} [Det18a]. For example, if $\alpha \leq 0$ then the number of isolated nodes is infinite, and thus P_{fc} can never be achieved, whereas when $\alpha > 0$ the behaviour is likely to be determined by highly isolated nodes [Det18a].

7.6.5 Routing

This work also highlights the need for flexible routing algorithms in mesh networks. Most routing algorithms in mesh networks fall between two extremal cases: proactive and reactive routing. The former is the case when

a node periodically exchanges information with its neighbours giving it an awareness of paths to other nodes in the network, but as a result has more drain on resources such as power, and can influence the connectivity of other nodes in its neighbourhood when interference is considered. Reactive routing on the other hand only looks for a path between nodes in a network when it is required, which helps to conserve resources but delays the time of information transfer as it needs to find a route. Naturally, most algorithms proposed fall somewhere in between these two extremes. One example is PathDetect, an example of a decentralised algorithm, discussed in Ref [Iye13]. In this model, local messages are exchanged between neighbouring nodes to achieve global knowledge of the network, ultimately allowing it to track temporal fluctuations in connectivity. The main problem is how to minimise the overheads in obtaining this global picture, which can be achieved through an understanding of the network topology, for example employing an adaptive power scheme based on the location of the user. Alternatively, one could employ multipath routing with network coding. In multipath routing, multiple paths are chosen between the source and destination nodes, meaning it is less probable that all the chosen paths will have broken links. In network coding, random linear combinations of original packets are transmitted, so even if one or two paths have broken links, the destination can still recover the original packets. With this assumption, it can be predicated that nodes near the boundary/sparse regions being in proactive routing mode and nodes in the bulk being in reactive routing mode will likely minimize the delay between the source and destination [Zha09].

Chapter 8

Isolated Clusters

So far we have explored the role isolated nodes have on connectivity in spatio-temporal networks, but what can we say about the structure of the graph beyond just isolated nodes? The aim is to go further than the previous chapter and analyse the clusters of size greater than one. For classical (uniform) RGGs isolated nodes are the obstacle to P_{fc} and these follow a limiting PPP if the distribution is uniform. This is a consequence of not being able to have two isolated nodes close together, as these themselves will connect. Namely, the probability a point being isolated, given that it lies in a cluster of finite size, goes to one in the dense network limit [Pen91]. This work has more recently been extended by Ref [Las18] to study the first and second order properties of SRGGs for a uniform PPP. In the non-uniform SRGG it is feasible that isolated subgraphs (cliques of size two or more) play an important role in P_{fc}; here we aim to explore this through the average number of clusters of size K. This work is an extension of the previous chapter and has not been published.

8.1 System Model

We adopt a similar to the model as in the previous chapter and aim to keep the analysis as general as possible. Let Φ denote a PPP in the triangular domain defined by

$$A = \{(x, y)|0 \leq x \leq L, 0 \leq y \leq \min[x \tan \phi, -(x - L) \tan \phi]\} \tag{8.1}$$

with the distribution of points being modelled by $\lambda(r, \theta)$. Once again let $\mathcal{H}(r)$ denote a connection function with infinite support with no directionality (i.e $\mathbb{P}[\boldsymbol{x} \rightarrow \boldsymbol{y}] = \mathbb{P}[\boldsymbol{y} \rightarrow \boldsymbol{x}]$). Furthermore, let the probability be independent of time and the rest of the points in Φ, therefore ignoring any interference. Finally, we once again assume that the time for a link to be realised is much smaller than the time for a node to move, hence, we can assume the nodes in Φ are not mobile between time slots. The difference from the previous chapter is that here we need to consider the connected subgraphs that are disconnected from the rest of the network. Let $\mathcal{G}_K$ denote a connected subgraph of K nodes, not necessarily in Φ. The question we aim to address is, *How long is a connected component $\mathcal{G}_K$ of size K isolated from any node in Φ?*

8.2 Probability a subgraph is isolated and its expectation

We proceed by providing a general analysis for T time slots, and a graph with K components in it that are all connected. We first write the probability of there being a subgraph $\mathcal{G}_K$ isolated from Φ conditioned on the locations of all the other nodes in Φ, then average over all possible realisations of the point process Φ. In this case we do not need to assume that the locations of the nodes in $\mathcal{G}_K$ have the same distribution as those in Φ, in fact they can be separate from Φ altogether. However, as later on in this section we use the fact that $\mathcal{G}_K \in \Phi$ and we will assume that this is the case here also,

and denote $\hat{\Phi} = \Phi \backslash \mathcal{G}_k$ as the set of points excluding the subgraph and apply Slivnyak's theorem (see Sec 2.1.1).

$$\begin{aligned}
\mathbb{P}^T_{\text{iso}}(\mathcal{G}_k) &= \mathbb{E}_\Phi \left[\left(\mathbb{P}[\mathcal{G}_K \text{ is connected}, \boldsymbol{y} \not\to \hat{\Phi} \forall \boldsymbol{y} \in \mathcal{G}_K | \Phi, \mathcal{G}_K] \right)^T \right] \\
&= \mathbb{E}_\Phi \left[\mathbb{P}[\mathcal{G}_K \text{ is connected} | \mathcal{G}_K]^T \mathbb{P}[\boldsymbol{y} \not\to \hat{\Phi} \forall \boldsymbol{y} \in \mathcal{G}_K | \Phi, \mathcal{G}_K] \right)^T \Big] \\
&= \mathbb{E}_\Phi \left[\mathbb{P}[\mathcal{G}_K \text{connected}]^T \prod_{\boldsymbol{x} \in \hat{\Phi}} \prod_{\boldsymbol{y} \in \mathcal{G}_K} (1 - \mathcal{H}(|\boldsymbol{x} - \boldsymbol{y}|))^T \right] \\
&= \mathbb{P}[\mathcal{G}_k \text{connected}]^T \exp\left(- \int_A \left(1 - \prod_{\boldsymbol{y} \in \mathcal{G}_k} (1 - \mathcal{H}(|\boldsymbol{x} - \boldsymbol{y}|))^T \right) \lambda(x, \theta) \mathrm{d}\boldsymbol{x} \right),
\end{aligned} \tag{8.2}$$

where in the last inequality we have used the PGFL in eq.(2.6) for a PPP. The integral in the exponential is the modified connectivity mass, which we denote $M^T_{\mathcal{G}_K}(\boldsymbol{y}_1, ..., \boldsymbol{y}_K)$, where for $T = 1$ and $\mathcal{G}_k = \boldsymbol{y}_1$ we retrieve the usual connectivity mass [Coo12a]. The structure of $\mathcal{G}_K$ has numerous possibilities. For small K the sequence of how many ways to construct a connected graph of size $1, 2, 3, 4, 5, ...$ goes like $1, 1, 4, 38, 278, ...$, [Wil05]. The two extremal cases for how the subgraph can be connected are the complete graph K_K and one which has exactly one Hamiltonian path L_K. The probability of being connected in both these cases are,

$$\mathbb{P}[\mathcal{G}_k \text{connected}] = \begin{cases} \frac{1}{k!} \prod_{i=1}^{k-1} \prod_{j=i+1}^{k} \mathcal{H}(|y_i - y_j|), & \text{for } K_K, \\ \frac{1}{k!} \prod_{i=1}^{k-1} \mathcal{H}(|y_i - y_{i+1}|), & \text{for } L_K. \end{cases} \tag{8.3}$$

The expected number of isolated subgraphs is found by averaging eq.(8.2) over all possible permutations of the graph $\mathcal{G}_K$, and is consistent with results

in [Las18].

$$\begin{aligned}\mathcal{C}^T_{\mathcal{G}_k} &= \mathbb{E}_{\mathcal{G}_k}\left[\left(\mathbb{P}[\mathcal{G}_k\text{connected}]^T \exp\left(-M^T_{\mathcal{G}_K}(\boldsymbol{y}_1,...,\boldsymbol{y}_K)\right)\right)\right] \\ &=^{(2)} \int_A ... \int_A \mathbb{P}[\mathcal{G}_k\text{is connected}]^T e^{-M^T_{\mathcal{G}_k}(\boldsymbol{y}_1,...,\boldsymbol{y}_K)} \lambda(\boldsymbol{y}_1)...\lambda(\boldsymbol{y}_K)\mathrm{d}\boldsymbol{y}_K...\mathrm{d}\boldsymbol{y}_1.\end{aligned} \tag{8.4}$$

This computation becomes very expensive very quickly. For example, even for a subgraph of size two it involves computing four integrals with the integrand itself having a double integral in an exponential. We remark however the condition for $\mathcal{G}_K$ to be connected is very restrictive in this case. For example, in reality it is likely we refer to $\mathcal{G}_K$ as connected if there is a multihop path between every node in $\mathcal{G}_K$ from the first time slot to some time T. In this case there may be multiple time slots in between where the edge set is empty, but the subgraph is still "connected" as all information is able to be relayed between all pairs of nodes by time T.

8.3 Discussion

In Fig 8.1 we show how the number of clusters of size K decays as a function of time. Clearly for isolated nodes this is non-increasing, but for clusters of size ≥ 2 this is not the case as smaller clusters combine to form bigger ones. Noticeably the number of isolated nodes decays quickly and then slows down as those remaining disconnected nodes are "more isolated", and it is those that obstruct full connectivity. Once again isolated the main obstruction to full connectivity, but those smaller clusters offer a correction term to that approximation.

Naturally, this model assumes a static distribution of points between time slots, but for mobile networks we should expect the number of isolated clusters to go to zero faster[1]. This work further highlights the need for

[1]Again we do not concern ourselves with the causal paths in the network and nodes

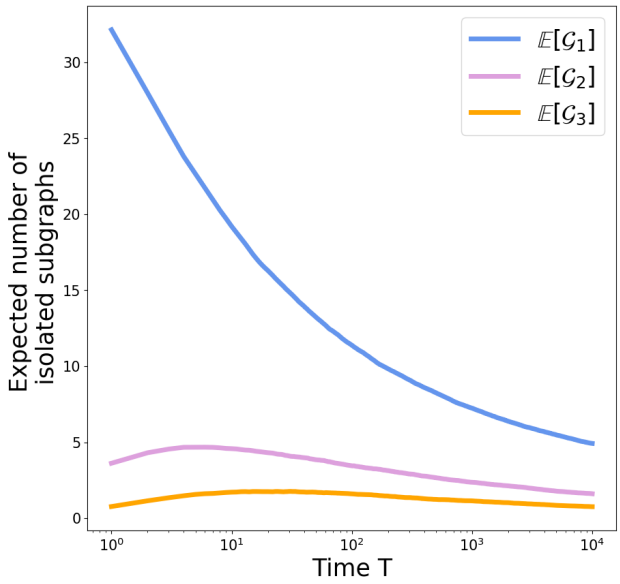

Figure 8.1: The expected number of isolated subgraphs in a spatio-temporal random graph as a function of time, where the spatial distribution of nodes is modelled by the RWP model in the triangle (see eq (3.23) in Sec 3). The connection function is the stretched exponential $\mathcal{H}(r) = e^{-\left(\frac{r}{r_0}\right)^\eta}$. Parameters: $L = 10, \lambda_0 = 1, \phi = \pi/3, r_0 = 0.25$ and $\eta = 2$.

support nodes near boundaries and less populated areas.

becoming connected and then disconnected between time slots.

Chapter 9

Conclusion

Mobility is playing an increasingly important role in wireless networks. As the number of hand-held smart devices continues to grow the networks are becoming increasingly dynamic. Mobility itself is a wide field of research with a wealth of literature dedicated to it, from the usual Random Walk models, to more simulation-based models such as the Self-similar Least Action Walk [Lee12]. Thus, characterising the impact of human mobility remains an important question [Sch17]. In this thesis we approach the problem by using a general non-uniform distribution to model the location of mobile devices, with a particular case being the stationary distribution of the Random Waypoint Model. In doing so, we are able to analyse how regions of low/high density and boundaries affect local and global connectivity, both as a single snapshot of the network and over multiple time slots.

9.1 Mobility

Analysing network performance under general human mobility models is notoriously difficult and results are normally given for very specific examples [Bro06, Ben07, Lee12] or in terms of thresholds of network performance [Tse05]. As such, we aim to focus on analysing networks with non-uniform

densities that are a consequence of mobility. Two models that are widely used throughout the wireless literature are the Random Walk (RW) and the Random Waypoint (RWP) models, with each converging to a stationary distribution of users for long times. The RW has a uniform stationary distribution of users (in 2 dimensions or less), whilst the RWP has a concave distribution of users where the density is higher in the bulk than at the boundaries. The latter provides an intuitive model for human mobility, whilst remaining tractable. We would expect, from simple observations, that in cities the density of users is higher in the centre than near the outskirts, particular at busy shopping time or working hours; this is exactly what the RWP models.

As a starting point our first result was to calculate the exact stationary distribution in rectangular and triangular regions and compare this with approximations. We observed that the stationary distributions of the exact and approximate forms both captured the key characteristics of the model, with the density being highest in the bulk and going to zero at the boundaries (when pause times are neglected) with the main discrepancy between the approximate and exact coming near the corners. Although the distributions do differ quantitatively, the increased tractability of the approximate form, and it capturing the key features of the RWP, led to us using this model in the subsequent discussions to study mean degree and coverage in 5G networks.

9.2 Mean Degree

Having now a method to analyse the impact of mobility, we began by analysing the mean degree (Chapter 4). The mean degree (the average number of links a node can make) is a standard metric for networks as it gives an indication to the global connectivity; a network is likely to be disconnected if the mean degree is small, and certainly will be if it is less than one. We studied three different types of SRGGs in this case, the disk model (RGGs), the Rayleigh model and the interference-limited case. For the first two cases the mean de-

gree scales with the number of nodes, regardless of the connection function being deterministic or probabilistic, with the mean degree being highest in more densely populated regions away from the boundaries.

For the interference model, the probability a pair of nodes form a link also depends on the other points in the network which often leads to some interesting behaviour. In particular for a singular and non-singular path loss model the results are very different. For a singular path loss model the mean degree increases with the number of nodes, then plateaus; whilst for the non-singular case it initially increases until some maximum then decays to zero. The latter seems to provide a more intuitive model: initially the benefit of having more nodes to connect to outweighs an increase in the interference field until some threshold density where the interference effects dominate and the mean degree decreases to zero. Moreover, this result can be related to one regarding percolation. The authors of [Dou06] showed that for a non-singular model percolation in SIR graphs occurs for an interval of densities. For the singular model, we should expect to see a more classical picture of percolation, namely the probability of percolation is non-decreasing.

Importantly we highlight how mobility impacts the connectivity of SRGGs, and extend our analysis to SRGGs with interference. In the typical model with uniform measure the interference field is independent of location (except near a boundary if there is one). We show that in a MANET it is beneficial to be in regions where the density is highest, even with the increased interference field. The only exception happens for the peculiar case when the density is highest at the boundary where it is better to be situated near the border instead.

9.3 Ultra-dense and Low Power networks

The variations in connectivity due to mobility raises the question how future networks should be deployed to cope with increasingly dynamic networks. 5G networks are expected to be extremely dense and comprised of a range

of different APs, each with different transmit powers. We addressed how APs should be deployed to meet the dynamic demand of mobile users in chapter 5. In this model a user connects only to its nearest AP and the user benefits from being in regions of high AP density. Through brute force optimisation techniques we show that APs should match the user profile when the profile of users is convex, but uniform for uniform or concave distribution of MUs. Therefore, through a simple ALOHA protocol network performance can easily be met by switching APs on or off to meet traffic demand; a result that can be used to influence how 5G networks should be deployed. We then extended this to cooperative networks, where the signal was the sum of a MU's K nearest neighbours, where we showed the increased diversity improved network coverage.

We also discuss the somewhat related problem of connectivity in Low Power wide area networks, and provide some initial approximations for typical network scenarios. Our approximations use the fact that the network is very sparse and thus the maximum interfering signal can be approximated as the closest one. In dense regimes closed form calculations are difficult since order statistics need to be used for the different connection criterion. However, the method we use is highly generalisable and can easily be extended to network optimisation and multiple gateways, which is discussed below regarding interesting open problems.

9.4 Spatio-temporal networks

Much of this work, and that in the literature, is for single snap shot analysis. In Chapter 7 we extend our approach to non-uniform SRGGs and analyse how long a node near a corner is isolated for over multiple time slots. For low power networks where the links are better modelled by SRGGs with compact support, the isolation depends greatly on the "local neighbourhood" of the node. Namely, there has to be a node within the support of the connection function for it to connect, meaning to mitigate node isolation

a more regular structure of support nodes is suitable. However, for longer range connection functions, it is those highly isolated nodes that are likely to be the bottleneck to P_{fc}. In particular, in mobile networks it is those few nodes that find themselves near a boundary (particularly corners) which are likely to be isolated, highlighting that support nodes need to be located near boundaries and areas where the density is low. In this case, to have efficient network routing boundary nodes should be proactive (periodically update its knowledge of neighbours), whilst nodes near the bulk should be reactive (only find a path when it is needed). To address full connectivity in these temporal networks is difficult, but by showing that it is those nodes near the boundaries which are last to connect we can see that it is once again those highly isolated nodes are the obstruction.

As a comparison we also looked at networks where nodes had infinite mobility, or alternatively where the assumed time scales had swapped, the typical time between transmissions was much larger than the time it took for nodes to move around the domain. In this case we showed that high mobility networks help to resolve these highly isolated nodes. As such the performance of realistic MANETs will fall somewhere in between the two scenarios, with more mobile networks being more connected.

Although posed in terms of MANETs, this has interesting connotations for HetNets, where the nodes in the domain are APs (assumed fixed) and the user is mobile. In this case, APs may be deployed near the centre to meet high traffic demand in working hours as in the coverage problem, but to maximise user experience, border nodes should be deployed to help support those highly isolated nodes. For example, in order to meet demand in 5G networks the distribution of APs should roughly mirror that of the spatial distribution of users, whilst also keeping residual border nodes to ensure users near the boundary don't become isolated.

Throughout this body of work we have shown the important role that mobility has on the performance of a wide range of communication networks, both current and future. Many of our results can be used to better under-

stand how future 5G and mobile ad hoc networks should be deployed to maximise experience, along with how information should be routed within dynamic networks. We now discuss some open problems that extend this work to different scenarios.

9.5 Outlook

We begin this discussion on some interesting open problems that arose whilst on my industrial placement regarding LoRa networks.

Referring back to the model outlined in Chapter 6, one important question still to ask is: given a distribution of end users, how should I draw my annuli to maximise the coverage in the network? This problem can easily be achieved through a brute force optimisation technique, but it would be interesting if a more elegant solution could be found.

Another related problem is how the network performs with multiple gateways. Typically, by adding network diversity (increasing the number of gateways) network performance should increase. In this model, an end user should aim to maximise both q_{SF} and its coverage probability (minimise the impact of interfering signals). Quantifying the impact this diversity has would be very interesting to study, particular when the gateways themselves are different; they have different spreading factors (q_{SF}) associated to different annuli which themselves may have different widths. One approach is to relax the constraint that a device would maximise the q_{SF} but instead transmit to its nearest gateway assuming they are identical. In particular, this model would be a suitable for a small γ, which is expected. In this case, all of the previous analysis can be used. Alternatively, the more complex scenario could easily be analysed through extensive simulations, but a more mathematical analysis may provide deeper insights into performance.

Another interesting problem is one of isolated clusters and their role in P_{fc}. We gave some brief discussions on how long a node is isolated for, and the expected number of isolated nodes at time T, but this is certainly not

the whole picture. For example, if an effective way to approximate isolated clusters in a network is achieved, then this may act as correction term for isolated nodes approximation. However, as we discussed previously, the approximations we used for the isolated nodes were no longer valid for the larger subgraphs. Furthermore, our notion of full connectivity is a weak one. It is feasible that the network may have nodes that are connected over a range of time slots, but disconnected from the rest of the network. For example, two (likely highly isolated) nodes could continually be connecting to one another, but no other nodes. Ideally we want to look at the time when every node has a causal path to every other, and what obstructs this. From this work we might expect that it is those highly isolated nodes that are the obstruction, but it would be nice to verify this.

Finally, an important question for the study of SRGGs is to look beyond the usual Poisson Point Process to capture an even more diverse network structure, including the attraction and repulsion of points through different point processes such as the determinantal, Cox and Gibbs processes.

9.6 Concluding Remarks

Soft Random Geometric Graphs have a wide range of applications, particularly to current and future communication networks. Of particular interest is how these networks are becoming increasingly dynamic as technology evolves and smart devices become more mobile. Through tools from stochastic geometry, we have explored how human mobility can impact upon the connectivity properties of a wide range of these communication networks. The non-uniform nature of mobile networks means the performance is highly location dependent. Particularly, the non-constant interference field whole regions can become disconnected from either having too few (the number of close neighbours is low) or too many devices (the interference field is too strong). Our results can be applied to a wide range of topics including: understanding percolation in interference-limited networks; the optimal de-

ployment of Access points in 5G networks and efficient routing algorithms in spatio-temporal networks, all with a focus on how the non-uniform distribution of devices induced by mobility causes the global connectivity picture to change.

Appendices

Appendix A

Publication List

During my thesis I have been listed as a co-author in the following publications:

1. Pratt, Pete, Carl P. Dettmann, and Orestis Georgiou. "How does mobility affect the connectivity of interference-limited ad hoc networks?." Modeling and Optimization in Mobile, Ad Hoc, and Wireless Networks (WiOpt), 2016 14th International Symposium on. IEEE, 2016.

2. Pratt, Pete, Carl P. Dettmann, and Orestis Georgiou. "Optimal Non-Uniform Deployments in Ultra-Dense Finite-Area Cellular Networks." IEEE Communications Letters 21.5 (2017): 1139-1142.

3. Pratt, Pete, Carl P. Dettmann, and Woon Hau Chin. "Temporal connectivity in finite networks with nonuniform measures." Physical Review E 98.5 (2018): 052310.

4. Dettmann, Carl P., Orestis Georgiou, and Pete Pratt. "Spatial networks with wireless applications." Comptes Rendus Physique 19.4 (2018): 187-204.

The above work was done in close collaboration with my supervisors who were also named as authors. Any simulations were done in Python3

along with the numerical integration using the Scipy package. Mathematica was also used for dealing with the special cases of the Gauss hypergeometric function. To clarify my contributions for each paper I give a summary below.

Paper 1 Calculating the exact spatial distribution for the Random Waypoint model; calculating the solvable cases of the interference-limited connection probability and mean degree for interference free networks, and the remaining numerical computations. The numerical integration was also carried out simultaneously by Dr Orestis Georgiou. I also helped to write this paper.

Paper 2 Calculating the nearest neighbour distribution and coverage probability for non-uniform networks, both analytically and numerically; numerically calculating the optimal distribution of points and writing the paper (and revisions) with guidance from my supervisors.

Paper 3 Choosing the initial problem; all the analytical and numerical calculations, including simulations, along with writing the paper and doing any revisions. It was pointed out to me that an alternate approach could be done by Professor Carl Dettmann hence why there are two methods to calculating the isolation probabilities, along with a more general choice of density to the one I had originally decided upon.

Paper 4 I helped to draft the review; complete suggested edits from the reviewer and wrote the sections on point processes (Sec 2 of Ref [Det18b]); percolation (Sec4.2 of Ref [Det18b]); temporal networks (Sec 7 of Ref [Det18b] and mobility (Sec 8 of Ref [Det18b]).

Appendix B

Python Code for a non-uniform PPP

Some example code to create a non-uniform PPP in a circular domain, written in python3. A more general approach can be used by passing the distribution function to the PPP function itself, but this becomes less readable.

```
from __future__ import division
import numpy as np
from scipy.stats import poisson

def dist_example(r, R, b = 0):
    '''
    Example of distribution of function that could be passed
    to PoissonPointProcess function.
    Default b value is zero
    if not specified when calling function
    '''
    return (1 - (b*R**2)/2 + b * r**2)

def PoissonPointProcess(rt, R, dist, dist_kwargs):
```

```
    '''
    Function that generates a PPP in a circle with
    distribution given by the function passed as  dist.
    R: Radius of circle
    rt: rate of PPP desired.
    dist: distribution of function for PPP
    dist_kwarg: keyword arguments passed to distribution function
    '''
    k = 2.3# Parameter ensuring mean_a > mean_b
    mean_a = rt * 4 * R**2 # Mean number of points in PPP A
    #Instance for how many point in original PPP
    N = poisson.rvs(k * mean_a)
    #Generate N points uniform - x direction
    x = np.random.uniform(-R, R, N)
    #Generate N points uniform - y direction
    y = np.random.uniform(-R, R, N)

    new_pts = [(i, j) for i, j in zip(x,y) if j**2 + i**2 <= R**2
              and  dist(np.sqrt(j**2 + i**2), R, **dist_kwargs)/k
                >= np.random.uniform(0, 1)   ]

    return new_pts
```

Appendix C

Random Waypoint Model

In this appendix we give a more detailed method for calculating the exact spatial distribution of the RWP in the rectangle and triangle, beginning with the former.

C.1 RWP Rectangle

We begin by reminding the reader that the aim is to solve the following integral,

$$\int_0^{\pi} a_1(x,y)a_2(x,y)(a_1(x,y)+a_2(x,y))\mathrm{d}\theta \tag{C.1}$$

where

$$\begin{aligned} a_1(x,y) &= \begin{cases} \frac{a-x}{\cos\theta} & 0 \le \theta < \arctan\left[\frac{b-y}{a-x}\right] \\ \frac{b-y}{\sin(\theta)} & \arctan\left[\frac{b-y}{a-x}\right] \le \theta < \pi - \arctan\left[\frac{b-y}{a+x}\right] \\ -\frac{(a+x)}{\cos(\theta)} & \pi - \arctan\left[\frac{b-y}{a+x}\right] \le \theta < \pi \end{cases} \\ a_2(x,y) &= \begin{cases} \frac{a+x}{\cos\theta} & 0 \le \theta < \arctan\left[\frac{b+y}{a+x}\right] \\ \frac{b+y}{\sin\theta} & \arctan\left[\frac{b+y}{a+x}\right] \le \theta < \pi - \arctan\left[\frac{b+y}{a-x}\right] \\ \frac{x-a}{\cos(\theta)} & \pi - \arctan\left[\frac{b+y}{a-x}\right] \le \theta < \pi \end{cases} \end{aligned} \tag{C.2}$$

To solve eq.(3.4) we split the integral into the five piecewise components and solve separately.

$$\begin{aligned}\int_0^{\pi} a_1a_2(a_1+a_2)\mathrm{d}\theta &= \int_0^{\arctan\left[\frac{b+y}{a+x}\right]} a_1a_2(a_1+a_2)\mathrm{d}\theta \\ &+ \int_{\arctan\left[\frac{b+y}{a+x}\right]}^{\arctan\left[\frac{b-y}{a-x}\right]} a_1a_2(a_1+a_2)\mathrm{d}\theta \\ &+ \int_{\arctan\left[\frac{b-y}{a-x}\right]}^{\pi-\arctan\left[\frac{b+y}{a-x}\right]} a_1a_2(a_1+a_2)\mathrm{d}\theta \\ &+ \int_{\pi-\arctan\left[\frac{b+y}{a-x}\right]}^{\pi-\arctan\left[\frac{b-y}{a+x}\right]} a_1a_2(a_1+a_2)\mathrm{d}\theta \\ &+ \int_{\pi-\arctan\left[\frac{b-y}{a+x}\right]}^{\pi} a_1a_2(a_1+a_2)\mathrm{d}\theta \\ &= I_1^{\square}+I_2^{\square}+I_3^{\square}+I_4^{\square}+I_5^{\square}\end{aligned} \tag{C.3}$$

Note that we have dropped the notation of writing $a_1(x,y), a_2(x,y)$ but instead use a_1, a_2 for brevity.

We now proceed by explicitly calculating the integrals starting with I_1.

$$\begin{aligned}I_1^{\square} &= \int_0^{\arctan\left[\frac{b+y}{a+x}\right]} a_1a_2(a_1+a_2)\mathrm{d}\theta = 2a(a-x)(a+x)\int_0^{\arctan\left[\frac{b+y}{a+x}\right]} \sec^3\theta\mathrm{d}\theta \\ &= a(a-x)(a+x)\Bigg(\frac{(b+y)\sqrt{(a+x)^2+(b+y)^2}}{(a+x)^2} \\ &+ \log\left[\frac{1}{a+x}\left(\sqrt{(a+x)^2+(b+y)^2}-(b+y)\right)\right]\Bigg) \\ &= \frac{a(a-x)(b+y)\sqrt{(a+x)^2+(b+y)^2}}{(a+x)} \\ &+ a(a-x)(a+x)\log\left[\frac{1}{a+x}\left(\sqrt{(a+x)^2+(b+y)^2}-(b+y)\right)\right]\Bigg) \\ &= \frac{a(a-x)(b+y)c_1}{(a+x)} + a(a-x)(a+x)\log\left[\frac{c_1-b-y}{a+x}\right]\Bigg)\end{aligned} \tag{C.4}$$

where we have defined $c_1 = \sqrt{(a+x)^2 + (b+y)^2}$.

To facilitate the calculation of I_2 we further split into a further two integrals.

$$\begin{aligned} I_2^{\square} &= \int_{\arctan\left[\frac{b+y}{a+x}\right]}^{\arctan\left[\frac{b-y}{a-x}\right]} a_1 a_2 (a_1 + a_2) \mathrm{d}\theta \\ &= (a-x)(b+y) \int \frac{(a-x)\cos\theta + (b+y)\sin\theta}{\sin^2\theta \cos^2\theta} \mathrm{d}\theta = I_{2a}^{\square} + I_{2b}^{\square} \end{aligned} \tag{C.5}$$

$$\begin{aligned} I_{2a}^{\square} &= \int_{\arctan\left[\frac{b+y}{a+x}\right]}^{\arctan\left[\frac{b-y}{a-x}\right]} \frac{(b+y)^2(a-x)}{\sin^2\theta\cos\theta} \mathrm{d}\theta \\ &= -\frac{(a-x)(b+y)^2\sqrt{(a-x)^2+(b-y)^2}}{b-y} \\ &+ \frac{(a-x)(b+y)^2\sqrt{(a+x)^2+(b+y)^2}}{b+y} \\ &+ (a-x)(b+y)^2 \log\left[\frac{\sqrt{(a-x)^2+(b-y)^2}+b-y}{a-x}\right] \\ &- (a-x)(b+y)^2 \log\left[\frac{\sqrt{(a+x)^2+(b+y)^2}+b+y}{a+x}\right] \\ &= -\frac{(a-x)(b+y)^2 c_2}{b-y} + \frac{(a-x)(b+y)^2 c_1}{b+y} \\ &+ (a-x)(b+y)^2 \log\left[\frac{c_2+b-y}{a-x}\right] - (a-x)(b+y)^2 \log\left[\frac{c_1+b+y}{a+x}\right] \end{aligned} \tag{C.6}$$

$c_2 = \sqrt{(a-x)^2 + (b-y)^2}$

$$I_{2b}^{\square} = \int_{\arctan\left[\frac{b+y}{a+x}\right]}^{\arctan\left[\frac{b-y}{a-x}\right]} \frac{(b+y)^2(a-x)}{\sin^2\theta\cos\theta} \mathrm{d}\theta \tag{C.7}$$

$$
\begin{aligned}
I_{2b}^{\square} &= -\frac{(a-x)^2(b+y)\sqrt{(a+x)^2+(b+y)^2}}{a+x} \\
&+ \frac{(a-x)^2(b+y)\sqrt{(a-x)^2+(b-y)^2}}{a-x} \\
&+ (a-x)^2(-(b+y))\log\left(\frac{\sqrt{(a-x)^2+(b-y)^2}+a-x}{b-y}\right) \\
&+ (a-x)^2(b+y)\log\left(\frac{\sqrt{(a+x)^2+(b+y)^2}+a+x}{b+y}\right) \\
&= -\frac{(a-x)^2(b+y)c_1}{a+x} + \frac{(a-x)^2(b+y)c_2}{a-x} \\
&- (a-x)^2(b+y)\log\left(\frac{c_2+a-x}{b-y}\right) + (a-x)^2(b+y)\log\left(\frac{c_1+a+x}{b+y}\right)
\end{aligned}
\tag{C.8}
$$

$$
\begin{aligned}
I_{3}^{\square} &= \int_{\arctan\left[\frac{b-y}{a-x}\right]}^{\pi-\arctan\left[\frac{b+y}{a-x}\right]} a_1 a_2 (a_1+a_2)\mathrm{d}\theta \\
&= \frac{b(a-x)(b+y)\sqrt{(a-x)^2+(b-y)^2}}{b-y} \\
&+ \frac{b(a-x)(b-y)\sqrt{(a-x)^2+(b+y)^2}}{b+y} \\
&+ b(b+y)(b-y)\log\left[\frac{\sqrt{(a-x)^2+(b-y)^2}+a-x}{b-y}\right] \\
&- b(b-y)(b+y)\log\left[\frac{\sqrt{(a-x)^2+(b+y)^2}-a+x}{b+y}\right] \\
&= \frac{b(a-x)(b+y)c_2}{b-y} + \frac{b(a-x)(b-y)c_3}{b+y} \\
&+ b(b+y)(b-y)\log\left[\frac{c_2+a-x}{b-y}\right] - b(b-y)(b+y)\log\left[\frac{c_3-a+x}{b+y}\right]
\end{aligned}
\tag{C.9}
$$

$c_3 = \sqrt{(a-x)^2+(b+y)^2}$.

To facilitate the calculation of I_4 we further split into a further two integrals.

$$
\begin{aligned}
I_{4a}^{\square} &= \int_{\pi-\arctan\left[\frac{b+y}{a-x}\right]}^{\pi-\arctan\left[\frac{b-y}{a+x}\right]} a_1^2 a_2 \mathrm{d}\theta \\
&\quad - (b-y)^2(a-x)\int_{\pi-\arctan\left[\frac{b+y}{a-x}\right]}^{\pi-\arctan\left[\frac{b-y}{a+x}\right]} \frac{1}{\sin^2\theta\cos\theta}\mathrm{d}\theta \\
&= -\frac{(a-x)(b-y)^2\sqrt{(a-x)^2+(b+y)^2}}{b+y} + (a-x)(b-y)\sqrt{(a+x)^2+(b-y)^2} \\
&\quad - (a-x)(b-y)^2\log\left[\frac{-\sqrt{(a+x)^2+(b-y)^2}-b+y}{a+x}\right] \\
&\quad + (a-x)(b-y)^2\log\left[\frac{-\sqrt{(a-x)^2+(b+y)^2}-b-y}{a-x}\right] \\
&= -\frac{(a-x)(b-y)^2 c_3}{b+y} + \frac{(a-x)(b-y)^2}{b-y}c_4 \\
&\quad - (a-x)(b-y)^2\log\left[\left|\frac{-c_4-b+y}{a+x}\right|\right] + (a-x)(b-y)^2\log\left[\left|\frac{-c_3-b-y}{a-x}\right|\right] \\
&= -\frac{(a-x)(b-y)^2 c_3}{b+y} + \frac{(a-x)(b-y)^2}{b-y}c_4 \\
&\quad - (a-x)(b-y)^2\log\left[\frac{c_4+b-y}{a+x}\right] + (a-x)(b-y)^2\log\left[\frac{c_3+b+y}{a-x}\right]
\end{aligned}
\tag{C.10}
$$

with $c_4 = \sqrt{(a+x)^2+(b-y)^2}$. Since both terms in the logarithms are negative we use the identity that $\log[-z] = \log[z] + i\pi$, where $z > 0$ and $z \in \mathbb{R}$, where, as we should expect, all imaginary parts cancel.

$$
\begin{aligned}
I_{4b}^{\square} &= \int_{\pi-\arctan\left[\frac{b+y}{a-x}\right]}^{\pi-\arctan\left[\frac{b-y}{a+x}\right]} a_1 a_2^2 \mathrm{d}\theta \\
&= -(a-x)^2(b-y)\int_{\pi-\arctan\left[\frac{b+y}{a-x}\right]}^{\pi-\arctan\left[\frac{b-y}{a+x}\right]} \frac{1}{\sin\theta\cos^2\theta}\mathrm{d}\theta
\end{aligned}
\tag{C.11}
$$

$$
\begin{aligned}
I_{4b}^{\square} &= -\frac{(a-x)^2(b-y)\sqrt{(a+x)^2+(b-y)^2}}{a+x} \\
&+ (a-x)(b-y)\sqrt{(a-x)^2+(b+y)^2} \\
&- (a-x)^2(b-y)\log\left[\frac{\sqrt{(a+x)^2+(b-y)^2}-a-x}{b-y}\right] \\
&+ (a-x)^2(b-y)\log\left[\frac{\sqrt{(a-x)^2+(b+y)^2}-a+x}{b+y}\right] \\
&= -\frac{(a-x)^2(b-y)c_4}{a+x} + \frac{(a-x)(b-y)^2}{b-y}c_3 \\
&- (a-x)^2(b-y)\log\left[\frac{c_4-a-x}{b-y}\right] + (a-x)^2(b-y)\log\left[\frac{c_3-a+x}{b+y}\right]
\end{aligned}
\tag{C.12}
$$

$$
\begin{aligned}
I_5^{\square} &= -2a(a-x)(a+x)\int_{\pi-\arctan\left[\frac{b-y}{a+x}\right]}^{\pi}\sec^3\mathrm{d}\theta \\
&= -a(a-x)(a+x)\pi i + \frac{a(a-x)(b-y)\sqrt{(a+x)^2+(b-y)^2}}{a+x} \\
&- a(a-x)(a+x)\log\left[\frac{b-y-\sqrt{(a+x)^2+(b-y)^2}}{a+x}\right] \\
&= \frac{a(a-x)(b-y)c_4}{a+x} - a(a-x)(a+x)\log\left[\frac{c_4-(b-y)}{a+x}\right]
\end{aligned}
\tag{C.13}
$$

Similar to before the imaginary parts cancel.

A summary of the constants introduced to reduce the formula are,

$$
\begin{aligned}
c_1&:\sqrt{(a+x)^2+(b+y)^2} \\
c_2&:\sqrt{(a-x)^2+(b-y)^2} \\
c_3&:\sqrt{(a-x)^2+(b+y)^2} \\
c_4&:\sqrt{(a+x)^2+(b-y)^2}
\end{aligned}
\tag{C.14}
$$

Combining all the above integral gives,

$$
\begin{aligned}
f^{A_1}_{\boldsymbol{X},m}(x,y) = & \frac{(2x+a)(b+y)(a-x)}{a+x}c_1 + \frac{(a-x)(b+y)(b-2y)}{b-y}c_2 \\
& \frac{(b-y)(a-x)(b+2y)}{b+y}c_3 + \frac{(a+2x)(b-y)(a-x)}{a+x}c_4 \\
& + (b-y)(a-x)^2 \log\left[\frac{(c_3+x-a)(b-y)}{(c_4-a-x)(b+y)}\right] \\
& + (b+y)(a-x)^2 \log\left[\frac{(a+x+c_1)(b-y)}{(b+y)(a-x+c_2)}\right] \\
& + (b+y)^2(a-x) \log\left[\frac{(b-y+c_2)(a+x)}{(a-x)(b+y+c_1)}\right] \\
& - a(a+x)(a-x) \log\left[\frac{-b+y+c_4}{c_1-y-b}\right] \\
& + (b-y)^2(a-x) \log\left[\frac{(b+y+c_3)(a+x)}{(a-x)(b-y+c_4)}\right] \\
& + b(b-y)(b+y) \log\left[\frac{(a-x+c_2)\,(b+y)}{(b-y)\,(-a+x+c_3)}\right]
\end{aligned}
\tag{C.15}
$$

C.2 Triangle

C.2.1 Mean leg length triangle

To calculate the mean leg length in the triangle we use eq.(3.6). Namely we need to compute the following,

$$
\bar{l}_{\triangle} = \frac{1}{|A|^2}\int_0^{2\pi}\int_0^{r_{\max}} r^2 |A \cap A_{\boldsymbol{r}}| \mathrm{d}r\mathrm{d}\theta \tag{C.16}
$$

where $A_{\boldsymbol{r}}$ denotes the domain shifted by a parameter $\boldsymbol{r}$, namely the original domain A is moved a distance $r_{\max}$ at an angle θ away. In fact the main part of this problem is finding $|A \cap A_{\boldsymbol{r}}|$, the rest follows from normal integration.

Lets first define $\hat{A} = |A \cap A|_{\boldsymbol{r}}$.

$$\hat{a} = \begin{cases} \frac{(2ab - ar\sin\theta - br\cos\theta)^2}{4ab} & 0 \leq \theta < \arctan\left[\frac{b}{a}\right] \\ \frac{a(b - r\sin\theta)^2}{b} & \arctan\left[\frac{b}{a}\right] \leq \theta < \pi - \arctan\left[\frac{b}{a}\right] \\ \frac{(2ab - ar\sin\theta + br\cos\theta)^2}{4ab} & \pi - \arctan\left[\frac{b}{a}\right] \leq \theta < \pi \\ \frac{(2ab + ar\sin\theta - br\cos\theta)^2}{4ab} & \pi \leq \theta < \pi + \arctan\left[\frac{b}{a}\right] \\ \frac{a(b + r\sin\theta)^2}{b} & \pi + \arctan\left[\frac{b}{a}\right] \leq \theta < 2\pi - \arctan\left[\frac{b}{a}\right] \\ \frac{(2ab + ar\sin\theta - br\cos\theta)^2}{4ab} & 2\pi - \arctan\left[\frac{b}{a}\right] \leq \theta < 2\pi \end{cases} \tag{C.17}$$

Immediately we notice from symmetry we will only need to solve two distinct integrals.

$$\begin{aligned} \bar{l}_{\triangle} &= \frac{1}{|A|^2}\int_0^{2\pi}\int_0^{r_{\max}} r^2 |A \cap A_{\boldsymbol{r}}| \mathrm{d}r\mathrm{d}\theta \\ &= \frac{4}{|A|^2}\int_0^{\arctan\left[\frac{b}{a}\right]}\int_0^{\frac{2ab}{\cos\theta(b + a\tan\theta)}} \frac{(2ab - ar\sin\theta - br\cos\theta)^2}{4ab} r^2 \mathrm{d}r\mathrm{d}\theta \\ &+ \frac{2}{|A|^2}\int_{\arctan\left[\frac{b}{a}\right]}^{\pi - \arctan\left[\frac{b}{a}\right]}\int_0^{\frac{b}{\sin\theta}} \frac{a(b - r\sin\theta)^2}{b} r^2 \mathrm{d}r\mathrm{d}\theta \\ &= 4\bar{l}^1_{\triangle} + 2\bar{l}^2_{\triangle} \end{aligned} \tag{C.18}$$

Consider first $\bar{l}^1_{\triangle}$.

$$\begin{aligned} \bar{l}^1_{\triangle} &= \frac{1}{(\frac{1}{2}(2ab))^2}\int_0^{\arctan\left[\frac{b}{a}\right]}\int_0^{\frac{2ab}{\cos\theta(b + a\tan\theta)}} \frac{(2ab - ar\sin\theta - br\cos\theta)^2}{4ab} r^2 \mathrm{d}r\mathrm{d}\theta \\ &= \frac{1}{a^2b^2}\int_0^{\arctan\left[\frac{b}{a}\right]} \frac{4a^4b^4}{15(b\cos\theta + a\sin\theta)^3}\mathrm{d}\theta \\ &= \frac{1}{30(a^2 + b^2)^{3/2}}\left(4a^2b^2\log\left[\frac{a}{a + \sqrt{a^2 + b^2}}\right] + b^4 - a^4 + 4a^3\sqrt{a^2 + b^2}\right) \end{aligned} \tag{C.19}$$

where we use $\tan x = \frac{\sin x}{1+\cos x}$, $\operatorname{arctanh} z = \frac{1}{2}\log\left[\frac{1+z}{1-z}\right]$, to help the simplification.

The calculation of $l_{\triangle}^2$ is much more straightforward.

$$\begin{aligned}\bar{l}_{\triangle}^2 &= \frac{2}{(ab)^2}\int_{\arctan\left[\frac{b}{a}\right]}^{\frac{\pi}{2}}\int_0^{\frac{b}{\sin\theta}}\frac{a(b-r\sin\theta)^2}{b}r^2\mathrm{d}r\mathrm{d}\theta = \int_{\arctan\left[\frac{b}{a}\right]}^{\frac{\pi}{2}}\frac{b^2\csc^3\theta}{15a}\mathrm{d}\theta \\ &= \frac{a\sqrt{a^2+b^2}+b^2\log\left[\frac{a+\sqrt{a^2+b^2}}{b}\right]}{30a}\end{aligned} \tag{C.20}$$

As a verification we see that for a triangle where $a=\sqrt{3}$ and $b=3$, $\bar{l}=1.263$ as in Ref [Hyy06].

C.2.2 Spatial distribution of the RWP in a triangle

Consider the RWP in a triangular region $\mathcal{T} = \{(x,y)| -a \le x \le a, 0 \le y \le \min[(x+a)\tan\phi, -(x-a)\tan\phi\}$ where a, b are parameters of the base and height of the triangle respectively, and $\phi = \arctan\left[\frac{b}{a}\right]$. As in the rectangle, we can use symmetry to reduce the amount of calculations needed, and focus only on the case when $0 \le x \le a$.

$$f_{\boldsymbol{X},m}^{\triangle}(x,y,a,b) = \begin{cases} f_{\boldsymbol{X},m}^{\triangle,+}(x,y,a,b) & x \ge 0 \\ f_{\boldsymbol{X},m}^{\triangle,-}(-x,y,a,b) & x \le 0 \end{cases} \tag{C.21}$$

We begin by defining a_1 and a_2.

$$\begin{aligned} a_1(x,y) &= \begin{cases} \frac{ab-ay-bx}{\cos\theta(b+a\tan\theta)} & 0 \le \theta < \frac{\pi}{2} + \arctan\left[\frac{x}{b-y}\right] \\ \frac{ab+bx-ay}{\cos\theta(a\tan\theta-b)} & \frac{\pi}{2} + \arctan\left[\frac{x}{b-y}\right] \le \theta < \pi \end{cases} \\ a_2(x,y) &= \begin{cases} \frac{ya-ba-ax}{\cos\theta(a\tan\theta-b)} & 0 \le \theta < \arctan\left[\frac{y}{x+a}\right] \\ \frac{y}{\sin\theta} & \arctan\left[\frac{y}{x+a}\right] \le \theta < \frac{\pi}{2} + \arctan\left[\frac{a-x}{y}\right] \\ \frac{ay+bx-ab}{\cos\theta(a\tan\theta+b)} & \frac{\pi}{2} + \arctan\left[\frac{a-x}{y}\right] \le \theta < \pi \end{cases} \end{aligned} \tag{C.22}$$

Again, we need to compute eq.(3.4), and proceed by breaking the integral of $\int_0^\pi a_1(x,y,\theta)a_2(x,y,\theta)(a_1(x,y,\theta)+a_2(x,y,\theta))\mathrm{d}theta$ into the different integration limits, resulting in four different integrals. The first integral we need to compute is is over the interval $\theta \in \left[0, \arctan\left[\frac{y}{x+a}\right]\right)$ and is denoted as $I^+_{1,\triangle}$. To simplify the expressions we use the constants $c_0 = \sqrt{a^2+b^2}, c_1 = \sqrt{(a+x)^2+y^2}, c_2 = \sqrt{x^2+(b-y)^2}$ and $c_3 = \sqrt{(a-x)^2+y^2}$.

$$
\begin{aligned}
I^{+}_{1,\triangle} &= \int_{0}^{\arctan\left[\frac{y}{x+a}\right]} \left(\frac{ab-ay-bx}{\cos\theta(b+a\tan\theta)}\right)\left(\frac{ya-ba-ax}{\cos\theta(a\tan\theta-b)}\right)\left(\frac{ab-ay-bx}{\cos\theta(b+a\tan\theta)}+\frac{ya-ba-ax}{\cos\theta(a\tan\theta-b)}\right)\mathrm{d}\theta \\
&= \frac{b+x-y}{2b^2c_0^2}\Bigg(a(b+x-y)(a(y-b)+bx)c_0+c_0^2(a(y-b)+bx)^2 \\
&+ \frac{1}{2}b^2c_0((a(y-b)+bx)^2-(b+x-y)(a(b-y)-bx))\log\left[\frac{(b^2y^2-(a+c_0)^2(a+c_1+x)^2)}{((a-c_0)(a+c_1+x)+by)^2}\right] \\
&+ \frac{1}{2}a^2c_0((b+x-y)(a(b-y)-bx)-(a(y-b)+bx)^2)\log\left[\frac{((a+c_0)(a+c_1+x)+by)}{((a+c_0)(a+c_1+x)-by)}\right] \\
&+ \frac{abc_0^2c_1(b+x-y)(a(b-y)-bx)}{ay-b(a+x)} - \frac{(a(y-b)+bx)^2bc_0^2c_1}{(a(b+y)+bx)} \\
&+ c_0b^2\log\left[\frac{c_0-a}{a+c_0}\right]\left(\frac{1}{a}(a(y-b)+bx)^2+(b+x-y)(a(y-b)+bx)\right)\Bigg)
\end{aligned}
\tag{C.23}
$$

$$
\begin{aligned}
I^{+}_{2,\triangle} &= \int_{\arctan\left[\frac{y}{x+a}\right]}^{\frac{\pi}{2}+\arctan\left[\frac{x}{b-y}\right]} \left(\frac{ab-ay-bx}{\cos\theta(b+a\tan\theta)}\right)\left(\frac{y}{\sin\theta}\right)\left(\frac{ab-ay-bx}{\cos\theta(b+a\tan\theta)}+\frac{y}{\sin\theta}\right)\mathrm{d}\theta \\
&= \frac{y(a(y-b)+bx)}{b^2}\Bigg(yc_0\log\left[\frac{((c_0-a)(a+c_1+x)+by)(-(a+c_0)(c_2-x)+b^2-by)}{((c_0+a)(a+c_1+x)-by)((a-c_0)(c_2-x)-b^2+by)}\right] \\
&+ \frac{b^2c_2}{b-y}-2bc_1+b(x+a)\log\left[\frac{y(b-y)}{(a+c_1+x)(c_2-x)}\right]+\frac{a(a(y-b)+bx)}{c_0}\log\left[\frac{(c_0+a)(a+c_2+x)-by)}{(a-c_0)(a+c_2+x)-by)}\right]\Bigg)
\end{aligned}
\tag{C.24}
$$

$$
\begin{aligned}
I^{+}_{3,\triangle} &= \int_{\frac{\pi}{2}+\arctan\left[\frac{x}{b-y}\right]}^{\frac{\pi}{2}+\arctan\left[\frac{a-x}{y}\right]} \left(\frac{ab+bx-ay}{\cos\theta(a\tan\theta-b)}\right)\left(\frac{y}{\sin\theta}\right)\left(\frac{ab+bx-ay}{\cos\theta(a\tan\theta-b)}+\frac{y}{\sin\theta}\right)\mathrm{d}\theta \\
&= \frac{1}{b^2}y\Bigg(-y(a(b-y)+bx)\Bigg(c_0\log\left[\frac{(ab-ay-bc_0+bc_2+c_0y)(-a^2+a(-c_0+c_3+x)+by+c_0(c_3+x))}{(a(y-b)-b(c_0+c_2)+c_0y)(a^2-a(c_0+c_3+x)-by+c_0(c_3+x))}\right] \\
&+ a\log\left[\frac{y(b-y)}{(c_2+x)(-a+c_3+x)}\right]-\frac{bc_2}{b-y}+\frac{bc_3}{y}\Bigg) \\
&+ (b(a+x)-ay)^2\Bigg(\frac{a}{c_0}\log\left[\frac{((a-c_0)(c_2-x)+b^2-by)(c_0(-a+c_3+x)+a(-a+c_3+x)+by)}{((a+c_0)(c_2-x)+b^2-by)(-a^2+a(c_0+c_3+x)+by-c_0(c_3+x))}\right] \\
&+ \log\left[\frac{y(b-y)}{(c_2-x)(-a+c_3+x)}\right]+\frac{bc_3}{bx-a(b+y)}+\frac{bc_2}{ab-ay+bx}\Bigg)\Bigg)
\end{aligned}
\tag{C.25}
$$

$$
\begin{aligned}
I^{+}_{4,\triangle} &= \int_{\frac{\pi}{2}+\arctan\left[\frac{a-x}{y}\right]}^{\pi} \left(\frac{ab+bx-ay}{\cos\theta(a\tan\theta-b)}\right)\left(\frac{ay+bx-ab}{\cos\theta(a\tan\theta+b)}\right)\left(\frac{ab+bx-ay}{\cos\theta(a\tan\theta-b)}+\frac{ay+bx-ab}{\cos\theta(a\tan\theta+b)}\right)\mathrm{d}\theta \\
&= \frac{axy^2}{b}+abx-2axy-\frac{bx^3}{a}-\frac{c_3(ay-bx)(a(y-b)+bx)}{ab}-\frac{a(b-y)(b^2x^2-a^2(b-y)^2)}{2c_0b^2}\log\left[\frac{bc_3+c_0y}{bc_3-c_0y}\right] \\
&- \frac{xb(b^2x^2-a^2(b-y)^2)}{2c_0a^2}\log\left[\frac{((a(c_0+c_3+x)-c_0(c_3+x)-a^2)^2-b^2y^2)}{((c_0(-a+c_3+x)+a(-a+c_3+x))^2-b^2y^2)}\right]
\end{aligned}
\tag{C.26}
$$

Therefore we can write the spatial distribution of the mobile part of the RWP model as the sum of the four previous integrals.

$$f_{\boldsymbol{X}}^{\triangle,+}(x,y,a,b) = I_{1,\triangle}^{+} + I_{2,\triangle}^{+} + I_{3,\triangle}^{+} + I_{4,\triangle}^{+} \tag{C.27}$$

In this case we leave it in this form, as combining them creates a very lengthy expression, with few terms cancelling.

Appendix D

Gauss Hypergeometric Function

To provide some mathematical insight into why we get this transitional behaviour when $\eta =$ dimension, we consider the series expansion of the hypergeometric function as $d_{\mathcal{R}} \to \infty$. To achieve the large parameter expansion it is convenient to use the integral representation of the hypergeometric function [Gog13],

$$ {}_2F_1\left(a,b;c;-z\right) = \frac{\Gamma[c]}{\Gamma[b]\Gamma[c-b]}\int_0^1 \frac{t^{b-1}(1-t)^{c-b-1}}{(1+tz)^a}\mathrm{d}t \quad c>b>0 \tag{D.1}$$

The second step is to use the analytic continuation formula for the hypergeometric function which allows for $|z|>1$, obtained through analysis of Barnes' integral [Gog13].

$$\begin{aligned} {}_2F_1\left(a,b;c;z\right) = &\frac{\Gamma[c]\Gamma[b-a]}{\Gamma[b]\Gamma[c-a]}(-z)^{-a}\,{}_2F_1\left(a,a+1-c;a+1-b;\frac{1}{z}\right) \\ &+\frac{\Gamma[c]\Gamma[a-b]}{\Gamma[a]\Gamma[c-b]}(-z)^{-b}\,{}_2F_1\left(b,b+1-c;b+1-a;\frac{1}{z}\right) \end{aligned} \tag{D.2}$$

The particular case we are interested allows for a significant simplification through the substitution of $c=b+1, a=1$, the integral representation given

in eq.(D.1) and noticing that ${}_2F_1(a,0;c;z)=1$.

$$
\begin{aligned}
{}_2F_1\left(1,b;b+1;-z\right) &= \frac{\Gamma[b+1]\Gamma[b-1]}{\Gamma[b]\Gamma[b]}(z)^{-1}\left(\frac{\Gamma[2-b]}{\Gamma[1-b]\Gamma[2-b-(1-b)]}\int_0^1 \frac{t^{-b}}{\left(1+t\frac{1}{z}\right)}\mathrm{d}t\right) \\
&+ \frac{\Gamma[b+1]\Gamma[1-b]}{\Gamma[1]\Gamma[1]}(z)^{-b} \\
&=^{(1)} \frac{b}{b-1}(z)^{-1}\left((1-b)\int_0^1 t^{-b}\left(1-\frac{t}{z}+\frac{t^{2-b}}{z^2}-\frac{t^{3-b}}{z^3}+O(z^4)\right)\mathrm{d}t\right) \\
&+ b\pi\csc(\pi b)z^{-b} \\
&= -\frac{b}{z}\left(\frac{1}{(1-b)}-\frac{1}{(2-b)z}+\frac{1}{(3-b)z^2}+...\right)+b\pi\csc(\pi b)z^{-b}
\end{aligned}
\tag{D.3}
$$

In (1) we have expanded the integrand in terms of large z, and used the definition of the Gamma function to provide further simplifications.

Therefore, multiplying the gauss hypergeometric function by z^{-b},

$$
\begin{aligned}
z^b\ {}_2F_1\left(1,b;b+1;-z\right) &= -z^{b-1}b\left(\frac{1}{(1-b)}-\frac{1}{(2-b)z}+\frac{1}{(3-b)z^2}+...\right)+b\pi\csc(\pi b) \\
&= \lim_{z\to\infty}\begin{cases} b\pi\csc(\pi b) & 0<b<1 \\ \infty & b\geq 1 \end{cases}
\end{aligned}
\tag{D.4}
$$

which is equivalent to that in eq.(4.14) once $b=\frac{2}{\eta}$ is substituted back in and the factor $\pi\lambda_0(q\gamma d_{\mathcal{R}}^{\eta})^{\frac{2}{\eta}}$ is accounted for.

Bibliography

[Abr70] N. Abramson, "The aloha system: another alternative for computer communications," in *Proceedings of the November 17-19, 1970, fall joint computer conference*, 281–285 (ACM, 1970).

[AlA17] A. AlAmmouri, J. G. Andrews and F. Baccelli, "Analysis of dense cellular networks with stretched exponential path loss," in *Signals, Systems, and Computers, 2017 51st Asilomar Conference on*, 1837–1847 (IEEE, 2017).

[And11] J. G. Andrews, F. Baccelli and R. K. Ganti, "A tractable approach to coverage and rate in cellular networks," IEEE Transactions on Communications **59**, 3122–3134 (2011).

[Asa14] A. Asadi, Q. Wang and V. Mancuso, "A survey on device-to-device communication in cellular networks," IEEE Communications Surveys Tutorials **16**, 1801–1819 (2014).

[Aug16] A. Augustin, J. Yi, T. Clausen and W. M. Townsley, "A study of lora: Long range & low power networks for the internet of things," Sensors **16**, 1466 (2016).

[Bac97] F. Baccelli, M. Klein, M. Lebourges and S. Zuyev, "Stochastic geometry and architecture of communication networks," Telecommunication Systems **7**, 209–227 (1997).

[Bac09] F. Baccelli and B. Blaszczyszyn, "Spatial modeling of wireless communicationsa stochastic geometry approach," Foundations and Trends in Networking, NOW Publishers (2009).

[Bac10a] F. Baccelli and B. Blaszczyszyn, "A new phase transitions for local delays in manets," in *INFOCOM, 2010 Proceedings IEEE*, 1–9 (IEEE, 2010).

[Bac10b] F. Baccelli, B. Błaszczyszyn et al., "Stochastic geometry and wireless networks: Volume ii applications," Foundations and Trends® in Networking **4**, 1–312 (2010).

[Bac11] F. Baccelli, B. Błaszczyszyn and M.-O. Haji-Mirsadeghi, "Optimal paths on the space-time sinr random graph," Advances in Applied Probability **43**, 131–150 (2011).

[Bad07] A. Baddeley, I. Bárány and R. Schneider, "Spatial point processes and their applications," Stochastic Geometry: Lectures given at the CIME Summer School held in Martina Franca, Italy, September 13–18, 2004 1–75 (2007).

[Bal06] F. Ballani, "On modelling of refractory castables by marked gibbs and gibbsian-like processes," in *Case studies in spatial point process modeling*, 153–167 (Springer, 2006).

[Bal08] P. Balister, A. Sarkar and B. Bollobás, "Percolation, connectivity, coverage and colouring of random geometric graphs," in *Handbook of large-scale random networks*, 117–142 (Springer, 2008).

[Ban07] S. Bandyopadhyay, E. J. Coyle and T. Falck, "Stochastic properties of mobility models in mobile ad hoc networks," IEEE Transactions on Mobile Computing **6**, 1218–1229 (2007).

[Bar11] M. Barthélemy, "Spatial networks," Physics Reports **499**, 1–101 (2011).

[Bat12] N. Batool and R. Chellappa, "A markov point process model for wrinkles in human faces," in *Image Processing (ICIP), 2012 19th IEEE International Conference on*, 1809–1812 (IEEE, 2012).

[Ben07] S. Benhamou, "How many animals really do the levy walk?" Ecology **88**, 1962–1969 (2007).

[Bet02] C. Bettstetter, C. Wagner et al., "The spatial node distribution of the random waypoint mobility model." WMAN **11**, 41–58 (2002).

[Bet03a] C. Bettstetter, G. Resta and P. Santi, "The node distribution of the random waypoint mobility model for wireless ad hoc networks," IEEE Transactions on mobile computing **2**, 257–269 (2003).

[Bet03b] C. Bettstetter, G. Resta and P. Santi, "The node distribution of the random waypoint mobility model for wireless ad hoc networks," IEEE Transactions on mobile computing **2**, 257–269 (2003).

[Bet04] C. Bettstetter, H. Hartenstein and X. Pérez-Costa, "Stochastic properties of the random waypoint mobility model," Wireless Networks **10**, 555–567 (2004).

[Bhu14] N. Bhushan, J. Li, D. Malladi, R. Gilmore, D. Brenner, A. Damnjanovic, R. T. Sukhavasi, C. Patel and S. Geirhofer, "Network densification: the dominant theme for wireless evolution into 5G," IEEE Communications Magazine **52**, 82–89 (2014).

[Bib13] M. Bibinger, "Notes on the sum and maximum of independent exponentially distributed random variables with different scale parameters," arXiv preprint arXiv:1307.3945 (2013).

[Bła18] B. Błaszczyszyn, M. Haenggi, P. Keeler and S. Mukherjee, *Stochastic geometry analysis of cellular networks* (Cambridge University Press, 2018).

[Boc14a] S. Boccaletti, G. Bianconi, R. Criado, C. I. Del Genio, J. Gómez-Gardenes, M. Romance, I. Sendina-Nadal, Z. Wang and M. Zanin, "The structure and dynamics of multilayer networks," Physics Reports **544**, 1–122 (2014).

[Boc14b] F. Boccardi, R. W. Heath, A. Lozano, T. L. Marzetta and P. Popovski, "Five disruptive technology directions for 5g," IEEE Communications Magazine **52**, 74–80 (2014).

[Bor88] M. Borkovec, H. F. Eicke, H. Hammerich and B. Das Gupta, "Two percolation processes in microemulsions," The Journal of Physical Chemistry **92**, 206–211 (1988).

[Bra14] M. Bradonjić, "Outbreak of infectious diseases through the weighted random connection model," Mathematical Modelling of Natural Phenomena **9**, 82–88 (2014).

[Bro57] S. R. Broadbent and J. M. Hammersley, "Percolation processes: I. crystals and mazes," in *Mathematical Proceedings of the Cambridge Philosophical Society*, volume 53, 629–641 (Cambridge University Press, 1957).

[Bro06] D. Brockmann, L. Hufnagel and T. Geisel, "The scaling laws of human travel," Nature **439**, 462–465 (2006).

[Cam02] T. Camp, J. Boleng and V. Davies, "A survey of mobility models for ad hoc network research," Wireless communications and mobile computing **2**, 483–502 (2002).

[Che06] A. V. Chechkin, V. Y. Gonchar, J. Klafter and R. Metzler, "Fundamentals of lévy flight processes," Fractals, Diffusion, and Relaxation in Disordered Complex Systems: Advances in Chemical Physics, Part B, Volume 133 439–496 (2006).

[Che08] A. V. Chechkin, R. Metzler, J. Klafter, V. Y. Gonchar et al., "Introduction to the theory of lévy flights," Anomalous transport: Foundations and applications 129–162 (2008).

[Che18a] Y. Chen, R. Li, Z. Zhao and H. Zhang, "On the capacity of d2d social networks with fractal communications," in *2018 25th International Conference on Telecommunications (ICT)*, 486–492 (IEEE, 2018).

[Che18b] V. V. Chetlur and H. S. Dhillon, "Coverage analysis of a vehicular network modeled as cox process driven by poisson line process," IEEE Transactions on Wireless Communications **17** (2018).

[Chi13] S. N. Chiu, D. Stoyan, W. S. Kendall and J. Mecke, *Stochastic geometry and its applications* (John Wiley & Sons, 2013).

[Cho03] C.-Y. Chong and S. P. Kumar, "Sensor networks: evolution, opportunities, and challenges," Proceedings of the IEEE **91**, 1247–1256 (2003).

[Cho11] E. Cho, S. A. Myers and J. Leskovec, "Friendship and mobility: user movement in location-based social networks," in *Proceedings of the 17th ACM SIGKDD international conference on Knowledge discovery and data mining*, 1082–1090 (ACM, 2011).

[Cla90] B. N. Clark, C. J. Colbourn and D. S. Johnson, "Unit disk graphs," Discrete mathematics **86**, 165–177 (1990).

[Coo12a] J. Coon, C. P. Dettmann and O. Georgiou, "Full connectivity: Corners, edges and faces," J. Stat. Phys. **147**, 758–778 (2012).

[Coo12b] J. Coon, C. P. Dettmann and O. Georgiou, "Impact of boundaries on fully connected random geometric networks," Phys. Rev. E **85**, 011138 (2012).

[Coo15] J. P. Coon, O. Georgiou and C. P. Dettmann, "Connectivity scaling laws in wireless networks," IEEE Wireless Communications Letters **4**, 629–632 (2015).

[Dal07] D. J. Daley and D. Vere-Jones, *An introduction to the theory of point processes: volume II: general theory and structure* (Springer Science & Business Media, 2007).

[Der17] D. Dereudre, "Introduction to the theory of gibbs point processes," arXiv preprint arXiv:1701.08105 (2017).

[Deta] C. P. Dettmann, J. Coon, M. Di Renzo and O. Georgiou, "Random graphs and wireless communication networks, part 8: Mobility," http://www.eng.ox.ac.uk/sen/files/course2016/lec8.pdf, last Accessed: 2017-09-10.

[Detb] C. P. Dettmann, J. Coon, M. Di Renzo and O. Georgiou, "Random graphs and wireless communication networks, part 8: Mobility," http://www.eng.ox.ac.uk/sen/files/course2016/lec8.pdf, last Accessed: 2017-09-10.

[Det16] C. P. Dettmann and O. Georgiou, "Random geometric graphs with general connection functions," Physical Review E **93**, 032313 (2016).

[Det17] C. P. Dettmann and O. Georgiou, "Isolation statistics in temporal spatial networks," EPL **119**, 28002 (2017).

[Det18a] C. P. Dettmann, "Isolation and connectivity in random geometric graphs with self-similar intensity measures," Journal of Statistical Physics **172**, 679–700 (2018).

[Det18b] C. P. Dettmann, O. Georgiou and P. Pratt, "Spatial networks with wireless applications," Comptes Rendus Physique **19**, 183–264 (2018).

[Dig03] P. A. Dighe, R. K. Mallik and S. S. Jamuar, "Analysis of transmit-receive diversity in rayleigh fading," IEEE Transactions on Communications **51**, 694–703 (2003).

[Dou06] O. Dousse, M. Franceschetti, N. Macris, R. Meester and P. Thiran, "Percolation in the signal to interference ratio graph," Journal of Applied Probability **43**, 552–562 (2006).

[DR13] M. Di Renzo, A. Guidotti and G. E. Corazza, "Average rate of downlink heterogeneous cellular networks over generalized fading channels: A stochastic geometry approach," IEEE Transactions on Communications **61**, 3050–3071 (2013).

[DR16] M. Di Renzo, W. Lu and P. Guan, "The intensity matching approach: A tractable stochastic geometry approximation to system-level analysis of cellular networks," IEEE Transactions on Wireless Communications **15**, 5963–5983 (2016).

[Fam95] E. F. Fama, "Random walks in stock market prices," Financial analysts journal **51**, 75–80 (1995).

[Fia18] V. Fialho and F. Azevedo, "Wireless communication based on chirp signals for lora iot devices," i-ETC: ISEL Academic Journal of Electronics Telecommunications and Computers **4**, 6 (2018).

[Fra07] M. Franceschetti, O. Dousse, D. N. Tse and P. Thiran, "Closing the gap in the capacity of wireless networks via percolation theory," Information Theory, IEEE Transactions on **53**, 1009–1018 (2007).

[Gan09] R. K. Ganti and M. Haenggi, "Bounds on the information propagation delay in interference-limited aloha networks," in *Modeling and Optimization in Mobile, Ad Hoc, and Wireless Networks, 2009. WiOPT 2009. 7th International Symposium on*, 1–7 (IEEE, 2009).

[Geo15] O. Georgiou, S. Wang, M. Z. Bocus, C. P. Dettmann and J. P. Coon, "Location, location, location: Border effects in interference limited ad hoc networks," in *Modeling and Optimization in Mobile, Ad Hoc, and Wireless Networks (WiOpt), 2015 13th International Symposium on*, 568–575 (IEEE, 2015).

[Geo17] O. Georgiou and U. Raza, "Low power wide area network analysis: Can lora scale?" IEEE Wireless Communications Letters **6**, 162–165 (2017).

[Gil] A. P. Giles, O. Georgiou and C. P. Dettmann, "Betweenness centrality in dense random geometric networks," in *2015 IEEE International Conference on Communications (ICC)*.

[Gil61] E. N. Gilbert, "Random plane networks," Journal of the Society for Industrial and Applied Mathematics **9**, 533–543 (1961).

[Gil16] A. P. Giles, O. Georgiou and C. P. Dettmann, "Connectivity of soft random geometric graphs over annuli," Journal of Statistical Physics **162**, 1068–1083 (2016).

[Gog13] A. O. Gogolin, *Lectures on complex integration* (Springer Science & Business Media, 2013).

[Gon08] M. C. Gonzalez, C. A. Hidalgo and A.-L. Barabasi, "Understanding individual human mobility patterns," Nature **453**, 779–782 (2008).

[Gon14] Z. Gong and M. Haenggi, "Interference and outage in mobile random networks: Expectation, distribution, and correlation," IEEE Transactions on Mobile Computing **13**, 337–349 (2014).

[Gra89] R. L. Graham, D. E. Knuth, O. Patashnik and S. Liu, "Concrete mathematics: a foundation for computer science," Computers in Physics **3**, 106–107 (1989).

[Gri99] G. Grimmett, "What is percolation?" in *Percolation*, 1–31 (Springer, 1999).

[Gro01] M. Grossglauser and D. Tse, "Mobility increases the capacity of ad-hoc wireless networks," in *INFOCOM 2001. Twentieth Annual Joint Conference of the IEEE Computer and Communications Societies. Proceedings. IEEE*, volume 3, 1360–1369 (IEEE, 2001).

[Gug12] L. Gugelmann, K. Panagiotou and U. Peter, "Random hyperbolic graphs: degree sequence and clustering," Automata, Languages, and Programming 573–585 (2012).

[Guo13] A. Guo and M. Haenggi, "Spatial stochastic models and metrics for the structure of base stations in cellular networks," IEEE Transactions on Wireless Communications **12**, 5800–5812 (2013).

[Gup00] P. Gupta and P. R. Kumar, "The capacity of wireless networks," IEEE Transactions on information theory **46**, 388–404 (2000).

[Hae09] M. Haenggi, J. G. Andrews, F. Baccelli, O. Dousse and M. Franceschetti, "Stochastic geometry and random graphs for the analysis and design of wireless networks," IEEE J. Select. Areas Comm. **27**, 1029–1046 (2009).

[Hae12] M. Haenggi, *Stochastic geometry for wireless networks* (Cambridge University Press, 2012).

[Hae13] M. Haenggi, "The local delay in poisson networks," IEEE Transactions on Information Theory **59**, 1788–1802 (2013).

[Hal85] P. Hall, "On continuum percolation," The Annals of Probability **13**, 1250–1266 (1985).

[Har09] J. Harri, F. Filali and C. Bonnet, "Mobility models for vehicular ad hoc networks: a survey and taxonomy," IEEE Communications Surveys & Tutorials **11** (2009).

[Hel14] D. Helen and D. Arivazhagan, "Applications, advantages and challenges of ad hoc networks," JAIR **2**, 453–7 (2014).

[Hof83] G. Hoffmann, "Optimization of brownian search strategies," Biological cybernetics **49**, 21–31 (1983).

[Hol12] P. Holme and J. Saramäki, "Temporal networks," Physics reports **519**, 97–125 (2012).

[Hsi05] T. Hsing and H. Rootzén, "Extremes on trees," Annals of probability 413–444 (2005).

[Hug95] B. D. Hughes, "Random walks and random environments," Oxford **2**, 1995–1996 (1995).

[Hyy05] E. Hyytiä and J. Virtamo, "Random waypoint model in n-dimensional space," Operations Research Letters **33**, 567–571 (2005).

[Hyy06] E. Hyytia, P. Lassila and J. Virtamo, "Spatial node distribution of the random waypoint mobility model with applications," IEEE Transactions on mobile computing **5**, 680–694 (2006).

[Iye12] S. K. Iyer and D. Thacker, "Nonuniform random geometric graphs with location-dependent radii," The Annals of Applied Probability **22**, 2048–2066 (2012).

[Iye13] V. Iyer, Q. Liu, S. Dulman and K. Langendoen, "Adaptive online estimation of temporal connectivity in dynamic wireless networks," in *Self-Adaptive and Self-Organizing Systems (SASO), 2013 IEEE 7th International Conference on*, 237–246 (IEEE, 2013).

[Iye18] S. K. Iyer, "The random connection model: Connectivity, edge lengths, and degree distributions," Random Structures & Algorithms **52**, 283–300 (2018).

[Kan02] M. Kang and M.-S. Alouini, "Performance analysis of mimo mrc systems over rician fading channels," in *Vehicular Technology Conference, 2002. Proceedings. VTC 2002-Fall. 2002 IEEE 56th*, volume 2, 869–873 (IEEE, 2002).

[Kan03a] M. Kang and M.-S. Alouini, "A comparative study on the performance of mimo mrc systems with and without co-channel interference," in *Communications, 2003. ICC'03. IEEE International Conference on*, volume 3, 2154–2158 (IEEE, 2003).

[Kan03b] M. Kang and M.-S. Alouini, "Largest eigenvalue of complex wishart matrices and performance analysis of mimo mrc systems," IEEE Journal on Selected Areas in Communications **21**, 418–426 (2003).

[Kar08] S. Kar and J. M. Moura, "Sensor networks with random links: Topology design for distributed consensus," IEEE Transactions on Signal Processing **56**, 3315–3326 (2008).

[Kar10] S. Kar and J. M. Moura, "Distributed consensus algorithms in sensor networks: Quantized data and random link failures," IEEE Transactions on Signal Processing **58**, 1383–1400 (2010).

[Ken10] W. S. Kendall and I. S. Molchanov, *New perspectives in stochastic geometry* (Oxford University Press, 2010).

[Kes82] H. Kesten, *Percolation theory for mathematicians* (Springer, 1982).

[KG16] A. P. Kartun-Giles, "Connectivity and centrality in dense random geometric graphs," arXiv preprint arXiv:1601.03296 (2016).

[Kha16] S. Khan, A.-S. K. Pathan and N. A. Alrajeh, *Wireless sensor networks: Current status and future trends* (CRC Press, 2016).

[Kiw01] M. Kiwi, J. Mejıa-López, I. K. Schuller and H. Suhl, "Percolation and magnetism: interplay and relevance," Journal of magnetism and magnetic materials **226**, 626–629 (2001).

[Kla96] J. Klafter, M. F. Shlesinger and G. Zumofen, "Beyond brownian motion," Physics today **49**, 33–39 (1996).

[Kle07] R. Kleinberg, "Geographic routing using hyperbolic space," in *INFOCOM 2007. 26th IEEE International Conference on Computer Communications. IEEE*, 1902–1909 (IEEE, 2007).

[Kol68] A. N. Kolmogorov and B. V. Gnedenko, *Limit distributions for sums of independent random variables* (Addison-Wesley, 1968).

[Kou16a] K. Koufos and C. P. Dettmann, "Distribution of cell size in bounded voronoi tesselations with application to secure local connectivity," arXiv preprint arXiv:1612.02375 (2016).

[Kou16b] K. Koufos and C. P. Dettmann, "Temporal correlation of interference in bounded mobile ad hoc networks with blockage," IEEE Communications Letters **20**, 2494–2497 (2016).

[Kou17] K. Koufos, C. P. Dettmann and J. P. Coon, "Correlated interference from uncorrelated users in bounded ad hoc networks with blockage," IEEE Wireless Communications Letters **6**, 114–117 (2017).

[Kri10] D. Krioukov, F. Papadopoulos, M. Kitsak, A. Vahdat and M. Boguná, "Hyperbolic geometry of complex networks," Physical Review E **82**, 036106 (2010).

[Kri16] D. Krioukov, "Clustering implies geometry in networks," Physical review letters **116**, 208302 (2016).

[Kul12] A. Kulesza, B. Taskar et al., "Determinantal point processes for machine learning," Foundations and Trends® in Machine Learning **5**, 123–286 (2012).

[Las17] G. Last and M. Penrose, *Lectures on the Poisson process*, volume 7 (Cambridge University Press, 2017).

[Las18] G. Last, F. Nestmann and M. Schulte, "The random connection model and functions of edge-marked poisson processes: second order properties and normal approximation," arXiv preprint arXiv:1808.01203 (2018).

[Lee11] K. Lee, Y. Kim, S. Chong, I. Rhee and Y. Yi, "Delay-capacity tradeoffs for mobile networks with lévy walks and lévy flights," in *INFOCOM, 2011 Proceedings IEEE*, 3128–3136 (IEEE, 2011).

[Lee12] K. Lee, S. Hong, S. J. Kim, I. Rhee and S. Chong, "Slaw: self-similar least-action human walk," IEEE/ACM Transactions on Networking (TON) **20**, 515–529 (2012).

[Li15] Y. Li, F. Baccelli, H. S. Dhillon and J. G. Andrews, "Statistical modeling and probabilistic analysis of cellular networks with determinantal point processes," IEEE Transactions on Communications **63**, 3405–3422 (2015).

[Lin04] X. Lin and N. B. Shroff, "The fundamental capacity-delay tradeoff in large mobile ad hoc networks," in *Third Annual Mediterranean Ad Hoc Networking Workshop* (2004).

[Lu14] N. Lu and X. S. Shen, "Scaling laws for throughput capacity and delay in wireless networksa survey," IEEE Communications Surveys & Tutorials **16**, 642–657 (2014).

[Lu15] W. Lu and M. Di Renzo, "Stochastic geometry modeling of cellular networks: Analysis, simulation and experimental validation,"

in *Proceedings of the 18th ACM International Conference on Modeling, Analysis and Simulation of Wireless and Mobile Systems*, 179–188 (ACM, 2015).

[Mac13] G. R. MacCartney, J. Zhang, S. Nie and T. S. Rappaport, "Path loss models for 5G millimeter wave propagation channels in urban microcells." in *Globecom*, 3948–3953 (2013).

[Man94] R. N. Mantegna and H. E. Stanley, "Stochastic process with ultraslow convergence to a gaussian: the truncated lévy flight," Physical Review Letters **73**, 29–46 (1994).

[Mao12] G. Mao and B. D. Anderson, "Towards a better understanding of large-scale network models," IEEE/ACM transactions on networking **20**, 408–421 (2012).

[Mao13] G. Mao and B. D. Anderson, "Connectivity of large wireless networks under a general connection model," Information Theory, IEEE Transactions on **59**, 1761–1772 (2013).

[Mao17] G. Mao, *Connectivity of Communication Networks* (Springer, 2017).

[MB06] M. A. Martínez-Beneito, J. J. Abellán, A. López-Quílez, H. Vanaclocha, O. Zurriaga, G. Jorques and J. Fenollar, "Source detection in an outbreak of legionnaires disease," in *Case studies in spatial point process modeling*, 169–182 (Springer, 2006).

[Miy14] N. Miyoshi and T. Shirai, "A cellular network model with ginibre configured base stations," Advances in Applied Probability **46**, 832–845 (2014).

[Mör10] P. Mörters and Y. Peres, *Brownian motion*, volume 30 (Cambridge University Press, 2010).

[Mül15] T. Müller and P. Prałat, "The acquaintance time of (percolated) random geometric graphs," European Journal of Combinatorics **48**, 198–214 (2015).

[Nee05] M. J. Neely and E. Modiano, "Capacity and delay tradeoffs for ad hoc mobile networks," IEEE Transactions on Information Theory **51**, 1917–1937 (2005).

[Nig14] G. Nigam, P. Minero and M. Haenggi, "Coordinated multipoint joint transmission in heterogeneous networks," IEEE Transactions on Communications **62**, 4134–4146 (2014).

[Nos97] R. M. Nosofsky and T. J. Palmeri, "An exemplar-based random walk model of speeded classification." Psychological review **104**, 266–300 (1997).

[OG06] J. Osorio-Guillén, S. Lany, S. Barabash and A. Zunger, "Magnetism without magnetic ions: percolation, exchange, and formation energies of magnetism-promoting intrinsic defects in cao," Physical review letters **96**, 107203 (2006).

[Ors17] A. Orsino, A. Ometov, G. Fodor, D. Moltchanov, L. Militano, S. Andreev, O. N. Yilmaz, T. Tirronen, J. Torsner, G. Araniti et al., "Effects of heterogeneous mobility on d2d-and drone-assisted mission-critical mtc in 5g," IEEE Communications Magazine **55**, 79–87 (2017).

[Pen91] M. D. Penrose, "On a continuum percolation model," Advances in applied probability **23**, 536–556 (1991).

[Pen97] M. D. Penrose, "The longest edge of the random minimal spanning tree," Ann. Appl. Prob. 340–361 (1997).

[Pen98] M. D. Penrose, "Extremes for the minimal spanning tree on normally distributed points," Advances in Applied Probability **30**, 628–639 (1998).

[Pen03] M. Penrose, *Random geometric graphs* (Oxford University Press, 2003).

[Pen16] M. D. Penrose, "Connectivity of soft random geometric graphs," The Annals of Applied Probability **26**, 986–1028 (2016).

[Per13] Y. Peres, A. Sinclair, P. Sousi and A. Stauffer, "Mobile geometric graphs: Detection, coverage and percolation," Probability Theory and Related Fields **156**, 273–305 (2013).

[Pra16] P. Pratt, C. P. Dettmann and O. Georgiou, "How does mobility affect the connectivity of interference-limited ad hoc networks?" in *Modeling and Optimization in Mobile, Ad Hoc, and Wireless Networks (WiOpt), 2016 14th International Symposium on*, 1–8 (IEEE, 2016).

[Pra17] P. Pratt, C. P. Dettmann and O. Georgiou, "Optimal non-uniform deployments in ultra-dense finite-area cellular networks," IEEE Communications Letters **21**, 1139–1142 (2017).

[Pra18] P. Pratt, C. P. Dettmann and W. H. Chin, "Temporal connectivity in finite networks with nonuniform measures," Physical Review E **98**, 052310 (2018).

[Raz17] U. Raza, P. Kulkarni and M. Sooriyabandara, "Low power wide area networks: An overview," IEEE Communications Surveys & Tutorials **19**, 855–873 (2017).

[Rhe11] I. Rhee, M. Shin, S. Hong, K. Lee, S. J. Kim and S. Chong, "On the levy-walk nature of human mobility," IEEE/ACM transactions on networking (TON) **19**, 630–643 (2011).

[Rin47] D. Ring and W. Young, "The hexagonal cells concept," Bell Labs Technical Journal (1947).

[Rom92] S. Roman, "The logarithmic binomial formula," The American mathematical monthly **99**, 641–648 (1992).

[Rou04] Y. Roudi and A. Treves, "An associative network with spatially organized connectivity," Journal of Statistical Mechanics: Theory and Experiment **2004**, 07010 (2004).

[San05] P. Santi, "The critical transmitting range for connectivity in mobile ad hoc networks," IEEE transactions on mobile computing **4**, 310–317 (2005).

[Sch12] U. Schilcher, C. Bettstetter and G. Brandner, "Temporal correlation of interference in wireless networks with rayleigh block fading," IEEE Transactions on Mobile Computing **11**, 2109–2120 (2012).

[Sch14] V. Schmidt, *Stochastic geometry, spatial statistics and random fields* (Springer, 2014).

[Sch17] U. Schilcher, G. Brandner and C. Bettstetter, "Quantifying inhomogeneity of spatial point patterns," Computer Networks **115**, 65–81 (2017).

[Sha04] G. Sharma and R. R. Mazumdar, "Scaling laws for capacity and delay in wireless ad hoc networks with random mobility," **7**, 3869–3873 (2004).

[Shi92] M. Shiino and T. Fukai, "Self-consistent signal-to-noise analysis and its application to analogue neural networks with asymmetric connections," Journal of Physics A: Mathematical and General **25**, L375 (1992).

[Shl86] M. F. Shlesinger and J. Klafter, "Lévy walks versus lévy flights," in *On growth and form*, 279–283 (Springer, 1986).

[Sos00] A. Soshnikov, "Determinantal random point fields," Russian Mathematical Surveys **55**, 923–975 (2000).

[Sri10] S. Srinivasa and M. Haenggi, "Distance distributions in finite uniformly random networks: Theory and applications," IEEE Transactions on Vehicular Technology **59**, 940–949 (2010).

[Taj17] S. E. Tajbakhsh, J. P. Coon and D. E. Simmons, "Accessibility and delay in random temporal networks," Physical Review E **96**, 032309 (2017).

[Teh14] M. N. Tehrani, M. Uysal and H. Yanikomeroglu, "Device-to-device communication in 5g cellular networks: challenges, solutions, and future directions," IEEE Communications Magazine **52**, 86–92 (2014).

[Tor08] S. Torquato, A. Scardicchio and C. E. Zachary, "Point processes in arbitrary dimension from fermionic gases, random matrix theory, and number theory," Journal of Statistical Mechanics: Theory and Experiment **2008**, P11019 (2008).

[Tse05] D. Tse and P. Viswanath, *Fundamentals of wireless communication* (Cambridge university press, 2005).

[Van15] L. Vangelista, A. Zanella and M. Zorzi, "Long-range iot technologies: The dawn of lora," in *Future Access Enablers of Ubiquitous and Intelligent Infrastructures*, 51–58 (Springer, 2015).

[Vaz12] R. Vaze, "Percolation and connectivity on the signal to interference ratio graph," in *INFOCOM, 2012 Proceedings IEEE*, 513–521 (IEEE, 2012).

[Wal11] M. Walters, "Random geometric graphs," Surveys in Combinatorics **392**, 365–402 (2011).

[Wat98] D. J. Watts and S. H. Strogatz, "Collective dynamics of small-worldnetworks," Nature **393**, 440 (1998).

[Wax88] B. M. Waxman, "Routing of multipoint connections," Selected Areas in Communications, IEEE Journal on **6**, 1617–1622 (1988).

[Wik18a] Wikipedia contributors, "Edgar Gilbert — Wikipedia, the free encyclopedia," `https://en.wikipedia.org/w/index.php?title=Edgar_Gilbert&oldid=839676809` (2018), [Online; accessed 7-September-2018].

[Wik18b] Wikipedia contributors, "Mobile ad hoc network — Wikipedia, the free encyclopedia," `https://en.wikipedia.org/w/index.php?title=Mobile_ad_hoc_network&oldid=857061538` (2018), [Online; accessed 7-September-2018].

[Wik18c] Wikipedia contributors, "Random geometric graph — Wikipedia, the free encyclopedia," `https://en.wikipedia.org/w/index.php?title=Random_geometric_graph&oldid=846741477` (2018), [Online; accessed 7-September-2018].

[Wil05] H. S. Wilf, *Generatingfunctionology* (AK Peters/CRC Press, 2005).

[Won06] L. H. Wong, P. Pattison and G. Robins, "A spatial model for social networks," Physica A: Statistical Mechanics and its Applications **360**, 99–120 (2006).

[Zha09] X. Zhang and B. Li, "Optimized multipath network coding in lossy wireless networks," IEEE journal on selected areas in communications **27**, 622–634 (2009).

[Zha15] X. Zhang and J. G. Andrews, "Downlink cellular network analysis with multi-slope path loss models," IEEE Transactions on Communications **63**, 1881–1894 (2015).

[Zho13] Y. Zhong and W. Zhang, "Multi-channel hybrid access femtocells: A stochastic geometric analysis," IEEE Transactions on Communications **61**, 3016–3026 (2013).